



University of Tennessee, Knoxville  
**Trace: Tennessee Research and Creative  
Exchange**

---

Doctoral Dissertations

Graduate School

---

5-2012

# Derivation of Correction Terms to the Eikonal Approximations in the Formulation of Analytical Abrasion-Ablation Model

Santosh Bhatt  
[sbhatt@utk.edu](mailto:sbhatt@utk.edu)

---

## Recommended Citation

Bhatt, Santosh, "Derivation of Correction Terms to the Eikonal Approximations in the Formulation of Analytical Abrasion-Ablation Model. " PhD diss., University of Tennessee, 2012.  
[https://trace.tennessee.edu/utk\\_graddiss/1268](https://trace.tennessee.edu/utk_graddiss/1268)

This Dissertation is brought to you for free and open access by the Graduate School at Trace: Tennessee Research and Creative Exchange. It has been accepted for inclusion in Doctoral Dissertations by an authorized administrator of Trace: Tennessee Research and Creative Exchange. For more information, please contact [trace@utk.edu](mailto:trace@utk.edu).

To the Graduate Council:

I am submitting herewith a dissertation written by Santosh Bhatt entitled "Derivation of Correction Terms to the Eikonal Approximations in the Formulation of Analytical Abrasion-Ablation Model." I have examined the final electronic copy of this dissertation for form and content and recommend that it be accepted in partial fulfillment of the requirements for the degree of Doctor of Philosophy, with a major in Nuclear Engineering.

Lawrence W. Townsend, Major Professor

We have read this dissertation and recommend its acceptance:

G. Ivan Maldonado, Lawrence H. Heilbronn, Thomas Handler

Accepted for the Council:

Dixie L. Thompson

Vice Provost and Dean of the Graduate School

(Original signatures are on file with official student records.)

---

# **Derivation of Correction Terms to the Eikonal Approximations in the Formulation of Analytical Abrasion-Ablation Model**

A Dissertation  
Presented for the  
Doctor of Philosophy  
Degree  
The University of Tennessee, Knoxville

**Santosh Bhatt**  
**May, 2012**

Copyright © 2012 by Santosh Bhatt  
All rights reserved.

## **Dedication**

To my loving parents

Padam Raj Bhatta  
&  
Kusum Bhatta

## **ACKNOWLEDGEMENTS**

I would like to sincerely thank my wonderful advisor Dr. Lawrence Townsend. I deeply appreciate his help, support and constant patience throughout this process. I could not have accomplished this work without his guidance. He has been an amazing advisor and a great role model. I would also like to thank Dr. Ivan Maldonado for his support and guidance ever since my days at the University of Cincinnati. He has been full of great advice and has always guided me to the right direction. I would like to thank Dr. Lawrence Heilbronn and Dr. Thomas Handler for their helpful suggestions and generous guidance throughout this work. My sincere thanks go to Dr. Arthur Ruggles. I have learned a lot from him both inside and outside the classroom, which has helped me develop as a better person.

I would also like to thank all my professors, teachers and friends for their support. I would like to especially thank my parents and all the family members for their love and for helping me achieve my personal and professional goals. Finally, I would like to thank Ms. Sadikshya Bhandari and Mr. Migun Shakya for constant support and encouragement.

## ABSTRACT

Analytical models for the quantitative predictions of spectra from the neutrons and light ions produced from the high energy, heavy ion (HZE) reactions are extremely important in assessment of the radiation damage during long duration deep space missions, and for various accelerator applications. The fundamental physics of the secondary particle production and transport from these HZE reactions is described using the abrasion-ablation model. The abrasion part of the model is based on the Glauber multiple scattering theory while the ablation process is based on statistical decay based on an evaporation model. The current formulations for the abrasion process are based on the Eikonal approximations, developed using the small angle approximations, which are considered in the strictly forward scattering, in the plane of incident momentum. However, neutron and light ion transport is inherently a three –dimensional problem and therefore requires nuclear models capable of generating double differential cross sections, both energy and angle, for use in the transport codes. This study relaxes the forward scattering, small angle approximation in the development of abrasion-ablation theory by adding higher order correction terms to the phase shift operator used in the abrasion formalism and thus improves the prediction of secondary particle production at different angular and spectral ranges. Four higher order correction terms to the Eikonal approximations were developed based on the previous work by Wallace. The optical potential used in the derivation of the phase functions was reformulated using Gaussian approximations to the nuclear single particle densities. The new formalism, with correction terms, was used to evaluate the total abrasion and the double differential cross sections of the secondary particles in HZE reactions. A comparison of total abrasions cross sections to evaluate the contributions of the individual higher order correction terms has been done. Also, the double differential cross sections were calculated using the current model with two correction terms and compared to the published measurements from accelerator studies.

## Table of Contents

1. Introduction .....	1
2. Eikonal Expansions and the Abrasion-Ablation Model .....	8
2.1. Brief Overview .....	8
2.2. Abrasion-Ablation Model .....	13
2.2.1. Abrasion Formalism .....	15
2.2.2. Ablation Formalism .....	20
3. Eikonal Corrections to the Phase Function .....	23
3.1. Formulation of the Scattering Amplitude .....	23
3.1.1. The Method of Partial Waves .....	24
3.1.2. Eikonal Approximation .....	26
3.2. Derivation of Correction Terms to the Scattering Amplitude .....	33
4. Optical Potential Derivation .....	40
4.1. Optical Model using Multiple Scattering Series .....	40
4.2. Nuclear Density Distribution Approximations .....	46
4.3. Validity of the Gaussian Approximations .....	54
4.4. Optical Potential and Phase Function Calculation .....	58
4.4.1. Phase Functions .....	67
4.5. Frame Transformations .....	70
5. Results .....	75
5.1. Comparison of Contributions of the Higher Order Correction Terms .....	75
5.2. Comparison to the Experimental Data .....	80
6. Conclusions and Future Work .....	92
LIST OF REFERENCES .....	94
APPENDIX .....	102
APPENDIX I .....	103
APPENDIX II .....	104
APPENDIX III .....	105



Phase Function Calculations.....	105
Appendix IV .....	110
Gaussian Quadrature.....	110
Appendix V .....	112
More Results:.....	112
Appendix VI.....	114
MATLAB code:.....	114
VITA .....	125

## LIST OF TABLES

Table	Page
Table 1: Parameters for the Momentum Distribution Model .....	18
Table 2: Total Abrasion Cross Section with Correction Terms for $^{12}\text{C}$ on $^{27}\text{Al}$ at 10 Degrees .....	76
Table 3: Total Abrasion Cross Section with Correction Terms for $^{20}\text{Ne}$ on $^{16}\text{O}$ at 20 Degrees .....	76
Table 4: Total Abrasion Cross Section with Correction Terms for $^{20}\text{Ne}$ on $^{64}\text{Cu}$ at 5 Degrees .....	112

## LIST OF FIGURES

Figure	Page
Figure 1: Schematic of abrasion-ablation model and the corresponding momenta distributions .....	4
Figure 2: Schematic diagram of Eikonal approximation scattering with straight line trajectory. ....	30
Figure 3: Comparison of Harmonic Well versus Gauss distribution for $^4\text{He}$ . ....	51
Figure 4: Comparison of Harmonic Well versus Gauss distribution for $^9\text{Be}$ . ....	52
Figure 5: Comparison of Wood Saxon versus Gauss distribution for $^{20}\text{Ne}$ . ....	52
Figure 6: Comparison of Wood Saxon versus Gauss distribution for $^{64}\text{Cu}$ . ....	53
Figure 7: Comparison of Wood Saxon versus Gauss distribution for $^{108}\text{Ag}$ . ....	53
Figure 8: Comparison of the Gaussian Model to the experimental data and parameterization by Townsend and Wilson for $^{12}\text{C}$ on $^{12}\text{C}$ . ....	56
Figure 9: Comparison of the Gaussian Model to the experimental data and parameterization by Townsend and Wilson for $^{12}\text{C}$ on $^{27}\text{Al}$ . ....	56
Figure 10: Comparison of the Gaussian Model to the parameterization by Townsend and Wilson for $^{20}\text{Ne}$ on $^{64}\text{Cu}$ . ....	57
Figure 11: Comparison of the Gaussian Model to the parameterization by Townsend and Wilson for $^{108}\text{Ag}$ on $^{208}\text{Pb}$ . ....	57
Figure 12: Comparison of differential cross section from abrasion process for 100 MeV/nucleon $^{12}\text{C}$ on $^{20}\text{Ne}$ at $20^\circ$ scattering angle for 0, 2 and 4 correction terms. ....	78
Figure 13: Comparison of differential cross section from ablation process for 100 MeV/nucleon $^{12}\text{C}$ on $^{20}\text{Ne}$ at $20^\circ$ scattering angle for 0, 2 and 4 correction terms. ....	78

Figure 14: Comparison of differential cross section from abrasion process for 400 MeV/nucleon $^{14}\text{N}$ on $^{12}\text{C}$ at $40^0$ scattering angle for 0, 2 and 4 correction terms. ....	79
Figure 15: Comparison of differential cross section from ablation process for 400 MeV/nucleon $^{14}\text{N}$ on $^{12}\text{C}$ at $40^0$ scattering angle for 0, 2 and 4 correction terms. ....	79
Figure 16: Double differential cross sections for 290 MeV/nucleon $^{12}\text{C}$ on $^{12}\text{C}$ at 5 degrees .....	81
Figure 17: Double differential cross sections for 290 MeV/nucleon $^{12}\text{C}$ on $^{12}\text{C}$ at 10 degrees .....	81
Figure 18: Double differential cross sections for 290 MeV/nucleon $^{12}\text{C}$ on $^{12}\text{C}$ at 20 degrees .....	82
Figure 19: Double differential cross sections for 290 MeV/nucleon $^{12}\text{C}$ on $^{12}\text{C}$ at 30 degrees .....	82
Figure 20: Double differential cross sections for 290 MeV/nucleon $^{12}\text{C}$ on $^{12}\text{C}$ at 40 degrees .....	83
Figure 21: Double differential cross sections for 290 MeV/nucleon $^{12}\text{C}$ on $^{12}\text{C}$ at 60 degrees .....	83
Figure 22: Double differential cross sections for 400 MeV/nucleon $^{20}\text{Ne}$ on $^{64}\text{Cu}$ at 5 degrees .....	84
Figure 23: Double differential cross sections for 400 MeV/nucleon $^{20}\text{Ne}$ on $^{64}\text{Cu}$ at 10 degrees .....	84
Figure 24: Double differential cross sections for 400 MeV/nucleon $^{20}\text{Ne}$ on $^{64}\text{Cu}$ at 20 degrees .....	85
Figure 25: Double differential cross sections for 400 MeV/nucleon $^{20}\text{Ne}$ on $^{64}\text{Cu}$ at 40 degrees .....	85
Figure 26: Double differential cross sections for 400 MeV/nucleon $^{14}\text{N}$ on $^{12}\text{C}$ at 5 degrees .....	86

Figure 27: Double differential cross sections for 400 MeV/nucleon $^{14}\text{N}$ on $^{12}\text{C}$ at 10 degrees .....	86
Figure 28: Double differential cross sections for 400 MeV/nucleon $^{14}\text{N}$ on $^{12}\text{C}$ at 20 degrees .....	87
Figure 29: Double differential cross sections for 400 MeV/nucleon $^{14}\text{N}$ on $^{12}\text{C}$ at 40 degrees .....	87
Figure 30: Double differential cross sections for 290 MeV/nucleon $^{12}\text{C}$ on $^{64}\text{Cu}$ at 5 degrees .....	88
Figure 31: Double differential cross sections for 290 MeV/nucleon $^{12}\text{C}$ on $^{64}\text{Cu}$ at 10 degrees .....	88
Figure 32: Double differential cross sections for 290 MeV/nucleon $^{12}\text{C}$ on $^{64}\text{Cu}$ at 20 degrees .....	89
Figure 33: Double differential cross sections for 290 MeV/nucleon $^{12}\text{C}$ on $^{64}\text{Cu}$ at 40 degrees .....	89
Figure 34: Surface plot of double differential cross section with two correction terms for 290 MeV/nucleon $^{12}\text{C}$ on $^{12}\text{C}$ .....	90
Figure 35: Same as Figure (34), except rotated .....	90
Figure 36: Surface plot of double differential cross section with two correction terms for 400 MeV/nucleon $^{20}\text{Ne}$ on $^{64}\text{Cu}$ .....	91
Figure 37: Same as Figure (36), except rotated .....	91
Figure 38: Double differential cross sections for 400 MeV/nucleon $^{84}\text{Kr}$ on $^{27}\text{Al}$ at 20 degrees .....	112
Figure 39: Surface plot of double differential cross section with two correction terms for 400 MeV/nucleon $^{84}\text{Kr}$ on $^{27}\text{Al}$ .....	113
Figure 40: Same as figure (39), except rotated .....	113

# 1. Introduction

The ionizing radiation environment in space is a major concern in planning for exploratory missions to Moon, Mars and beyond Earth's orbit. During long duration, deep space missions, safety of the space craft components and the human crews from exposure to such harmful ionizing radiation must be properly addressed. The ionizing radiation environment in space is very complex in nature as it consists of different types of particles over wide ranges of energies. The major sources of ionizing radiation in space are galactic cosmic rays (GCR), transient solar particle events (SPE), and the trapped electron and proton radiation belts [1],[2]. The GCR energy range extends up to TeV energies and consists of about 98% protons and heavy ions and 2% electrons. A SPE contains about 80-90% protons, 10-20% helium and about 1% heavy ions. During SPEs, the flux, particle composition and energy spectrum of SPE varies widely, up to orders of magnitude, with energies ranging from few MeV to tens of GeV in magnitude [1],[3]. Once the spacecraft leaves Earth's protective magnetic field, it is constantly bombarded with the entire spectrum of cosmic radiation of galactic and solar origin. The interaction of such cosmic radiation with the spacecraft structural shielding or the self shielding of human body leads to production of neutrons and light ion fragments, which are responsible for a large fraction of energy depositions, and thus doses, to the space crew and the space craft components. These secondary neutrons and light ion fragments can further undergo nuclear interactions producing more secondaries, which can result in deeper penetration into the material. Although the nuclear reactions leading to production of secondary particles are dominated by the nucleon component of cosmic radiation, a significant fraction of neutron production is also due to interactions of

primary helium and heavy ion components of cosmic rays with the shielding material[4]. The models for characterizing transport of neutrons produced in high energy, heavy ion (HZE) reactions are therefore extremely important in the assessment of radiation damage from cosmic radiation. Thus proper knowledge of neutron transport is essential as neutrons can be extremely damaging to biological tissue and spacecraft components due to their depths of penetration. Studies have also indicated that some of the secondary particles can also penetrate the Earth's atmosphere and are possible source of radiation exposure to airplane crews and passengers on long distance high latitude and altitude flights. Hence to establish proper protection from these high energy radiations and their secondaries during the space missions, we need accurate and efficient radiation transport models along with relevant nuclear databases. Precise transport models and rich nuclear cross-section databases enable us to calculate better radiation dose and exposure estimates, and also help us in effective shielding design [4],[5]. In this work, the fundamental physics for secondary particle production and transport is described using the abrasion-ablation process. The analytical abrasion-ablation model has been widely used to describe the fundamental physics of secondary particle production from high energy nucleon-nucleus and nucleus-nucleus collision. The current formulations for the abrasion-ablation model are based on the Eikonal approximation, developed using the Glauber multiple scattering theory, which considers scattering strictly in the forward direction, in the plane of incident momentum [6]. However, neutron and light ion transport is inherently a three-dimensional problem and therefore requires nuclear models capable of generating double differential cross sections, both energy and angle, for use in the transport codes. The main purpose of the current study is to relax the forward scattering, small angle approximation in the development of abrasion-ablation

theory. This is achieved by adding higher order correction terms to the phase shift operator used in the abrasion formalism, so as to eliminate the small angle approximation and thus improve the prediction of secondary particle production at different angular and spectral ranges.

The abrasion-ablation model is based on fragmentation theory which implies that the secondary particle production from high energy heavy ion collisions is a two stage process that involves the interaction between two relativistic heavy particles [7],[8]. In the first stage, also known as the abrasion or knockout process, a relativistic particle, projectile P, moving at an initial momentum,  $p$ , with respect to the stationary target T, collides with the target and thus their overlapping volumes get sheared off. After the abrasion process, the remaining pieces of projectile P and target T can be highly excited. The remaining piece of projectile P, known as the projectile pre-fragment, continues more or less on its initial trajectory with its pre-collision velocity. The projectile pre-fragment, which is now in the excited state, decays by emitting gamma rays and/or disintegrates into fragments and nucleons. This step is known as the ablation process. The abrasion-ablation process is schematically illustrated in Figure 1.



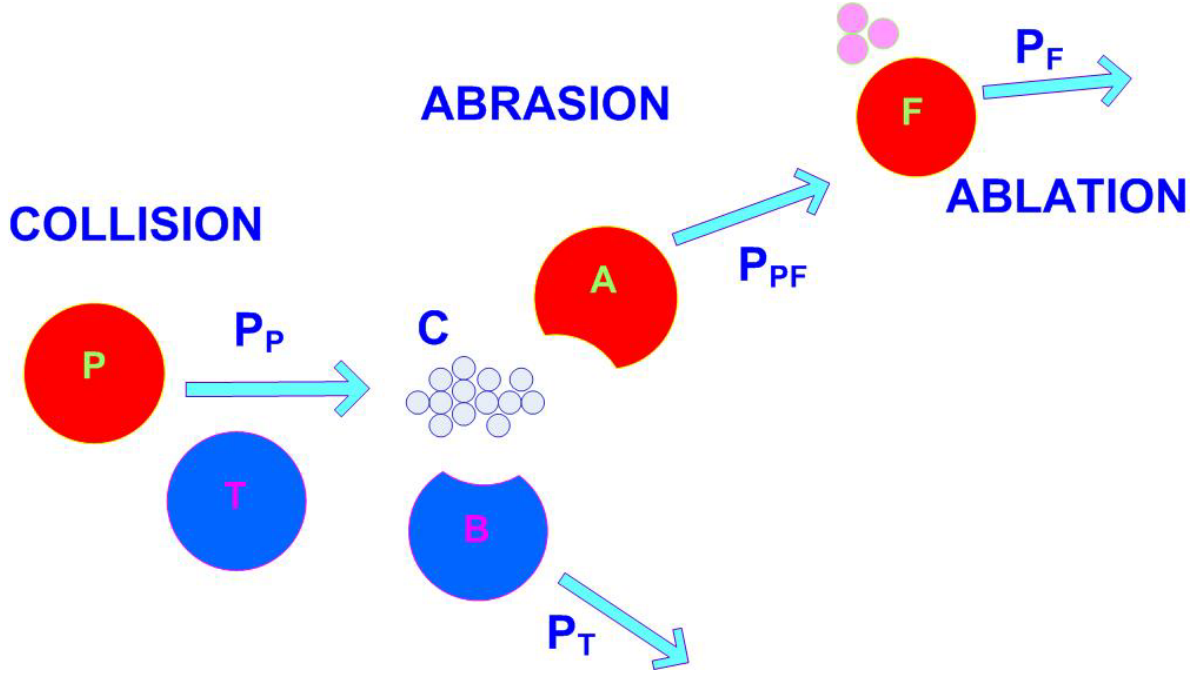


**Figure 1:** Schematic of abrasion-ablation model and the corresponding momenta distributions at different steps

Figure adapted from Giacomelli et al.[9].

The abrasion-ablation model was initially formulated by Bowman, Swiatecki and Tsang [7] and extended by Hufner, Schaffer, and Schurmann and others [8],[10],[11],[12],[13],[14]. It was further extended to the evaluation of neutron momentum distributions by Cucinotta et al. [5],[4]. The abrasion formalism of the current model for predicting secondary particle production is based on the Glauber multiple scattering theory, which applies the optical limit potential approximation to the nucleus-nucleus multiple scattering series, and its further expansion in terms of the Eikonal differential approximations. The ablation process of the model uses the classical evaporation model developed by Weisskopf and Ewing, where the statistical probability

of particle emission from excited nuclei are treated as competing processes [15],[6],[16],[17]. The Eikonal expansions in the Glauber model are considered in terms of a small angle, high energy approximation which assumes that the total Eikonal phase for the scattering is equal to the sum of the Eikonal phases for scattering of the projectile off each target constituent. This results into a finite multiple scattering series which terminates when the number of terms equals the target mass number. For heavy ion scattering, where the full series becomes too difficult to sum due to realistic nuclear densities, an alternative approach is used where the semi-classical solutions to effective coupled-channel equations are derived using Watson's approach. The equivalence of the semi-classical coupled-channel equations to the Glauber amplitude for heavy ion scattering was shown by Cucinotta [16]. Although the Glauber model has been widely used with reasonable success, the validity of the small angle approximations made in the model are not clear for systems with three or more particles in the final state, and at lower energies where medium effects come into play [18]. Light ion production ( $z \leq 2$ ), is also inherently three dimensional, and is not properly described by a small angle approximation. There have been various different approaches to the correction of Eikonal expansions in the Glauber multiple scattering series. Most derivations of Eikonal approximations require a small scattering angle in some sense, which has resulted into many variants of the approximations in order to extend the angular range of validity. However there is no compelling argument showing that any method is valid at large scattering angles [19],[20],[21].

In this work, we have used the Eikonal expansions developed by Wallace [19],[21] to include higher order correction terms to the phase shift operator used in the Glauber model. Wallace

converts the partial wave series into a Fourier-Bessel expansion, based on an expansion of Legendre functions, thus creating an infinite series, where the leading term in the phase shift operator is the same as the Glauber model and additional terms are the higher order Eikonal correction terms to the Glauber phase shift operator [17],[19],[21],[22]. This expansion is exact in the sense that there is no small angle assumption made. In the following sections, we have developed four higher order correction terms to the phase shift operator using Wallace's approach and incorporated them in the current abrasion-ablation formalism. The improved formalism, with correction terms, has been used to evaluate cross-sections and momentum distributions of secondary particles in the high energy heavy ion reactions. A comparison of angular distributions for elastic scattering amplitude, Lorentz invariant cross sections and double differential cross sections using the current model with correction terms correspond to the existing model and experimental data are presented.

The remaining chapters in this report are divided as follows: Chapter 2 gives a brief overview of the development of high energy scattering and Eikonal expansions along with the fundamental formalism of the abrasion-ablation model in the context of Eikonal approximations. The chapter also discusses various studies that have presented approximations for Eikonal expansions with reference to Glauber multiple scattering theory. Chapter 3 discusses the development of higher order correction terms to the Eikonal scattering using the formalism developed by Wallace [19]. In that chapter, starting with the partial wave representation of scattering amplitude, we have developed four higher order correction terms to the phase shift operator in accordance with the approach presented by Waxman et al. for the correction terms developed by Wallace [20].

Chapter 4 looks into the derivation of an optical potential with Gaussian approximations to nuclear densities and incorporates the correction terms presented in Chapter 3 to the phase shift operator calculated using nuclear density approximations to the optical potential. This chapter also presents brief discussion on frame transformations between laboratory and projectile frames. Chapter 5 presents calculations of total abrasion cross sections and double differential cross-sections by incorporating the correction terms to the current model. A comparison between contributions of the two and four correction terms, along with comparisons to the experimental data is presented. Chapter 6 includes conclusions and suggestions for future work, which is followed by a list of references, appendices and the MATLAB code used in the calculations.

## 2. Eikonal Expansions and the Abrasion-Ablation Model

### 2.1. Brief Overview

The investigation of high energy, heavy ion collisions has appeared in many studies [23],[24],[25],[26],[6],[19]. The development and use of the cloud chamber and nuclear emulsion began to reveal the details of high energy interactions after the discovery of cosmic rays through ionization phenomena [1]. In one of the earliest studies of high energy interactions, Serber suggested that the fast particles produced in high-energy proton and neutron reactions are the result of direct knockouts in the scattering process with individual nuclear constituents [23]. He developed a two step model suggesting the evaporation decay of residual nuclei following the direct knock out process. Goldberger later implemented the first step of the Serber model using semi classical methods and Monte Carlo techniques [24]. A corresponding quantum mechanical model was then developed by Chew in his impulse approximation [27]. Watson later derived a complete quantum mechanical formulation of the first step in the Serber model in terms of a multiple scattering series, where the impulse approximation from Chew was the first term in the series [28]. The Watson multiple scattering series rearranges the Born series, which is expressed in terms of the nucleon-nucleon potential as the two body amplitude for the scattering of a projectile nucleon off the target nucleon. The Watson series is an infinite series as it allows for re-scattering off the target constituents. Glauber later presented a great simplification to the quantum theory with the introduction of Eikonal expansions [29], which led to a successful yet simple derivation of a multiple scattering series in terms of Eikonal expansions by Franco [30]. The work used an empirical optical limit approach that depends on fluctuations and correlations of the individual nucleons. The Glauber multiple scattering series has also been extensively

studied with various extensions to the optical potential method with corrections and correlations to usual optical limit approach [31],[32],[30],[33]. A formal relation between the Watson multiple scattering series and the Glauber multiple-scattering was formulated by Remler [34] and has been presented in various other studies [35]. Glauber multiple scattering theory, based on Eikonal approximations, is one of the most successful theories in describing high energy scattering. Glauber in his work noted the advantages of a straight line path parallel to the average momentum, and thus obtained a Fourier-Bessel representation of the scattering amplitude. Blankenbecler and Goldberger later showed that the Fourier-Bessel representation is very handy as it can be justified for all scattering angles on general grounds of analyticity in momentum transfer and yields a general means for calculating cross sections from complex scattering problems [36]. A generalized formulation of elastic scattering amplitudes at small scattering angles for composite particles was later developed by Czyz and Maximon [31]. This work involved calculation of elastic scattering using matter densities of the composite units. The new formulation when compared to measured data showed the need of a more refined version of the multiple scattering approach to account for the scattering at larger angles. Another study by Harrington indicated that the cancellation of off-shell corrections by the higher order terms in the multiple-scattering expansion is necessary for the validity of the Glauber theory in high-energy small-angle optical potential method with two body interactions. He demonstrated that the cancellations can be obtained, and also formulated expressions for off-shell two particle  $t$ -matrices, the Green's function and the time dependent operator using Eikonal approximations [37]. Similar work was also presented by Osborn where he derived the Glauber theory without the Eikonal approximation [38]. To tackle the limitations resulting from the lack of the additional

correlation terms for treating the spreading of the center-of-mass wave function and the elastic scattering divergence of momentum transfer as nuclear mass becomes larger, Franco and Tekou developed a more general approach [39]. In a subsequent study, using the previously derived expressions Franco developed the numerical analysis for any nucleon in projectile or target to undergo multiple-scattering collisions. This approach is known as the optical phase shift potential, and is extensively used in predicting total and fragmentation cross-sections for nucleus-nucleus potentials [25].

The studies discussed above mostly used the corrections and extensions of the optical model to develop optical phase shift approach and applied them to Glauber multiple scattering theory. Another method developed and studied during that period was based on an impulse approximation approach [40],[26],[41],[42],[28]. The impulse approximation is understood using the fundamental assumptions that there is only a single interaction of incident particle with target nuclei at a time, and the amplitude of the incident wave stays almost same while the binding force during strong collision phase is negligible. Using these assumptions, an explicit formula for double scattering process based on the impulse approximation was presented [40]. The treatments described in these studies however were too complicated to use to describe a systematic multiple scattering problem and derive the optical models. Thus, Watson introduced an approximation based on separation of the coherent and incoherent effects in the solution to the Schrodinger equation with the fundamental assumption of large number of scattering nucleons [28]. Watson, however, noted the difficulty faced by the model is describing nucleon-nucleon interactions due to lack of detailed knowledge of two nucleon interaction process at the time.

Detailed studies of both experimental and the theoretical expressions for such nucleon-nucleon scattering amplitudes at high energies were published [43],[44]. Works by Bethe [45] and Kerman et al. [46] demonstrated success in using these nucleon-nucleon scattering amplitude expressions and derived the optical potential model based on the nucleon-nucleon transition amplitude. Later, a study by Feshbach and Hufner [47] derived the relation between the generalized semi-classical coupled solutions using the optical potential scattering and the Glauber multiple scattering series. The authors also reported that the work by Kerman et al. contains a highly complicated phase due to its dependency on dynamic structures of both projectile and target nuclei [47]. Studies published by Wilson later showed a simple but precise form of two body elastic double scattering amplitude including both the projectile and target recoil evaluated explicitly within the context of a Gaussian model [48]. Wilson also extended the expression for the optical potential operator and evaluated the new multiple scattering series for composite systems [12]. Wilson and Townsend later showed that this new optical model gave better convergence at large momentum transfers, and yielded more precise predictions for high-energy heavy-ion scattering compared to the classical model [49]. The calculations performed by Wilson [48],[12] were very successful at describing the measured angular distributions of cross section and polarization for measurements for 146 MeV protons done by Postma and Wilson [50]. These studies provided great success to applying multiple scattering theory to the three body nuclear problem.

Though the application of Glauber Model and its different variants have been used to study high energy scattering with reasonable success, the accuracy of such models for studying these



reactions came into question for the basic reasons that conservation of energy is ignored in the Glauber model, and also for the questionable validity of small angle approximations for reactions with three or more particles in final state [16]. Unlike production of heavy ion fragments, where the forward angle strictly dominates and a small angle approximation can be applied. For the systems with nucleons and light ion production, such an assumption may not provide accurate results. Hence, there have been several attempts to derive an Eikonal approximation that extends its angular range of validity. Theoretically, the number of possible variants of the Eikonal approximation is unlimited. For the non-forward scattering, the set of rays which represent the Eikonal approximation to the scattering wave function can be imagined to propagate through the interaction in as many ways as possible, each leading to a new variant of the approximation [19],[51]. Glauber, in his scattering model, basically obtained a Fourier-Bessel representation of the scattering amplitude and showed that the average-momentum directional approach used in his formulation can be obtained by replacing the Legendre polynomials with zeroth order Bessel functions  $J_0(qb)$ , where the momentum transfer  $q$  is expressed in terms of the incident momentum  $k$  and the scattering angle  $\theta$ , as  $q = 2k \sin \theta / 2$ . The impact parameter  $b$  is given by  $b = (l + 1/2) / k$ , where  $l$  is the angular momentum [19],[6]. Although this assumption eliminates the assumptions based on ray paths, a small angle approximation still remains as there are terms that are ignored because they are small at small scattering angles. Other studies have shown that for all physical angles,  $0 \leq \theta \leq \pi$ , an exact Fourier-Bessel representation can be obtained, given that the scattering amplitude is zero for angles beyond the physical range [52],[53]. However, Wallace [19] states that this assumption is too restrictive as it destroys the analyticity in the momentum transfer. Baker has derived the Eikonal approximation to the

potential scattering to the second order using the same assumptions and restrictions based on the model introduced by Glauber, except that the derivation is carried out one order further [54]. Other studies by Schiff [55],[56] and Ross [57] have developed a formalism for the Eikonal approximation for moderately large angles. However, this method is restrictive in its approach. Another study by Sarkar [58] develops the higher order terms in the Eikonal expansion for the potential scattering, which itself is an extension to work by Wallace [19]. In a series of works, Wallace has derived systematic corrections to the Eikonal phase by direct conversion of partial wave sums to the Fourier-Bessel integrals based on the Legendre Polynomials, and by thus deriving a infinite series where the leading term in phase shift operator is same as the Glauber model and higher order terms are the corrections to the phase shift operator [51],[19],[59]. This expansion is exact in the sense that no small angle approximation is made. This Eikonal expansion for the potential scattering was presented in compact representation by Waxman et al. [20] and has been studied for various potentials by Carstoiu et al. [18]. This work uses the correction terms to the Eikonal expansions derived by Wallace, and further presented by Waxman et al., to derive correction terms to the phase shift operator used in the development of an abrasion-ablation model.

## **2.2. Abrasion-Ablation Model**

The abrasion-ablation model has been developed in two different ways using a classical geometrical overlap model and using expressions based on Glauber multiple scattering theory [7],[11],[60],[8]. The classical overlap model uses a simple concept where the colliding nuclei are treated as spheres with uniform densities, sharp surfaces, and straight-line trajectories

[13],[61]. The number of abraded nucleons is related to overlapping volume of the nuclei, which are defined using the liquid drop model. The cross sections of abraded nuclei in this model are thus given by [7], [11]:

$$\sigma_{abr}(A_{pF}) = \pi[b(A_{pF} + 0.5)^2 - b(A_{pF} - 0.5)^2] \quad (2.1)$$

where  $b$  is the abrasion impact parameter and  $A_{pF}$  is the prefragment mass number. Here  $A_{pF} = A_p - n$ , with  $A_p$  being the projectile mass number and  $n$  the number of abraded nucleons. The geometric abrasion model assumes that there is no energy dependence in any variable and no nuclear surface diffusivity [13]. The second model, based on Glauber multiple-scattering, uses a quantum mechanical formulation based on optical limit approximation to the nucleus-nucleus multiple scattering series [10]. This model is energy dependent, uses realistic nuclear density distributions and includes the effects of finite nuclear force effects for a nucleon-nucleon interaction [1],[62]. For this work, we will use the second model based on Glauber multiple scattering theory. The abrasion formalism, based on a multiple scattering series, treats abrasion as an inelastic process and develops approximations including the optical phase shift model. The frictional spectator interactions (FSI) effects were also included in the formalism to improve the calculations [63]. The FSI effects are caused when a participant nucleon scatters through the remaining fragment matter of spectator depositing additional energy before it leaves the nucleus. The ablation part of the model is based on an evaporation model, where the statistical probability of a particle decaying off the prefragment is given as a competing process between all possible emissions [4],[5],[64]. The abrasion-ablation model was later extended to the evaluation of neutron momentum distributions by Cucinotta et al. [4],[5].

### 2.2.1. Abrasion Formalism

From Bleszynski and Sander [60], the cross section for abrading  $n$  projectile nucleons is given by

$$\sigma_n = \binom{A_p}{n} 2\pi \int \left[1 - P(\vec{b})\right]^n P(\vec{b})^{A_F} b db \quad (2.2)$$

where  $\binom{A_p}{n}$  is the binomial coefficient reflecting the number of possible combinations of  $n$  nucleons taken from an ensemble of  $A_p$  identical nucleons and  $A_F = A_p - n$ . With respect to the abrasion cross section, the total absorption cross section

$$\sigma_{abs} = 2\pi \int \left[1 - P(\vec{b})\right]^{A_p} b db \quad (2.3)$$

is obtained by summing over all values of  $n$ ,

$$\sigma_{abs} = \sum_{n=1}^{A_p} \sigma_n \quad (2.4)$$

In the above equations (2.2) and (2.3)  $P(\vec{b})$  is the nucleon non-removal probability as a function of impact parameter  $b$ , hence  $1 - P(\vec{b})$  is the nucleon removal probability.

The total absorption cross section in the optical potential model can also be represented using the Eikonal approximation as

$$\sigma_{abs} = 2\pi \int \left\{ 1 - \exp \left[ -2 \operatorname{Im} \chi(\vec{b}) \right] \right\} b db \quad (2.5)$$

where the Eikonal phase function  $\chi(\vec{b})$  in the Glauber model [6] is given as

$$\chi(\vec{b}) = -\frac{1}{\hbar v} \int_{-\infty}^{\infty} V(\vec{r}) dz \quad (2.6)$$

with  $V(\vec{r})$  being the optical potential and  $v$  being the relative velocity of the incoming particle momentum, in the  $z$  direction.

From equations (2.3) and (2.5) it can be implied that [14]

$$P(\vec{b})^{A_p} = \exp \left[ -2 \operatorname{Im} \chi(\vec{b}) \right] \quad (2.7)$$

And thus

$$P(\vec{b}) = \exp \left[ \frac{-2 \operatorname{Im} \chi(\vec{b})}{A_p} \right] \quad (2.8)$$

Finally, substituting equation (2.7) and (2.8) into equation (2.2) gives the abrasion cross section in terms of phase functions as

$$\sigma_n = \binom{A_p}{n} 2\pi \int \left[ 1 - \exp \left[ \frac{-2 \operatorname{Im} \chi(\vec{b})}{A_p} \right] \right]^n \left( \exp \left[ \frac{-2 \operatorname{Im} \chi(\vec{b})}{A_p} \right] \right)^{A_p} b db \quad (2.9)$$

Equation (2.9) treats all nucleons as identical objects. To differentiate between the protons and neutrons, the above equation can be replaced by [10]

$$\sigma_{nz} = \binom{N_p}{n} \binom{Z_p}{z} 2\pi \int \left[ 1 - \exp \left[ \frac{-2 \operatorname{Im} \chi(\vec{b})}{A_p} \right] \right]^{n+z} \left( \exp \left[ \frac{-2 \operatorname{Im} \chi(\vec{b})}{A_p} \right] \right)^{A_p - n - z} b db \quad (2.10)$$

where  $\sigma_{nz}$  is the cross section for abrading  $n$  out of  $N_p$  neutrons and  $z$  out of  $Z_p$  protons. It is implicitly assumed in the above expression that the neutron and proton distributions in the projectile are completely uncorrelated. This oversimplification of the complex nature of the nucleon correlations helps us obtain analytical simplicity as a convenient starting point for the cross section formulation [1].

Since we are interested in the momentum distributions of the projectile fragments, the nucleon momentum distributions in the rest frame of the projectile are given from work by Haneishi and Fujita as [65]

$$n(\mathbf{p}) = n_0 \sum_{i=1}^3 C_i \exp \left( \frac{-p_i^2}{2 p_i^2} \right) \quad (2.11)$$

where  $p_n$  is the momentum of the nucleon in the projectile rest frame,  $p_i$  is the momentum width parameter given in terms of the Fermi momentum  $k_F$  and  $n_0$  is the normalization constant. The normalization constant  $n_0$  can be given as:

$$n_0 = \frac{1}{\left\{ \left( C_1 2\pi p_1^2 \right)^{3/2} + \left( C_2 2\pi p_2^2 \right)^{3/2} + \left( C_3 2\pi p_3^2 \right)^{3/2} \right\}} \quad (2.12)$$

The values for parameters  $C_i$  and  $p_i$  are taken from Cucinotta et al. [4] and are listed below in Table 1.

*Table 1: Parameters for the Momentum Distribution Model*

$i$	$C_i$	$p_i \text{ MeV} / c$
1	1	$k_F \sqrt{(2/5)}$
2	0.03	$k_F \sqrt{(6/5)}$
3	0.0008	500

The values of the Fermi momentum,  $k_F$ , are taken from the experimental values given in Cucinotta et al. [4] for various nuclei, and for the purpose of this work have been extended to other nuclei using a simple logarithmic distribution

$$k_F \text{ (MeV} / c) = 26 \log(A_p) + 129 \quad (2.13)$$

where  $A_p$  is the mass number of the nucleus.

In the rest frame of projectile, integrating over all solid angle and momentum distribution should produce the total reaction cross section for fragment of interest. Thus equation (2.11) can be expressed as

$$\frac{d^3\sigma}{dp_n^3} = \sigma_R \left( n_0 \sum_{i=1}^3 C_i \exp\left(\frac{-p_n^2}{2p_i^2}\right) \right) \quad (2.14)$$

and the nucleon momentum distribution for abrading the sum of 1 through  $n$  projectile nucleons is given using equation (2.14) as

$$\left( \frac{d^3\sigma}{dp_n^3} \right)_{abr} = \left( \sum_1^n \sigma_n \right) \left( n_0 \sum_{i=1}^3 C_i \exp\left(\frac{-p_n^2}{2p_i^2}\right) \right) \quad (2.15)$$

where  $\sum_1^n \sigma_n$  is the sum of total abrasion cross section for abrading up to  $n$  projectile nucleons.

From the momentum distribution above, we can get the Lorentz invariant cross-section as

$$\sigma_{inv}^{abr} = E_p \left( \frac{d^3\sigma}{dp_n^3} \right)_{abr} \quad (2.16)$$

The invariant in equation (2.16) can be related to the double differential cross section as



$$\left( \frac{d^2\sigma}{dE_L d\Omega_L} \right)_{abr} = p_L E_p \left( \frac{d^3\sigma}{dp_n^3} \right)_{abr} \quad (2.17)$$

where  $p_L$  and  $d\Omega_L$  are momentum and direction of the outgoing nucleon in the laboratory frame and  $E_p$  is the kinetic energy in the projectile rest frame. It is important to note here that evaluation of nucleon differential cross section and its momentum distribution occurs in the rest frame of the projectile. However, the differential cross sections are required to be evaluated in the laboratory frame. A brief discussion of frame transformations from rest frame of projectile to laboratory frame is given in Chapter 4.5.

### 2.2.2. Ablation Formalism

After the abrasion process, the prefragment nuclei are in the excited state. In the ablation stage, these prefragment give up their excess energies by evaporating nucleons, light ion clusters and gamma rays to decay into the ground state [10],[64]. The ablation process is quite complicated and its calculation requires knowledge of the prefragment thermalization, temperature dependence of the fragments and also the physics behind the evaporation model. In this work, the ablation model has been derived using previous works by Cucinotta et al. [4],[5] and, Kikuchi & Kawai [64]. In the ablation stage, the rate of prefragment decay by the excited nuclei is directly related to the strength of the excitation energies. The nucleon emission spectrum from the ablation process is thus given by Weisskopf-Ewing statistical decay model [17]. The probability function for the emission of a particle is given by the statistical decay model as

$$P(\varepsilon_i)d\varepsilon_i = \frac{g_i m_i}{\pi^2 \hbar^3} \sigma_{CN}^i \frac{w_i}{w_c} \varepsilon_i d\varepsilon_i \quad (2.18)$$

where  $P(\varepsilon_i)d\varepsilon_i$  is the probability per unit time of emission of a particle  $i$  with kinetic energy between  $\varepsilon_i$  and  $\varepsilon_i + d\varepsilon_i$ ,  $\sigma_{CN}^i$  is the cross section for formation of a compound nucleus in the inverse process,  $g_i$  is the statistical weight,  $w_c$  and  $w_i$  are the level densities of initial and final nuclei respectively, and are functions of mass charge and excitation energy [64]. From the works by Cucinotta et al.[4],[5], with the assumption of an isotropic emission spectrum for nucleon and substantially large prefragment mass, the probability function can be expressed as

$$P_i(j, E_i) = \frac{2\mu_i g_i E_i \sigma_{CN} w_0 (E_j^* - E_i)}{(E_i^* - S_j)} \int_0^{(E_i^* - S_j)} P_l(j, E) dE \quad (2.19)$$

where  $\mu_i$  is the nucleon reduced mass. The secondary nucleon momentum distribution for the ablation process can be expressed in terms of the probability function as

$$\left( \frac{d^3 \sigma}{dp^3} \right)_{abl} = \sum_j \sigma_{abr} (A_j, Z_j, E_j^*) P_i(j, \mathbf{k}) \quad (2.20)$$

with total abrasion cross section being derived from equation (2.10), and  $P_i(j, \mathbf{k})$  being the probability that a prefragment labeled  $j$ , with mass number  $A_j$ , charge number  $Z_j$ , and

excitation energy  $E_j^*$ , emits a particle of momentum  $\mathbf{k}$ .

The values for  $P_i(j, \mathbf{k})$  used in this work are calculated using UBERNSPEC code [66],[2].

Finally,

$$\left(\frac{d^3\sigma}{dp^3}\right)_{total} = \left(\frac{d^3\sigma}{dp^3}\right)_{abr} + \left(\frac{d^3\sigma}{dp^3}\right)_{abl} \quad (2.21)$$

It must be noted that the calculations for  $\left(\frac{d^3\sigma}{dp^3}\right)_{abl}$  are carried out in the projectile rest frame.

They can be formed into Lorentz invariant cross sections and double differential cross sections in the laboratory frame by using the same treatment as given in equations (2.16) and (2.17).

### 3. Eikonal Corrections to the Phase Function

#### 3.1. Formulation of the Scattering Amplitude

The scattering problem in quantum mechanics can be formulated by solution of the Schrödinger Equation.

$$\left[ -\frac{\hbar^2}{2m} \nabla^2 + V(\vec{r}, t) \right] \psi'(\vec{r}, t) = i\hbar \frac{\partial}{\partial t} \psi'(\vec{r}, t) \quad (3.1)$$

which describes a particle of mass  $m$ , with the potential  $V(\vec{r}, t)$ , governing the evolution of wave function  $\psi'(\vec{r}, t)$  [67]. For a typical scattering problem, the boundary conditions are imposed such that the wave function  $\psi'(\vec{r}, t)$  must have a component involving an incident plane wave with momentum  $k$  moving in the positive  $z$  direction, and another component that involves a spherical outgoing wave. The energy of the incident plane wave is given by  $E = \frac{\hbar^2 k^2}{2m}$

For the case where the initial beam can be defined by a state of definite energy, and the potential does not explicitly depend on time, we can express the wave function using separation of variables as

$$\psi'(\vec{r}, t) = e^{-\frac{i}{\hbar} E t} \psi(\vec{r}) \quad (3.2)$$

where  $\psi(\vec{r})$  satisfies the differential equation

$$\left[ \nabla^2 + k^2 \right] \psi(\vec{r}) = U(\vec{r}) \psi(\vec{r}) \quad (3.3)$$

with  $U(\vec{r}) = \frac{2m}{\hbar^2} V(\vec{r})$ , and the boundary conditions on  $\psi(\vec{r})$  dictated by the boundary conditions on  $\psi'(\vec{r}, t)$ .

### 3.1.1. The Method of Partial Waves

For the case of a spherically symmetric potential, we can write the solution to equation (3.3), in terms of the partial wave expression as [68], [69]

$$\psi(\vec{r}) = \sum_{l=0}^{\infty} (2l+1) i^l R_l(r) P_l(\cos \theta) \quad (3.4)$$

where  $P_l(\cos \theta)$  is the  $l^{\text{th}}$  Legendre polynomial, expressed as

$$P_l(\cos \theta) = \frac{(-1)^l}{2^l l!} \frac{d^l (1 - \cos^2 \theta)}{d(\cos \theta)^l} \quad (3.5)$$

and  $R_l(r)$  is the solution to the radial differential equation

$$\frac{d^2 R_l(r)}{dr^2} + \frac{2}{r} \frac{dR_l(r)}{dr} + \left[ k^2 - \frac{l(l+1)}{r^2} - U(r) \right] R_l(r) = 0 \quad (3.6)$$

For the potentials that fall off faster than  $1/r^2$ , the solution to equation (3.5) as  $r \rightarrow \infty$  can be given as

$$\lim_{r \rightarrow \infty} R_l(r) = C_l \left[ \cos \delta_l \left( \lim_{r \rightarrow \infty} j_l(kr) \right) - \sin \delta_l \left( \lim_{r \rightarrow \infty} \eta_l(kr) \right) \right] \quad (3.7)$$

where  $\delta_l$  is the phase shift.

Upon substituting equation (3.7) into (3.1), and using the identity

$$e^{ikr \cos \theta} = \sum_{l=0}^{\infty} (2l+1) i^l j_l(kr) P_l(\cos \theta) \quad (3.8)$$

the scattering amplitude can be written in terms of the partial wave sum as

$$f(\theta, \phi) \frac{e^{ikr}}{r} = \sum_{l=0}^{\infty} (2l+1) i^l P_l(\cos \theta) \left[ (C_l \cos \delta_l - 1) \left( \lim_{r \rightarrow \infty} j_l(kr) \right) - C_l \sin \delta_l \left( \lim_{r \rightarrow \infty} \eta_l(kr) \right) \right] \quad (3.9)$$

Now, applying

$$\lim_{r \rightarrow \infty} j_l(kr) = \frac{1}{2kr} \left[ i^{-(l+1)} e^{ikr} + i^{+(l+1)} e^{-ikr} \right] \quad (3.10)$$

$$\lim_{r \rightarrow \infty} \eta_l(kr) = \frac{1}{2kr} \left[ i^{-(l+2)} e^{ikr} + i^{+(l)} e^{-ikr} \right] \quad (3.11)$$

in equation (3.9) and equating the coefficients of  $e^{ikr}$  and  $e^{-ikr}$ , we get

$$f(\theta) = \frac{1}{2k} \sum_{l=0}^{\infty} (2l+1) i^l P_l(\cos \theta) i^{-(l+1)} [C_l e^{+i\delta_l} - 1] \quad (3.12)$$

and

$$0 = \frac{1}{2k} \sum_{l=0}^{\infty} (2l+1) i^l P_l(\cos \theta) i^{+(l+1)} [C_l e^{-i\delta_l} - 1] \quad (3.13)$$

Equation (3.13) reduces to  $C_l = e^{+i\delta_l}$ , and thus equation (3.11) can be expressed as

$$f(\theta) = \frac{1}{2ik} \sum_{l=0}^{\infty} (2l+1) P_l(\cos \theta) [e^{i\delta_l} - 1] \quad (3.14)$$

Equation (3.13) is the standard expression for the scattering amplitude in terms of sum of the partial waves, with  $\delta_l$  being defined as the phase shift in terms of the Bessel functions.

### 3.1.2. Eikonal Approximation

The scattering amplitude can be also expressed in terms of the Eikonal approximations in the Glauber multiple scattering theory. We will now derive the scattering amplitude in terms of the Eikonal approximations closely following the work presented by Glauber [6] and its derivations given by Sakurai [68].

The basic assumption here is that the potential  $V(\vec{r})$  varies very slowly over a distance of order of the wavelength. The potential itself does not have to be weak as long as it satisfies that the incident energy  $E \gg |V(\vec{r})|$ . Using the above mentioned assumptions, we can now express the wave function in terms of the semi-classical solution as

$$\psi(\vec{r}) \propto e^{\frac{iS(\vec{r})}{\hbar}} \quad (3.15)$$

where the interpretation of  $S(\vec{x})$  can be obtained from the Hamilton-Jacobi equation

$$\frac{(\nabla S(\vec{r}))^2}{2m} + V = E = \frac{\hbar^2 k^2}{2m} \quad (3.16)$$

With the further assumption that the trajectory of the scattered wave is a straight line path, which should be a satisfactory assumption for small angles at high energy, we can solve equation (3.16) for  $S(\vec{x})$  by integration along the  $z$ -direction, which is assumed to be the direction of the straight line trajectory. Thus

$$\frac{S(\vec{r})}{\hbar} = \int_{-\infty}^z \left[ k^2 - \frac{2m}{\hbar^2} V(\sqrt{b^2 + z'^2}) \right]^{\frac{1}{2}} dz' + C \quad (3.17)$$

Here, the constant  $C$  is to be chosen in such a way that  $\frac{S(\vec{r})}{\hbar} \rightarrow kz$  as  $V \rightarrow 0$ .



Equation (3.17) can now be written as

$$\frac{S(\vec{r})}{\hbar} = kz + \int_{-\infty}^z \left[ k^2 - \frac{2m}{\hbar^2} V(\sqrt{b^2 + z'^2}) - k \right]^{\frac{1}{2}} dz' \quad (3.18)$$

For  $E \ll |V(\vec{r})|$ , we can use the approximation

$$\left[ k^2 - \frac{2m}{\hbar^2} V(\sqrt{b^2 + z'^2}) \right]^{\frac{1}{2}} \approx k - \frac{mV(\sqrt{b^2 + z'^2})}{\hbar^2 k} \quad (3.19)$$

which allows for equation (3.18) to be written as

$$\frac{S(\vec{r})}{\hbar} = kz - \frac{m}{\hbar^2 k} \int_{-\infty}^z V(\sqrt{b^2 + z'^2}) dz' \quad (3.20)$$

From equation (3.20), we can now rewrite equation (3.15) as

$$\psi(\vec{r}) \approx \frac{1}{(2\pi)^{\frac{3}{2}}} e^{ikz} e^{-\frac{im}{\hbar^2 k} \int_{-\infty}^z V(\sqrt{b^2 + z'^2}) dz'} \quad (3.21)$$

The scattering amplitude has its usual representation

$$f(\vec{k}', \vec{k}) = -\frac{1}{4\pi} \int d^3 r' e^{-i\vec{k}' \cdot \vec{r}'} V(\vec{r}') \psi(\vec{r}') \quad (3.22)$$

Equation (3.22) can be expressed by using equation (3.21) as

$$f(\vec{k}', \vec{k}) = -\frac{1}{4\pi} \frac{2m}{\hbar^2} \int d^3 r' e^{-i\vec{k}' \cdot \vec{r}'} V\left(\sqrt{b^2 + z'^2}\right) e^{i\vec{k} \cdot \vec{r}'} e^{-\frac{im}{\hbar^2 k} \int_{-\infty}^{z'} V\left(\sqrt{b^2 + z''^2}\right) dz''} \quad (3.23)$$

The  $d^3 r'$  integration can be performed using the cylindrical coordinates, where  $d^3 r' = b db d\phi dz'$ .

Also using  $\vec{k} \perp \vec{b}$  and  $(\vec{k} - \vec{k}') \cdot \hat{z} \approx 0(\theta^2)$ , which can be ignored for small scattering angles,

we can approximate

$$(\vec{k} - \vec{k}') \cdot \vec{r}' = (\vec{k} - \vec{k}') \cdot (\vec{b} + z' \hat{z}) \approx -\vec{k}' \cdot \vec{b} \quad (3.24)$$

The variables listed in Equation (3.24) are illustrated in Figure 2.

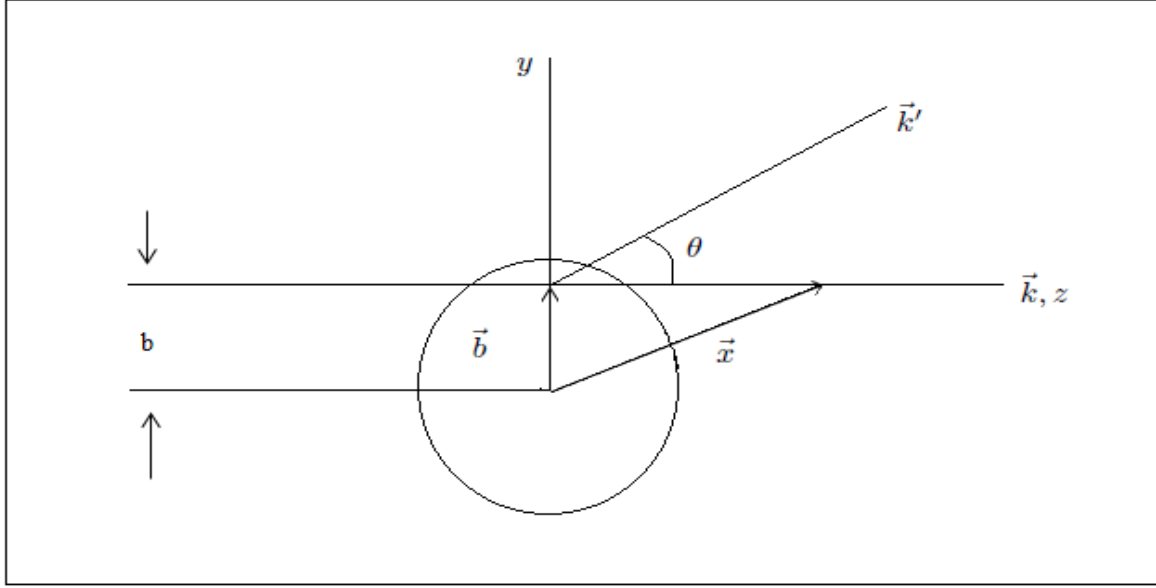


**Figure 2:** Schematic diagram of Eikonal approximation scattering with straight line trajectory.

For large incoming momentum and small scattering angles, we can choose scattering to be in the  $xz$ -plane and use the approximation that

$$\vec{k}' \cdot \vec{b} = (k \sin \theta \cdot \hat{r} + k \cos \theta \cdot \hat{z}) \cdot (b \cos \phi \cdot \hat{r} + b \sin \phi \cdot \hat{y}) \approx kb \theta \cos \phi \quad (3.25)$$

Thus, the expression for scattering amplitude in equation (3.23) becomes

$$f(\vec{k}', \vec{k}) = -\frac{1}{4\pi} \frac{2m}{\hbar^2} \int_0^\infty b \, db \int_0^{2\pi} d\phi \, e^{-ikb\theta \cos \phi} \int_{-\infty}^\infty dz \, V e^{-\frac{im}{\hbar^2 k} \int_{-\infty}^{z'} V dz'} \quad (3.26)$$

The second integration in the above equation with respect to  $\phi$  can be given as

$$\int_0^{2\pi} d\phi e^{-ikb\theta \cos \phi} = 2\pi J_0(kb\theta) \quad (3.27)$$

and the last part of the integral can be expressed as

$$\int_{-\infty}^{\infty} dz V e^{-\frac{im}{\hbar^2 k} \int_{-\infty}^{z'} V dz'} = -\frac{i\hbar^2 k}{m} e^{-\frac{im}{\hbar^2 k} \int_{-\infty}^{z'} V dz'} \Bigg|_{z=-\infty}^{z=\infty} \quad (3.28)$$

where the contributions from  $z = -\infty$  drop off and we can finally write the scattering amplitude as

$$f(\theta) = f(\vec{k}', \vec{k}) = ik \int_0^{\infty} J_0(qb) (1 - \exp(i\chi(b))) b db \quad (3.29)$$

where

$$\chi(\vec{b}) = -\frac{m}{2\hbar^2 k} \int_{-\infty}^{\infty} V(\vec{r}) dz \quad (3.30)$$

and the wave number  $k$  is related to the scattering angle  $\theta$  and the momentum transfer  $q$  by

$q = 2k \sin\left(\frac{\theta}{2}\right)$ , and  $J_0(qb)$  gives the zeroth order Bessel functions.

Recall that  $m$  is the nucleon mass, given in terms of  $MeV/c^2$ ,  $\hbar$  is the reduced Planck's constant, given as  $6.58212 \times 10^{-22} MeV s$  and,  $c = 2.99792 \times 10^{10} cm/s$  is the speed of light in vacuum.

It is more convenient to represent the nucleon mass  $m$  in terms of  $MeV$ . Hence, by the use of natural units, we note that

$$1 cm = \frac{1 cm}{\hbar c} \approx 5.1 \times 10^{10} MeV^{-1} \quad (3.31)$$

and

$$\hbar^2 c^2 = (6.58212 \times 10^{-22} MeV s)^2 \times (2.99792 \times 10^{10} \times 5.1 \times 10^{10} MeV^{-1} s^{-1})^2 \approx 1 \quad (3.32)$$

Thus, by the use of equation (3.32), we can now write the phase shift in equation (3.30) as

$$\chi(\vec{b}) = -\frac{m}{2k} \int_{-\infty}^{\infty} V(\vec{r}) dz \quad (3.33)$$

Equation (3.33) is the standard form of the impact parameter representation of the phase shift operator, developed by Glauber [6].

### 3.2. Derivation of Correction Terms to the Scattering Amplitude

We shall now consider Wallace's approach to derive the higher order terms for the correction of small angle approximation in the impact parameter representation of the scattering amplitude [19],[51]. This work closely follows the study of Wallace's method by Waxman et al. [20].

Wallace [19],[59] derives a relation between the two different representations of the scattering amplitudes given in equations (3.14) and (3.29) using an expansion of the Legendre Polynomials in terms of zeroth order Bessel functions as

$$P_l(z) = \sum_{m=0}^{\infty} \frac{1}{(2m)!} \left( \frac{\partial}{\partial l} \right)^{2m} b_m \left( \frac{1}{4} \frac{\partial}{\partial l} (2l+1) \right) J_0 \left\{ (2l+1) \left( \frac{(1-z)}{2} \right)^{\frac{1}{2}} \right\} \quad (3.34)$$

where  $b_m(x)$  are generalized Bernoulli polynomials with  $b_0(x)=1$  and  $b_1(x)=-x/6$ . A complete list of generalized Bernoulli polynomials from [19] is given in Appendix I.

The Eikonal phase factor  $e^{i\chi(b)}$  in equation (3.29) can now be related to phase shifts  $e^{i\delta_l}$ , in equation (3.14), in terms of Bessel functions as

$$e^{i\chi(b)} = \frac{1}{b} \sum_{m=0}^{\infty} \frac{1}{(2m)!} b_m \left( -\frac{1}{2} b \frac{d}{db} \right) \left( \frac{1}{k} \frac{d}{db} \right)^{2m} b e^{i\delta_l} \quad (3.35)$$

For the case of well behaved potentials, which allow the phase shifts to be smoothly interpolated for all real values of angular momentum  $l$ , the equation (3.35) can be written as

$$e^{i\chi(b)} = (2l+1)^{-1} W(2l+1) e^{2i\delta_l} \quad (3.36)$$

where the operator  $W$  has been expressed by Waxman et al. [20] as

$$W = \sum_{m=0}^{\infty} \frac{1}{(2m)!} b_m \left[ -\frac{1}{4} (2l+1) \frac{\partial}{\partial l} \right] \left( \frac{\partial}{\partial l} \right)^{2m} \quad (3.37)$$

with the impact parameter having its usual definition  $kb = l + \frac{1}{2}$ .

The series in equation (3.35) converges rapidly for the phase shifts varying regularly with  $l$ .

Thus a good approximation at high energies can be given by

$$e^{i\chi(b)} \approx \left[ 1 + \frac{1}{48} \left( \frac{\partial}{\partial l} \right)^3 (2l+1) \right] e^{2i\delta_l} \quad (3.38)$$

Wallace [19], at this point, applies the Wentzel-Kramers-Brillouin (WKB) approximation and its generalization to the phase shifts. The WKB approximation for the phase shifts can be given by

$$\delta^{WKB}(l) = \int_{r_0}^{\Lambda} dr \left[ k^2 - \frac{\left(l + \frac{1}{2}\right)^2}{r^2} - 2mV(\vec{r}) \right]^{\frac{1}{2}} - \int_{\frac{l+\frac{1}{2}}{k}}^{\Lambda} dr \left[ k^2 - \frac{\left(l + \frac{1}{2}\right)^2}{r^2} \right]^{\frac{1}{2}} \quad (3.39)$$

where  $r_0$  is the turning point for a particle of mass  $m$  and a potential field  $V(\vec{r})$ , with limit

$\Lambda \rightarrow \infty$ .

Equation (3.39) can be expressed in terms of expansion of a power series in the strength of the potential as

$$\delta^{WKB}(l) = \sum_{n=0}^{\infty} \delta_n(l) \quad (3.40)$$

where

$$\delta_n(l) = -\frac{k \left(\frac{\mu}{k^2}\right)^{n+1}}{(n+1)! b^{2n}} \left[ b^2 \left( 1 + b \frac{d}{db} \right) \right]^n \int_0^{\infty} V^{n+1} \left( (b^2 + z^2)^{\frac{1}{2}} \right) dz \quad (3.41)$$

It can be shown by induction that equation (3.41) is equivalent to

$$\delta_n(l) = -\frac{(\mu)^{n+1}}{k(n+1)!} \left[ \left( \frac{b}{k} \frac{\partial}{\partial b} - \frac{\partial}{\partial k} \right) \frac{1}{k} \right]^n \int_0^{\infty} V^{n+1} \left( (b^2 + z^2)^{\frac{1}{2}} \right) dz \quad (3.42)$$

with the differentiations  $\frac{\partial}{\partial b}$  and  $\frac{\partial}{\partial k}$  being carried out at fixed  $k$  and  $b$  respectively and  $\mu$  is

the reduced mass.



Various forms of differential operator in equation (3.42) have been derived with the assumption that the potential doesn't explicitly depend on the orbital angular momentum  $l$  [20]. However, from the definition  $kb = l + \frac{1}{2}$ , it can be shown that

$$\frac{b}{k} \left[ \frac{\partial}{\partial b} \right]_k - \left[ \frac{\partial}{\partial k} \right]_b = - \left[ \frac{\partial}{\partial k} \right]_l \quad (3.43)$$

which gives us that in terms of differentiation with respect to  $k$  at fixed  $l$

$$\delta_n(l) = -\frac{1}{2} \frac{(2\mu)^{n+1}}{(n+1)!} \left[ \left( -\frac{\partial}{\partial k^2} \right)_l \right]^n \frac{1}{k} \int_0^\infty V^{n+1} \left( \left( \frac{(l + \frac{1}{2})^2}{k^2} + z^2 \right)^{\frac{1}{2}} \right) dz \quad (3.44)$$

Waxman et al. [20] show that using the expansion and integration of  $\delta_m(l)$  in terms of WKB approximation, the desired form in the equation (3.44) can be arrived, hence, concluding that equation (3.42) is valid even for the cases where the potential does depend on the orbital angular momentum.

From equation (3.42), the first two terms in the Wallace expansions can be given as

$$\delta_0(l) = -\frac{\mu}{k} \int_0^\infty V(\bar{r}) dz \quad (3.45)$$

$$\delta_1(l) = -\frac{\mu^2}{2k^3} \left[ 1 + b \frac{\partial}{\partial b} - k \frac{\partial}{\partial k} \right] \int_0^\infty V^2(\vec{r}) dz \quad (3.46)$$

Waxman et al. [20] mention that if the phase shift  $\delta_0(l)$  equation (3.45) was interpreted as half of the Eikonal phase,  $\frac{1}{2} \chi(b)$ , it would represent the Born approximation. Thus for practical applications in the high energy scattering, where the first correction term in the expansion of equation (3.42) is dominant itself, the Wallace Eikonal phase can be expressed as

$$\chi_n(b) = -\frac{(\mu)^{n+1}}{k(n+1)!} \left[ \left( \frac{b}{k} \frac{\partial}{\partial b} - \frac{\partial}{\partial k} \right) \frac{1}{k} \right]^n \int_{-\infty}^\infty V^{n+1} \left( (b^2 + z^2)^{1/2} \right) dz \quad (3.47)$$

and the total Eikonal phase, as the sum of the zeroth order term and higher correction terms, can be expressed as [18]

$$\chi(b) = \sum_n -\frac{(\mu)^{n+1}}{k(n+1)!} \left[ \left( \frac{b}{k} \frac{\partial}{\partial b} - \frac{\partial}{\partial k} \right) \frac{1}{k} \right]^n \int_{-\infty}^\infty V^{n+1}(\vec{r}) dz \quad (3.48)$$

with  $r = (b^2 + z^2)^{1/2}$ .

Note that the zeroth order term in equation (3.48) yields same result as the Glauber phase shift operator. The higher order terms are correction terms to the Eikonal phase shift, to account for the small angle approximation made in the Glauber multiple scattering theory.

One of the major concerns in the development of correction terms as an infinite series is the convergence of the series and also its validity with respect to the quantum mechanical results. Carstoiu et al. [18] studied the expansion for various realistic potentials to calculate the total and reaction cross sections and concluded that the series shows good convergence, particularly for potentials with Gaussian shapes, and also are in good agreement with the quantum mechanical results.

In this work, we have used four higher order correction terms to the Glauber Eikonal phase, developed using the above derived formalism by Wallace. The zeroth order and higher corrections terms for the series given in equation (3.48) can be shown as

$$\chi_0(b) = -\frac{\mu}{k} \int_{-\infty}^{\infty} V(\vec{r}) dz \quad (3.49)$$

$$\chi_1(b) = -\frac{\mu^2}{2k^3} \left[ 1 + b \frac{\partial}{\partial b} - k \frac{\partial}{\partial k} \right] \int_{-\infty}^{\infty} V^2(\vec{r}) dz \quad (3.50)$$

$$\chi_2(b) = -\frac{\mu^3}{6k^5} \left[ b^2 \frac{\partial^2}{\partial b^2} + 5b \frac{\partial}{\partial b} - 2bk \frac{\partial}{\partial b} \frac{\partial}{\partial k} - 3k \frac{\partial}{\partial k} + k^2 \frac{\partial^2}{\partial k^2} + 3 \right] \int_{-\infty}^{\infty} V^3(\vec{r}) dz \quad (3.51)$$

$$\chi_3(b) = -\frac{\mu^4}{27k^7} \left[ b^3 \frac{\partial^3}{\partial b^3} + 13b^2 \frac{\partial^2}{\partial b^2} + 30b \frac{\partial}{\partial b} - 3b^2k \frac{\partial^2}{\partial b^2} \frac{\partial}{\partial k} - 18bk \frac{\partial}{\partial b} \frac{\partial}{\partial k} \right. \\ \left. + 3bk^2 \frac{\partial}{\partial b} \frac{\partial^2}{\partial k^2} + 6k^2 \frac{\partial^2}{\partial k^2} - 12k \frac{\partial}{\partial k} - k^3 \frac{\partial^3}{\partial k^3} + 15 \right] \int_{-\infty}^{\infty} V^4(\vec{r}) dz \quad (3.52)$$

$$\chi_4(b) = -\frac{\mu^5}{108k^9} \left[ b^4 \frac{\partial^4}{\partial b^4} + 23b^3 \frac{\partial^3}{\partial b^3} + 147b^2 \frac{\partial^2}{\partial b^2} + 240b \frac{\partial}{\partial b} - 4b^3k \frac{\partial^3}{\partial b^3} \frac{\partial}{\partial k} \right. \\ - 55b^2k \frac{\partial^2}{\partial b^2} \frac{\partial}{\partial k} - 178bk \frac{\partial}{\partial b} \frac{\partial}{\partial k} + 6b^2k^2 \frac{\partial^2}{\partial b^2} \frac{\partial^2}{\partial k^2} + 42bk^2 \frac{\partial}{\partial b} \frac{\partial^2}{\partial k^2} \\ \left. - 4bk^3 \frac{\partial}{\partial b} \frac{\partial^3}{\partial k^3} + 42k^2 \frac{\partial^2}{\partial k^2} - 72k \frac{\partial}{\partial k} - 10k^3 \frac{\partial^3}{\partial k^3} + k^4 \frac{\partial^4}{\partial k^4} + 95 \right] \int_{-\infty}^{\infty} V^5(\vec{r}) dz \quad (3.53)$$

We will now look into the formalism for the development of the optical potential, and thus, implement the correction terms obtained here to obtain the Eikonal phase shift in terms of the optical potential.

## 4. Optical Potential Derivation

In this chapter we will consider the derivation of optical potential for the nucleus-nucleus scattering and its further approximation in the context of high energy, using the one body Schrodinger equation, by applying the closure approximation [1],[49]. The optical potential will then be calculated using the Gaussian approximations for the single particle nuclear densities, which will be further used to develop the phase shift operator and its higher order correction terms, as discussed in chapter 3.

### 4.1. Optical Model using Multiple Scattering Series

For a system with an energetic projectile nucleus with well defined momentum, colliding with a target nucleus, the Hamiltonian for the combined system of N number of nucleons interacting through two body potentials can be given by [49]

$$H = \sum_j T_j + \sum_{i < j} V_{ij} + \sum_\alpha T_\alpha + \sum_{\beta < \alpha} V_{\beta\alpha} + \sum_{\alpha j} V_{\alpha j} \quad (4.1)$$

where the Roman subscripts refer to the projectile constituent nucleons, Greek subscripts refer to the target and  $T$  is the transition operator. The transformations from free initial state to final scattered state is given using the wave operator

$$\Omega = 1 + GV\Omega \quad (4.2)$$

with interaction potential being given as

$$V = \sum_{\alpha j} V_{\alpha j} \quad (4.3)$$

and  $G$  is the complete non-interacting systems Green's function.

To find a series for the transition operator  $T$  in terms of simpler functions, it is defined for scattering of the  $\alpha$  target constituents with  $j$  projectile constituents as

$$t_{\alpha j} = V_{\alpha j} + V_{\alpha j} G t_{\alpha j} \quad (4.4)$$

and the wave operator that transforms the entering free state up to the collision of the  $\alpha$  and  $j$  constituents is given by

$$\omega_{\alpha j} = 1 + \sum_{(\beta, k) \neq (\alpha, j)} G t_{\beta k} \omega_{\beta k} \quad (4.5)$$

Following the derivations given in works by Wilson et al. [1],[49], we can now write the multiple-scattering series as

$$T = \sum_{\alpha j} t_{\alpha j} + \sum_{(\beta, k) \neq (\alpha, j)} t_{\alpha j} G t_{\beta k} + \dots \quad (4.6)$$

Equation (4.6) constitutes a formal solution to the exact scattering problem. For high energy problems, the binding effects become negligible and thus the Green's function  $G$  can be

replaced by the N-body free Green's function  $G_0$ , given in terms of the total kinetic energy and its constituent kinetic energy operator as

$$G \rightarrow G_0 \equiv \frac{1}{E - \sum_j T_j - \sum_\alpha T_\alpha} \quad (4.7)$$

The approximation in equation (4.7) essentially turns the transition amplitude  $t_{\alpha j}$  into a two body operator and thus equation (4.6) becomes a series of sequential two body operators.

Wilson et al. [49] show that the equivalent one body Schrodinger equation for the optical model can be written as

$$(\nabla^2 + k^2)\psi(\vec{\xi}_P, \vec{\xi}_T, \vec{r}) = \frac{2mA_P A_T}{N} V_{OPT}(\vec{\xi}_P, \vec{\xi}_T, \vec{x})\psi(\vec{\xi}_P, \vec{\xi}_T, \vec{r}) \quad (4.8)$$

where

$\vec{\xi}_{P,T}$  = internal projectile/target coordinates,

$\vec{r}$  = relative position of projectile in center of mass (CM) to target CM,

$m$  = nucleon mass and

$$N = A_P + A_T$$

The optical potential  $V_{OPT}(\vec{\xi}_P, \vec{\xi}_T, \vec{r})$  can be expressed in terms of the transition operator as

$$V_{OPT}(\vec{\xi}_P, \vec{\xi}_T, \vec{r}) = \sum_{\alpha j} t_{\alpha j}(\vec{r}_\alpha, \vec{r}_i) \quad (4.9)$$

Following the derivations given in works [1],[49],[61], the optical model can be defined as the approximation for the elastic scattered part of the wave function using the closure approximation as

$$(\nabla^2 + k^2)\psi(\vec{r}) = \frac{2mA_P A_T}{N} W(\vec{r})\psi(\vec{r}) \quad (4.10)$$

where

$$W(\vec{r}) = A_P A_T \int d^3 z \rho_T(\vec{z}) \int d^3 y \rho_P(\vec{x} + \vec{y} + \vec{z}) \tilde{t}(e, \vec{y}) \quad (4.11)$$

with  $\rho_T(\vec{z})$  and  $\rho_P(\vec{x} + \vec{y} + \vec{z})$  being the target and the projectile single particle nuclear densities respectively and  $\tilde{t}(e, \vec{y})$  being the nucleon-nucleon transition amplitude.

Now, letting

$$V(\vec{r}) = \frac{2mA_P A_T}{N} W(\vec{r}) \quad (4.12)$$

equation (4.10) can be re-written as

$$(\nabla^2 + k^2)\psi(\vec{r}) = V(\vec{r})\psi(\vec{r}) \quad (4.13)$$

and



$$V(\vec{r}) = \frac{2mA_p^2 A_r^2}{N} \int d^3z \rho_T(\vec{z}) \int d^3y \rho_p(\vec{x} + \vec{y} + \vec{z}) \tilde{t}(e, \vec{y}) \quad (4.14)$$

Calculation of optical potential given in equation (4.14) requires knowledge of the projectile and the target nuclear densities, and the two body transition amplitude. We will first begin by developing a parameterization of the transition amplitude. Calculation of the nuclear densities will follow in the following sub-section.

The two particle transition amplitude is expressed as [1],[49]

$$\tilde{t}(e, \vec{y}) = -\sqrt{\frac{e}{m}} \sigma(e) [\alpha(e) + i] (2\pi B(e))^{-\frac{3}{2}} \exp\left(-\frac{y^2}{2B(e)}\right) \quad (4.15)$$

where

$e$  = energy in the two body center of mass frame,

$\sigma(e)$  = energy dependent total nucleon-nucleon cross section,

$\alpha(e)$  = energy dependent ratio of the real to the imaginary parts of the forward scattering amplitude,

$B(e)$  = slope parameter (related to the range of interaction)

The transition amplitude has the real and imaginary components to it, which gives rise to the real and imaginary parts of the optical potential and consequently the phase function. Calculations of

the total reaction cross section and double differential cross section from the ablation process, however, only requires the knowledge of the imaginary part.

The values for total nuclear cross sections are taken from experimental data and are parameterized by Wilson et al. [1] as

$$\sigma(e) = \frac{Z_P + Z_T}{A_P + A_T} \sigma_{pp}(e) + \frac{N_P + N_T}{A_P + A_T} \sigma_{pn}(e) \quad (4.16)$$

where  $Z_{P,T}$  are the nuclei charge number,  $N_{P,T}$  represent the neutron number in the projectile and the target nuclei respectively and

$$\sigma_{pp}(E) = \begin{cases} \left(1 + \frac{5}{E}\right) \left\{ 40 + 109 \cos(0.199\sqrt{E}) \exp(-0.451(E-25)^{0.258}) \right\} & \text{for } E \geq 25 \text{ MeV} \\ \exp \left\{ 6.51 \left[ \exp \left( -\frac{E}{134} \right)^{0.7} \right] \right\} & \text{for } E < 25 \text{ MeV} \end{cases} \quad (4.17)$$

$$\sigma_{np}(E) = \begin{cases} 38 + 12500 \exp \left[ -1.187 (E - 0.1)^{0.35} \right] & \text{for } E \geq 0.1 \text{ MeV} \\ 26000 \exp \left( -\frac{E}{0.282} \right)^{0.3} & \text{for } E < 0.1 \text{ MeV} \end{cases} \quad (4.18)$$

The values for slope parameter  $B(e)$  are taken from Ringia et al. [70] as given in [1] as

$$B(e) = 10 + 0.5 \ln \left( \frac{s'}{s_0} \right) \quad (4.19)$$

where  $s'$  is the square of the nucleon-nucleon center of mass energy and  $s_0 = 1 \text{ (GeV / c)}^{-2}$ .

It must be noted that the units on  $B(e)$  are  $(\text{GeV / c})^{-2}$ . To convert these units to  $\text{fm}^2$ , we use the multiplicative factor 0.0389.

Further, the units on  $\sigma(e)$  in equation (4.16) are in millibarns (mb). We can convert from  $\text{mb}$  to  $\text{fm}^2$  using the conversion factor  $1 \text{ mb} = 10 \text{ fm}^2$ .

The values of  $\alpha(e)$ , though not used in the calculations in this work, can be found in the works by De Jager and De Vries [71].

## 4.2. Nuclear Density Distribution Approximations

The nuclear density distributions for the projectile and the target nuclei, used to calculate the optical potential in equation (4.14), are given by the ground state-single particle nuclear densities. These density distributions for the collision pair are calculated from the experimentally determined charge density distributions, given as [1]

$$\rho_c(\vec{r}) = \int \rho_p(\vec{r}') \rho_A(\vec{r} + \vec{r}') d^3\vec{r}' \quad (4.20)$$

where  $\rho_A$  is the desired nuclear single-particle density,  $\rho_c$  is the nuclear charge density and  $\rho_p$  is the proton charge distribution, expressed in terms of Gaussian distribution as

$$\rho_p(\vec{r}) = \left( \frac{3}{2\pi r_p^2} \right)^{\frac{3}{2}} \exp\left( -\frac{3r^2}{2r_p^2} \right) \quad (4.21)$$

with  $r_p = 0.87 \text{ fm}$  being the proton root-mean-square charge radius [72].

For lighter nuclei ( $A < 20$ ), the nuclear charge distribution is assumed to have harmonic well (HW) form [71]

$$\rho_c(\vec{r}) = \rho_0 \left[ 1 + \gamma \left( \frac{r}{a} \right)^2 \right] \exp\left( -\frac{r^2}{a^2} \right) \quad (4.22)$$

which upon inserting equation (4.22) into equation (4.20), and performing necessary integration yields [73]

$$\rho_A(\vec{r}) = \rho_0 \frac{a^3}{8s^3} \left[ 1 + \frac{3\gamma}{2} - \frac{3\gamma a^2}{8s^2} + \frac{\gamma a^2 r^2}{16s^4} \right] \exp\left( -\frac{r^2}{4s^2} \right) \quad (4.23)$$

$$\text{with } s^2 = \frac{a^2}{4} - \frac{r_p^2}{6}$$

In equation (4.23)  $r$  is the radial coordinate,  $a$  and  $\gamma$  are charge parameters and  $\rho_0$  is the normalization constant, calculated by normalizing to unity as

$$\int \rho_A(\vec{r}) d^3\vec{r} = 1 \quad (4.24)$$

and can be given as

$$\rho_0 = \frac{1}{\left( \left( \pi/D \right)^{\frac{3}{2}} + \left( 3B/2 \right) \sqrt{\frac{\pi^3}{D^5}} \right)} \quad (4.25)$$

$$\text{with } D = \frac{1}{4s^2} \text{ and } B = \frac{a^3}{8s^3} \frac{\gamma a^2}{16s^4}.$$

The values for charge parameters  $a$  and  $\gamma$  are taken from De Jager and De Vries [71].

A list of these parameters for several nuclei, adapted from [1], is given in the Appendix II.

For heavier nuclei ( $A \geq 20$ ), the charge distribution is assumed to have Wood-Saxon (WS) form, which is calculated from the charge distribution  $\rho_c$ , and is given by Wilson and Costner [74] as

$$\rho_A(\vec{r}) = \frac{\rho_0}{1 + \exp\left(\frac{r - R}{t_A}\right)} \quad (4.26)$$

where

$$t_A = \frac{8.8r_p}{\sqrt{3}} \left[ \ln\left(\frac{3\beta - 1}{3 - \beta}\right) \right]^{-1} \quad (4.27)$$

and

$$\beta = \exp\left(\frac{4.4r_p}{\left(\frac{t}{4.4}\right)\sqrt{3}}\right) \quad (4.28)$$

The values of charge parameters  $R$  and  $t$  are taken from De Jager and De Vries [71] and a list of these parameters for several nuclei is listed in Appendix II.

The normalization constant  $\rho_0$  is calculated using approach similar to the one described in Muang et al. [75] and can be given as

$$\rho_0 = \frac{1}{4\pi \left( \frac{R^3}{3} + \frac{1}{3} \pi^2 t_A^2 R \right)} \quad (4.29)$$

The calculation of optical potential requires integration of the single-particle nuclear densities. It must be noted that the integrations of the nuclear densities mentioned above, both analytic and numerical solutions, are complex in nature and lead to too many terms in the final solution [75],[76]. This becomes even more challenging when we derive the optical potential for the higher order correction terms. A simpler form for the nuclear densities in the calculation of the optical potential can be obtained by using a Gaussian approximation for the distributions. In this work, we have developed Gaussian approximations to the nuclear densities by using the same normalization constant and charge parameters as described in the equations above. The approximations are given below.

For the lighter nuclei ( $A < 20$ ), the HW distribution given in equation (4.23) can be approximated using a Gaussian form as

$$\rho_A(\vec{r}) = 0.66 \rho_0 \frac{a^3}{8s^3} \left[ 1.5 + \frac{3\gamma}{2} - \frac{3\gamma a^2}{8s^2} + \frac{\gamma a^2}{16s^4} \right] \exp\left(-\frac{r^2}{4(1+0.52\gamma)s^2}\right) \quad (4.30)$$

and for the heavier nuclei ( $A \geq 20$ ), the WS distribution given in equation (4.26) can be expressed in terms of Gaussian form as

$$\rho_A(\vec{r}) = \rho_0 \left(\frac{R}{t}\right)^{0.3} \exp(-Dr^2) \quad (4.31)$$

with  $D = -0.0109R + 0.1234$

The normalization constant and the charge parameters given in equations (4.30) and (4.31) are same as the ones given in equations (4.23) and (4.26) respectively.

Equations (4.30) and (4.31) provide a simplified form to the nuclear densities since both equations can be written as

$$\rho_A(\vec{r}) = C_i \exp(-D_i r^2) \quad (4.32)$$

where  $i = P, T$  represent the projectile and target constituents respectively.

Presented in figures (3) to (7) are the comparisons of the Gaussian approximations developed herein to the HW and the WS model respectively.

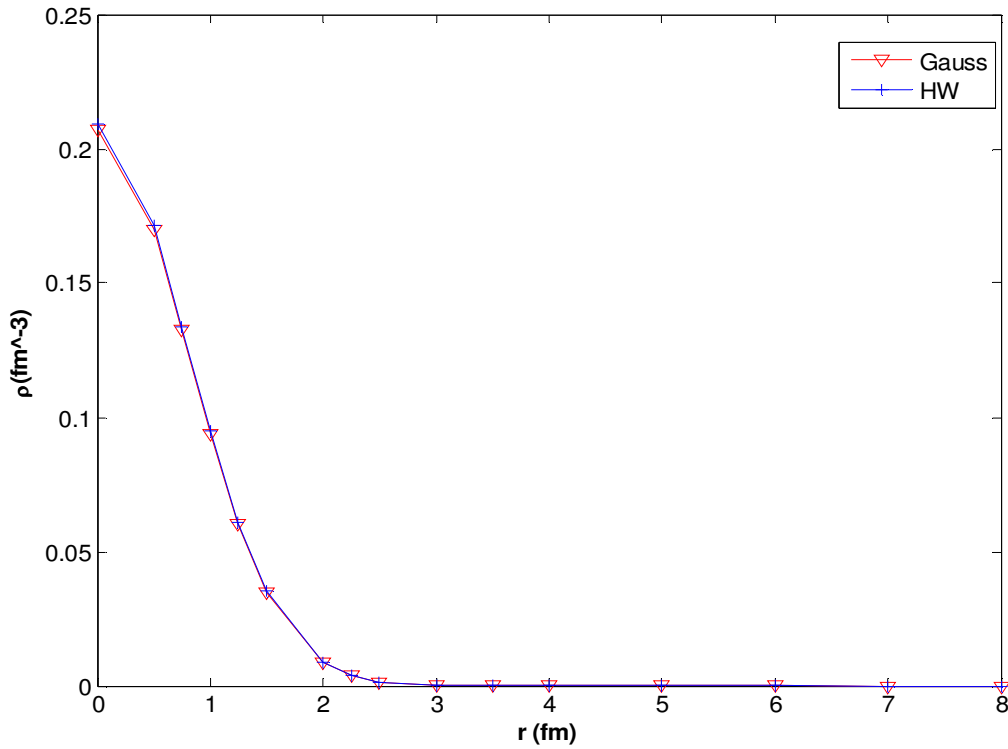


**Figure 3:** Comparison of Harmonic Well versus Gauss distribution for  ${}^4\text{He}$ .



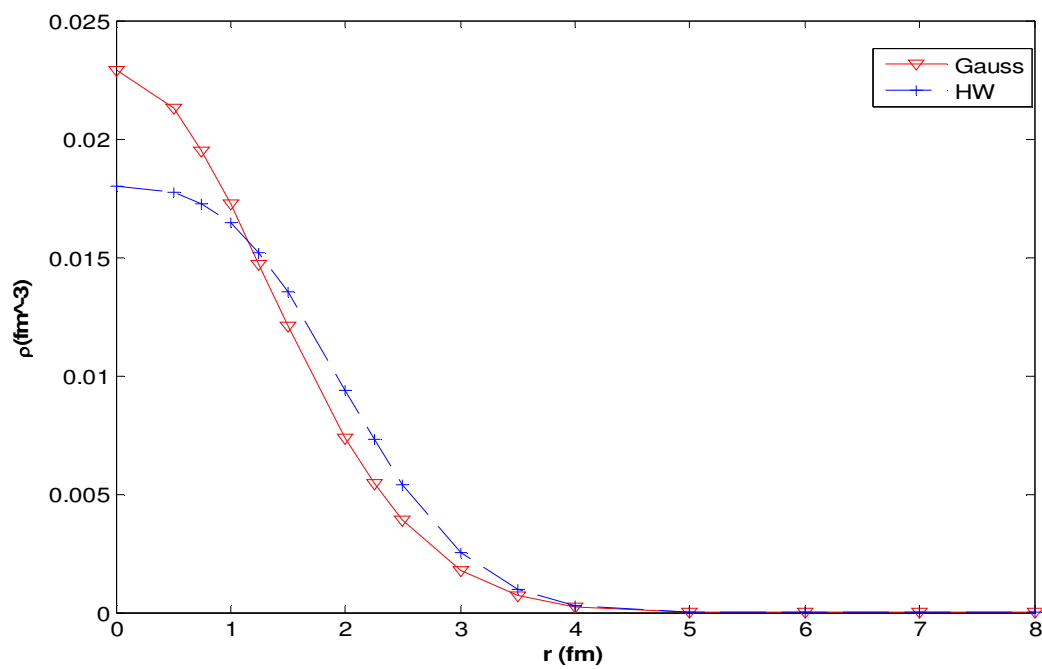


**Figure 4:** Comparison of Harmonic Well versus Gauss distribution for  ${}^9\text{Be}$ .

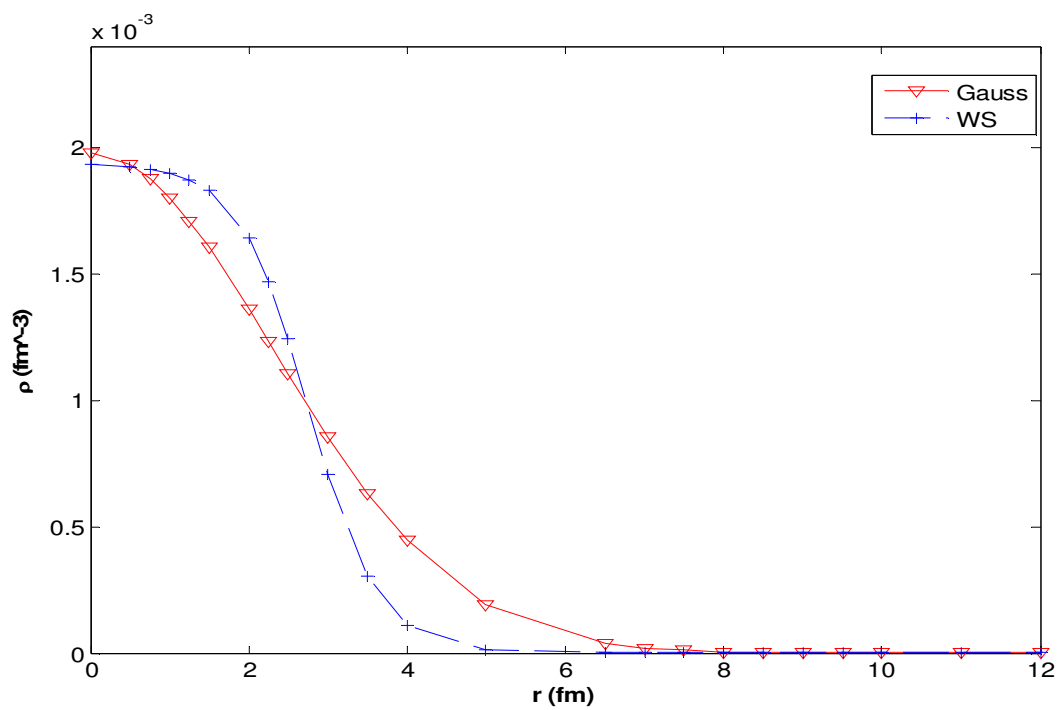


**Figure 5:** Comparison of Wood Saxon versus Gauss distribution for  ${}^{20}\text{Ne}$ .

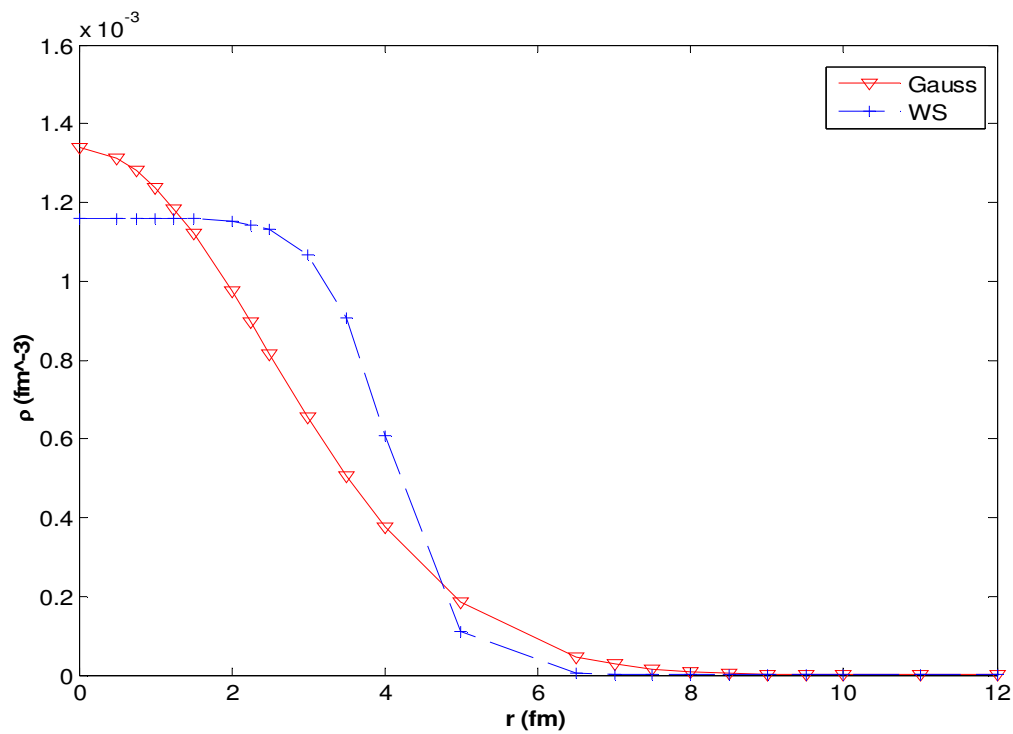


**Figure 6:** Comparison of Wood Saxon versus Gauss distribution for  $^{64}\text{Cu}$ .

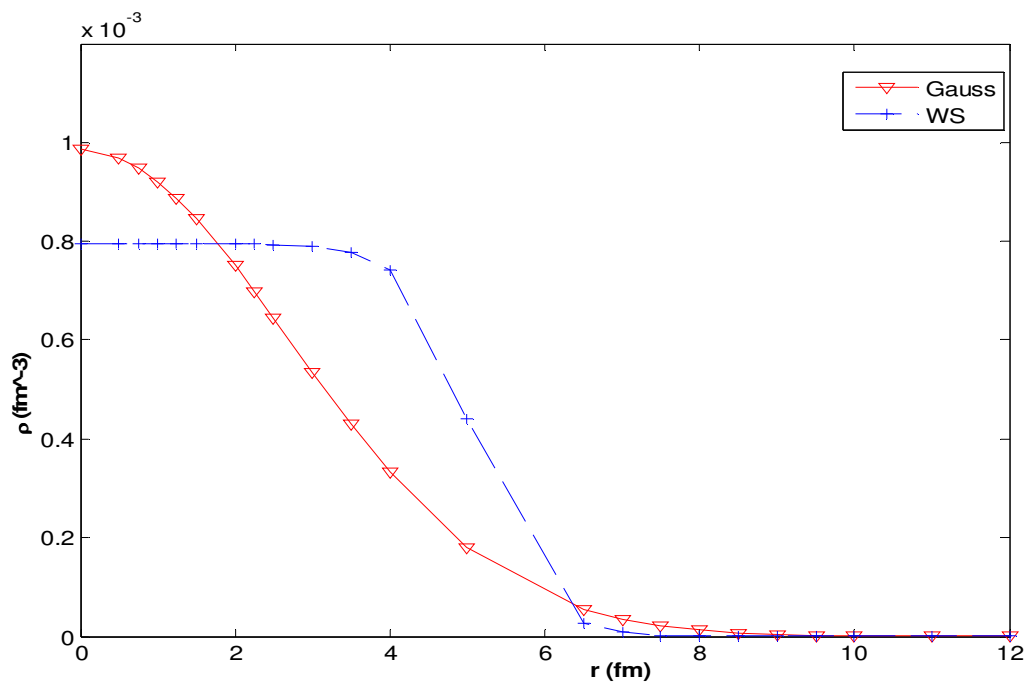


**Figure 7:** Comparison of Wood Saxon versus Gauss distribution for  $^{108}\text{Ag}$ .

### 4.3. Validity of the Gaussian Approximations

The Gaussian approximations given in the section 4.2 provide a reasonable fit when compared to the density distributions from HW distributions for lighter nuclei and the WS distributions for the heavier nuclei. However, it is important to check the validity of these approximations. In this section, an attempt is made to compare the total absorption cross sections calculated using Gaussian approximations to the experimental data and the energy dependent parameterization developed by Wilson and Townsend [77].

From equation (2.5), the total absorption cross section can be given as

$$\sigma_{abs} = 2\pi \int \left\{ 1 - \exp \left[ -2 \operatorname{Im} \chi(\vec{b}) \right] \right\} b db \quad (4.33)$$

where the phase function is related to optical potential, without the correction terms as

$$\chi(\vec{b}) = -\frac{m}{2k} \int_{-\infty}^{\infty} V(\vec{r}) dz \quad (4.34)$$

Inserting the Gaussian approximations from equation (4.32) into equation (4.14), we can re-write the optical potential as

$$V(\vec{r}) = \frac{2mA_p^2 A_T^2}{N} \int d^3z C_T \exp(-D_T \vec{z}^2) \int d^3y C_p \exp(-D_p (\vec{r} + \vec{y})^2) \tilde{t}(e, \vec{y}) \quad (4.35)$$

where subscripts  $P$  and  $T$  denote the projectile and the target constituents respectively. Note that the optical potential term described in equation (4.34) has the nucleon mass term,  $m$ , outside the integral as compared to the term in equation (4.35).

The total absorption cross section calculated using equation (4.33) is compared to the experimental data given in [78] and also the energy dependent parameterization by Townsend and Wilson [77]. The parameterization is given as

$$\sigma_{abs} = \pi r_0^2 (1 + 5E^{-1}) \left( A_p^{1/3} + A_T^{1/3} - \delta^2 \right)^2 \quad (4.36)$$

where

$$\delta = 0.200 + A_p^{-1} + A_T^{-1} - 0.292 \exp\left(-\frac{E}{792}\right) \cos\left(0.229 E^{0.453}\right) \quad (4.37)$$

$A_p$  and  $A_T$  are the projectile and the target mass numbers respectively, and  $E$  is the projectile energy expressed in terms of MeV/nucleon.

The plots in figures (8) through (11) show that the total absorption cross section calculated using the Gauss approximation show a good fit when compared to the experimental data and the energy dependent parameterization, and thus provide validity to the approximations made in section 4.2.

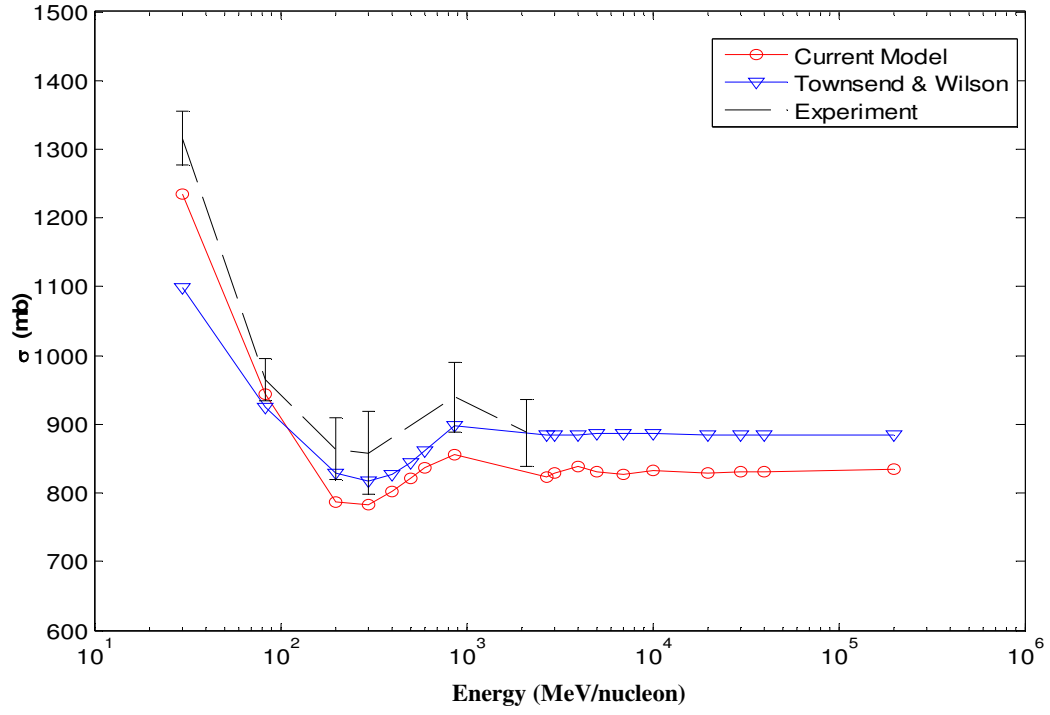


**Figure 8:** Comparison of the Gaussian Model to the experimental data and parameterization by Townsend and Wilson for  $^{12}\text{C}$  on  $^{12}\text{C}$ .

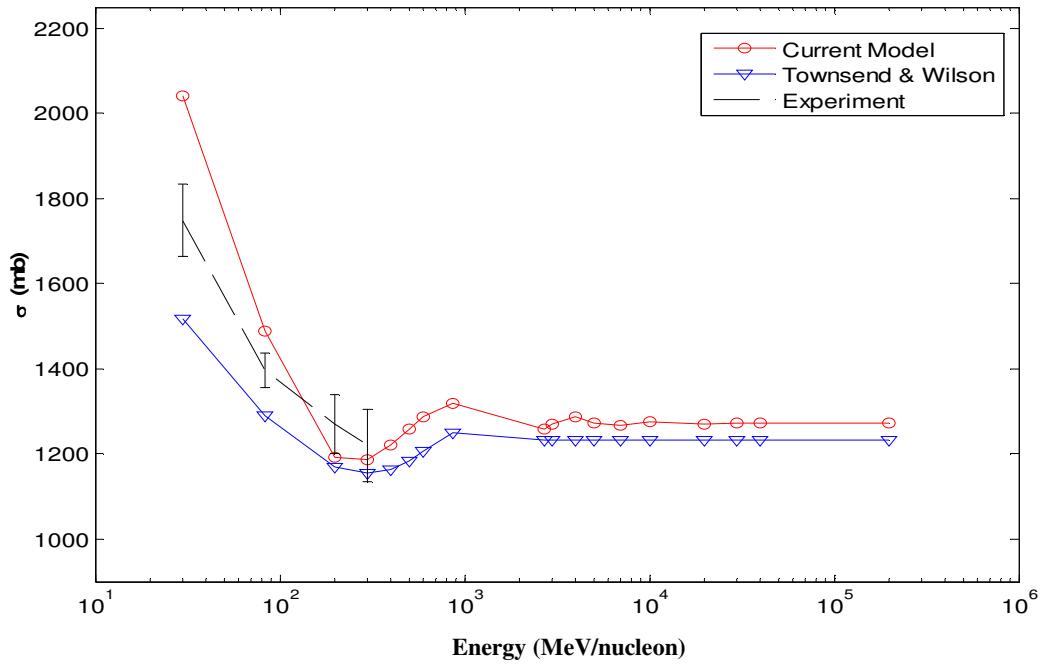


**Figure 9:** Comparison of the Gaussian Model to the experimental data and parameterization by Townsend and Wilson for  $^{12}\text{C}$  on  $^{27}\text{Al}$ .

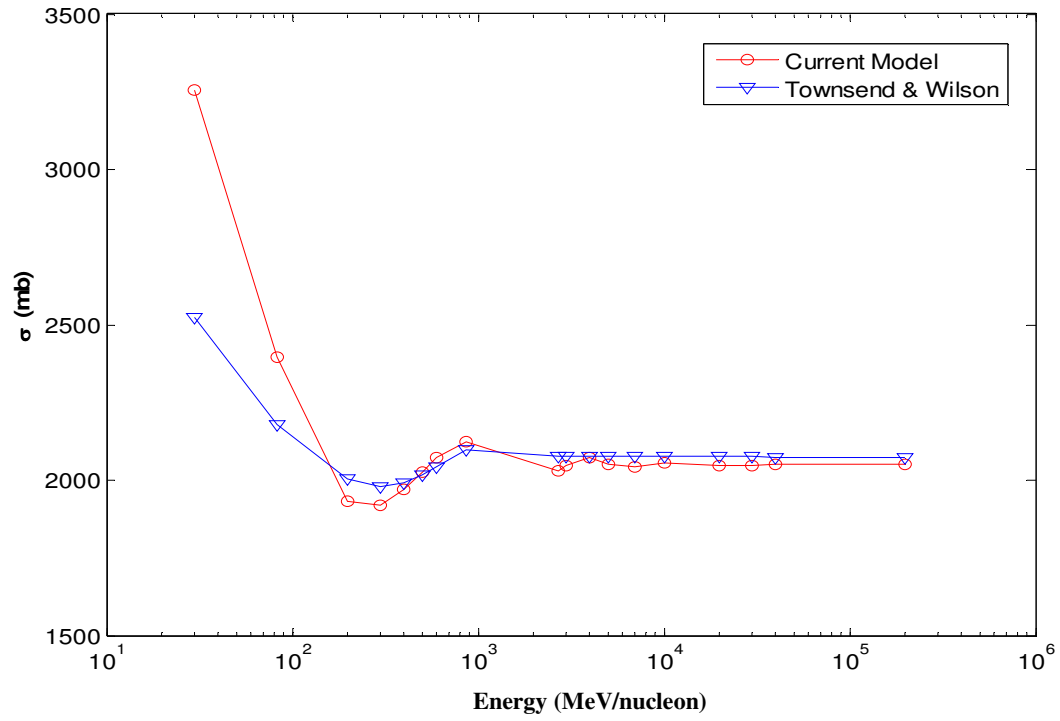


**Figure 10:** Comparison of the Gaussian Model to the parameterization by Townsend and Wilson for  $^{20}\text{Ne}$  on  $^{64}\text{Cu}$ .

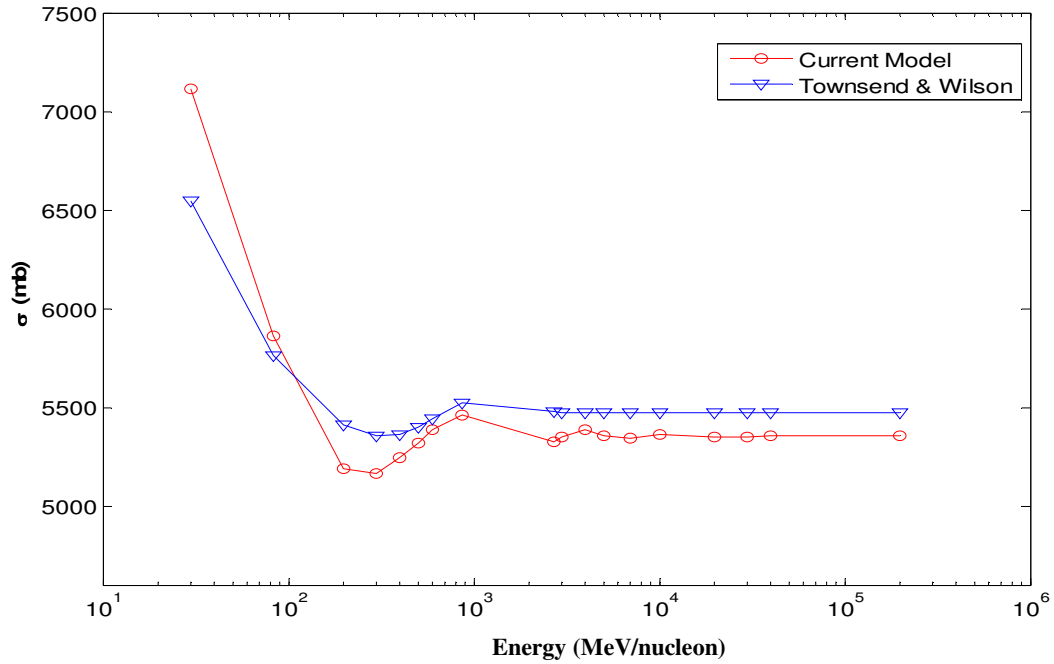


**Figure 11:** Comparison of the Gaussian Model to the parameterization by Townsend and Wilson for  $^{108}\text{Ag}$  on  $^{208}\text{Pb}$ .

#### 4.4. Optical Potential and Phase Function Calculation

Calculation of the optical potential derived in equation (4.35) requires performing the necessary integrations of the projectile and the target nuclear densities and also the two body transition amplitude. In this section, we will obtain a solution for the optical potential and also calculate the phase function with the correction terms as given by equations (3.49) to (3.53). The calculations below have been performed using a similar approach as given in the reference [61]

Recall that the optical potential can be expressed using equation (4.35) as

$$V(\vec{r}) = \frac{2mA_p^2 A_T^2}{N} \int d^3z C_T \exp(-D_T \vec{z}^2) \int d^3y C_p \exp(-D_p (\vec{r} + \vec{y})^2) \tilde{t}(e, \vec{y}) \quad (4.38)$$

where the two body transition amplitude is given by equation (4.15) as

$$\tilde{t}(e, \vec{y}) = -\sqrt{\frac{e}{m}} \sigma(e) [\alpha(e) + i] (2\pi B(e))^{-\frac{3}{2}} \exp\left(-\frac{y^2}{2B(e)}\right) \quad (4.39)$$

The two body center of mass energy,  $e$ , in equation (4.39) can be expressed as

$$e = \frac{1}{2} \mu v^2 \quad (4.40)$$

where  $\mu = m/2$  is the reduced mass, and the relative velocity  $v$  is given by

$$v = \frac{Nk}{mA_P A_T} \quad (4.41)$$

Inserting equation (4.40) and (4.41) into equation (4.39) yields

$$\tilde{t}(e, \vec{y}) = -\frac{Nk}{2mA_P A_T} \sigma(e) [\alpha(e) + i] (2\pi B(e))^{-\frac{3}{2}} \exp\left(-\frac{y^2}{2B(e)}\right) \quad (4.42)$$

The optical potential in equation (4.38) thus can be simplified to

$$V(\vec{r}) = G_1 \int d^3 z \exp(-D_r \vec{z}^2) \int d^3 y \exp(-D_p (\vec{r} + \vec{y})^2) \exp\left(-\frac{y^2}{2B(e)}\right) \quad (4.43)$$

with

$$G_1 = -kA_P A_T C_T C_P \sigma(e) [\alpha(e) + i] (2\pi B(e))^{-\frac{3}{2}} \quad (4.44)$$

where subscripts  $P$  and  $T$  denote the projectile and the target constituents respectively, and  $k$  is the wave number of the outgoing nucleons.

Now, using the identity  $(\vec{r} + \vec{y})^2 = r^2 + y^2 + 2ry \cos \theta$  and  $d^3 y = y^2 dy \sin \theta d\theta d\phi$ , the last part of the integral in equation (4.43) can be given as



$$I_1 = \int \exp(-D_P r^2) \exp \left[ - \left( D_P + \frac{1}{2B(e)} \right) y^2 \right] \exp(-D_P 2ry \cos \theta) y^2 dy \sin \theta d\theta d\phi \quad (4.45)$$

which can be further simplified to

$$I_1 = 2\pi \exp(-D_P r^2) \int_0^\infty y^2 \exp \left[ - \left( D_P + \frac{1}{2B(e)} \right) y^2 \right] dy \int_0^\pi \exp(-D_P 2ry \cos \theta) \sin \theta d\theta \quad (4.46)$$

The integration with respect to  $\theta$  in equation (4.46) can be solved using the form

$$\int_0^\pi \exp(-D_P 2ry \cos \theta) \sin \theta d\theta = \frac{1}{2D_P ry} \left[ \exp(2D_P ry) - \exp(-2D_P ry) \right] \quad (4.47)$$

and thus equation (4.46) can be re-written as

$$I_1 = 2\pi \exp(-D_P r^2) \frac{1}{2D_P r} \int_0^\infty y \exp \left[ - \left( D_P + \frac{1}{2B(e)} \right) y^2 \right] \left[ \exp(2D_P ry) - \exp(-2D_P ry) \right] dy \quad (4.48)$$

The last part of the integral in equation (4.48) has the form

$$J_1 = \int_0^\infty y dy \exp \left[ - \left( D_P + \frac{1}{2B(e)} \right) y^2 \right] \left[ \exp(\pm 2D_P ry) \right] \quad (4.49)$$

$$= \int_0^\infty y dy \exp \left[ - \left( D_P + \frac{1}{2B(e)} \right) \left[ y^2 \mp \frac{2D_P r y}{\left( D_P + \frac{1}{2B(e)} \right)} \right] \right] \quad (4.50)$$

$$= \exp \left( \frac{r^2 D_P^2}{\left( D_P + \frac{1}{2B(e)} \right)} \right) \int_0^\infty y dy \exp \left\{ - \left( D_P + \frac{1}{2B(e)} \right) \left[ y \mp \frac{D_P r}{\left( D_P + \frac{1}{2B(e)} \right)} \right]^2 \right\} \quad (4.51)$$

Now, let  $p = y \mp \frac{D_P r}{\left( D_P + \frac{1}{2B(e)} \right)}$ ,

which gives  $y = p \pm \frac{D_P r}{\left( D_P + \frac{1}{2B(e)} \right)}$  and  $dy = dp$ . This allows us to write equation (4.51) as

$$= \exp \left( \frac{r^2 D_P^2}{\left( D_P + \frac{1}{2B(e)} \right)} \right) \int_0^\infty dp \left[ p \exp \left\{ -p^2 \left( D_P + \frac{1}{2B(e)} \right) \right\} \pm \frac{D_P r}{\left( D_P + \frac{1}{2B(e)} \right)} \exp \left\{ -p^2 \left( D_P + \frac{1}{2B(e)} \right) \right\} \right] \quad (4.52)$$

The integrations in equation (4.52) have the form

$$\int_0^{\infty} x e^{-Ax^2} dx = \frac{1}{2A} \quad \text{and} \quad \int_0^{\infty} e^{-Ax^2} dx = \frac{1}{2} \sqrt{\frac{\pi}{A}}$$

Using the identities above, we can write equation (4.52) as

$$J_1 = \exp\left(\frac{r^2 D_p^2}{\left(D_p + \frac{1}{2B(e)}\right)}\right) \left[ \frac{1}{2\left(D_p + \frac{1}{2B(e)}\right)} \pm \frac{D_p r}{\left(D_p + \frac{1}{2B(e)}\right)} \frac{1}{2} \sqrt{\frac{\pi}{\left(D_p + \frac{1}{2B(e)}\right)}} \right] \quad (4.53)$$

Inserting the solutions from equation (4.53) into equation (4.48) and further simplifying gives

$$I_1 = 2\pi \exp(-D_p r^2) \frac{1}{2D_p r} \left\{ \exp\left(\frac{r^2 D_p^2}{\left(D_p + \frac{1}{2B(e)}\right)}\right) \left[ \frac{D_p r}{\left(D_p + \frac{1}{2B(e)}\right)} \sqrt{\frac{\pi}{\left(D_p + \frac{1}{2B(e)}\right)}} \right] \right\} \quad (4.54)$$

And inserting this into the optical potential equation (4.43) yields

$$V(\vec{r}) = \frac{\pi}{D_p} G_1 \int d^3 z \exp(-D_T \vec{z}^2) \exp(-D_p r^2) \left\{ \exp \left( \frac{r^2 D_p^2}{\left( D_p + \frac{1}{2B(e)} \right)} \right) \left[ \frac{D_p}{\left( D_p + \frac{1}{2B(e)} \right)} \sqrt{\frac{\pi}{\left( D_p + \frac{1}{2B(e)} \right)}} \right] \right\} \quad (4.55)$$

$$= \pi G_1 \left[ \frac{1}{\left( D_p + \frac{1}{2B(e)} \right)} \sqrt{\frac{\pi}{\left( D_p + \frac{1}{2B(e)} \right)}} \int d^3 z \exp(-D_T \vec{z}^2) \exp \left( -r^2 \left\{ D_p - \frac{D_p^2}{\left( D_p + \frac{1}{2B(e)} \right)} \right\} \right) \right] \quad (4.56)$$

$$= G_1 \left( \frac{\pi}{\left( D_p + \frac{1}{2B(e)} \right)} \right)^{\frac{3}{2}} \int d^3 z \exp(-D_T \vec{z}^2) \exp \left( -r^2 \left\{ D_p - \frac{D_p^2}{\left( D_p + \frac{1}{2B(e)} \right)} \right\} \right) \quad (4.57)$$

Now, again using the identity  $r^2 = x^2 + z^2 + 2xz \cos \theta$  and  $d^3 z = z^2 dz \sin \theta d\theta d\phi$ , the last part of the integral in equation (4.57) can be written as

$$I_2 = \int \exp(-D_T z^2) \exp(-z^2 L) \exp(-x^2 L) \exp(-2xzL \cos \theta) z^2 dz \sin \theta d\theta d\phi \quad (4.58)$$

with

$$L = \left\{ D_p - \frac{D_p^2}{\left( D_p + \frac{1}{2B(e)} \right)} \right\} \quad (4.59)$$

Re-arranging equation (4.58) gives

$$I_2 = 2\pi \exp(-x^2 L) \int_0^\infty z^2 \exp(-z^2 (D_T + L)) dz \int_0^\pi \exp(-2xzL \cos \theta) \sin \theta d\theta \quad (4.60)$$

The integration with respect to  $\theta$  in equation (4.60) can be simplified using the form

$$\int_0^\pi \exp(-2xzL \cos \theta) \sin \theta d\theta = \frac{1}{2xzL} [\exp(2xzL) - \exp(-2xzL)] \quad (4.61)$$

Thus, equation (4.60) can be given as

$$I_2 = \frac{\pi}{xL} \exp(-x^2 L) \int_0^\infty z \exp(-z^2 (D_T + L)) [\exp(2xzL) - \exp(-2xzL)] dz \quad (4.62)$$

Equation (4.62) has the same form as equation (4.48). Thus, solving for the integral, using a similar approach like the one used in equations (4.49) through (4.57), we have

$$I_2 = \left( \frac{\pi}{D_T + L} \right)^{\frac{3}{2}} \exp \left[ -x^2 \left( L - \frac{L^2}{D_T + L} \right) \right] \quad (4.63)$$

which upon substituting the value of  $L$  from equation (4.59) becomes

$$I_2 = \left( \frac{\pi}{D_T + D_P - \frac{D_P^2}{\left( D_P + \frac{1}{2B(e)} \right)}} \right)^{\frac{3}{2}} \exp \left[ -x^2 \left\{ D_P - \frac{D_P^2}{\left( D_P + \frac{1}{2B(e)} \right)} - \frac{\left\{ D_P - \frac{D_P^2}{\left( D_P + \frac{1}{2B(e)} \right)} \right\}^2}{\left\{ D_T + D_P - \frac{D_P^2}{\left( D_P + \frac{1}{2B(e)} \right)} \right\}} \right] \right] \quad (4.64)$$

We now obtain an expression for the optical potential in equation (4.43) by substituting the values obtained from equation (4.64) into equation (4.57), and inserting the value of  $G_1$  from equation (4.55), given as

$$V(\vec{r}) = -k M \exp(-Nx^2) \quad (4.65)$$

where

$$M = \pi^3 A_p A_T C_T C_p \sigma(e) [\alpha(e) + i] (2\pi B(e))^{-\frac{3}{2}} \left( \left( D_p + \frac{1}{2B(e)} \right) \right)^{-\frac{3}{2}} \left\{ D_T + D_p - \frac{D_p^2}{\left( D_p + \frac{1}{2B(e)} \right)} \right\}^{-\frac{3}{2}} \quad (4.66)$$

And

$$N = \left( \left\{ D_p - \frac{D_p^2}{\left( D_p + \frac{1}{2B(e)} \right)} \right\} - \frac{\left\{ D_p - \frac{D_p^2}{\left( D_p + \frac{1}{2B(e)} \right)} \right\}^2}{\left\{ D_T + D_p - \frac{D_p^2}{\left( D_p + \frac{1}{2B(e)} \right)} \right\}} \right) \quad (4.67)$$

where the parameters  $C_{p,T}$  and  $D_{p,T}$  are taken from the nuclear density parameters given in equation (4.30) and (4.31),  $A_p$  and  $A_T$  are the projectile and the target mass numbers, and  $B(e)$ ,  $\sigma(e)$  and  $\alpha(e)$  are the two nucleon transition amplitude parameters defined in equation (4.15)

#### 4.4.1. Phase Functions

Recall that the total phase function, defined as the sum of the zeroth order phase function term and the higher order correction terms, can be given by equation (3.48)

$$\chi(b) = \sum_n -\frac{(\mu)^{n+1}}{k(n+1)!} \left[ \left( \frac{b}{k} \frac{\partial}{\partial b} - \frac{\partial}{\partial k} \right) \frac{1}{k} \right]^n \int_{-\infty}^{\infty} V^{n+1}(\vec{r}) dz \quad (4.68)$$

Inserting the optical potential form derived in equation (4.65) into equation (4.68) allows us to write the zeroth order phase function as

$$\chi_0(b) = -\frac{1}{2k} \int_{-\infty}^{\infty} -kM \exp(-Nx^2) dz \quad (4.69)$$

Note that the reduced nucleon mass  $\mu = m/2$  has been already accounted for in the derivation of the optical potential. Separating  $x^2 = b^2 + z^2$ , allows us to write the equation above as

$$\chi_0(b) = \frac{1}{2} M \exp(-Nb^2) \int_{-\infty}^{\infty} \exp(-Nz^2) dz \quad (4.70)$$

and further reduces to

$$\chi_0(b) = \frac{1}{2} \sqrt{\frac{\pi}{N}} M \exp(-Nb^2) \quad (4.71)$$



Similarly, the correction terms to the phase function after performing the necessary derivatives to the equations (3.50) through (3.53) can be expressed as

$$\chi_1(b) = \frac{1}{4k} \sqrt{\frac{\pi}{2N}} M^2 (4Nb^2 + 1) \exp(-2Nb^2) \quad (4.72)$$

$$\chi_2 = -\frac{1}{12k^2} \sqrt{\frac{\pi}{3N}} M^3 (-36b^4N^2) \exp(-3Nb^2) \quad (4.73)$$

$$\chi_3 = \frac{1}{48k^3} \sqrt{\frac{\pi}{4N}} M^4 (-24b^2N - 192b^4N^2 + 512b^6N^3 - 3) \exp(-4Nb^2) \quad (4.74)$$

$$\chi_4 = -\frac{1}{240k^4} \sqrt{\frac{\pi}{5N}} M^5 (8000b^6N^3 - 10000b^8N^4) \exp(-5Nb^2) \quad (4.75)$$

with

$$\chi(b) = \chi_0(b) + \chi_1(b) + \chi_2(b) + \chi_3(b) + \chi_4(b) + \dots \quad (4.76)$$

The detailed derivations of the phase functions above are given in the Appendix III.

It must be noted here that the  $n^{th}$  order correction terms have the wave number  $k$  raised to the power  $n$  in the denominator. The wave number  $k$  is related to the momentum transfer  $q$  and the scattering angle  $\theta$  as

$$k = \frac{q}{2 \sin\left(\frac{\theta}{2}\right)} \quad (4.77)$$

For the strictly forward scattering, at  $\theta = 0^0$ , the correction terms go to zero, and we get the same result for the phase function as derived by the Glauber multiple scattering theory. The contribution of the correction terms gets bigger as the scattering angle gets larger. For the small scattering angles, the series converges rapidly since the power of the wave number  $k$  increases with the increasing order of the correction terms.

The phase function terms derived above are used to calculate the total abrasion cross sections, which further allow us to calculate the momentum distributions from both abrasion and ablation process, and also the double differential cross sections.

Recall that the cross section for abrading  $n$  nucleons from a projectile nucleus is given by equation (2.9) as

$$\sigma_n = \binom{A_p}{n} 2\pi \int \left[ 1 - \exp\left[\frac{-2\text{Im}\chi(\vec{b})}{A_p}\right] \right]^n \left( \exp\left[\frac{-2\text{Im}\chi(\vec{b})}{A_p}\right] \right)^{A_F} b db \quad (4.78)$$

where  $\text{Im}\chi(\vec{b})$  denotes the imaginary part of the phase function.

The integrations with respect to the impact parameter  $b$  require numerical integration. In this work the integrals have been calculated using a Gaussian quadrature integration method [79],[80]. The method uses the approximation

$$\int_{-1}^1 f(x) dx \approx \sum_{i=0}^{n-1} w_i f(x_i) \quad (4.79)$$

where  $f$  is the desired function,  $x_i$  are the roots of Legendre Polynomials,  $n$  is the number of Gaussian points over which the function is summed over, and  $w_i$  are the weights determined from the derivatives of the Legendre polynomials. The integral with respect to  $b$  in the equation (4.78) has limits  $[0, \infty]$ , which can be transformed to limits  $[-1, 1]$  using a transformation of variables, and thus the approximation given in equation (4.79) can be applied. The integrations for this work were performed using 1000 Gaussian points and respective weights.

A brief discussion on the Gaussian quadrature adapted from Werneth et al.[80] is given in the Appendix IV.

The roots of the Legendre Polynomials  $x_i$  and the weights  $w_i$ , have been calculated using an open source MATLAB code written by Greg Von Winckel [81]

## 4.5. Frame Transformations

The calculation of the cross section from the abrasion-ablation process, and the further evaluation of the neutron momentum distributions and the double differential cross sections

requires calculation of the energy and the momentum of the projectile and the target in their respective frame of reference. Recall from Chapter 2, the nucleon momentum distribution for abrading  $n$  projectile nucleons is given by equation (2.15) as

$$\left( \frac{d^3\sigma}{dp_n^3} \right)_{abr} = \left( \sum_1^n \sigma_n \right) \left( n_0 \sum_{i=1}^3 C_i \exp \left( \frac{-p_n^2}{2p_i^2} \right) \right) \quad (4.80)$$

where  $\sum_1^n \sigma_n$  is sum of the total abrasion cross section for abrading up to  $n$  projectile nucleons,  $p_n$  is the momentum of the outgoing nucleon on the rest frame of projectile,  $n_0$  is the normalization constant, and the values of  $C_i$  and  $p_i$  are listed in Table 1.

Similarly, the momentum distribution in equation (4.80) can be related to the double differential cross section as given by equation (2.17)

$$\left( \frac{d^2\sigma}{dE_L d\Omega_L} \right)_{abr} = p_L E_p \left( \frac{d^3\sigma}{dp_n^3} \right)_{abr} \quad (4.81)$$

where  $p_L$  and  $d\Omega_L$  are the momentum and direction of the outgoing nucleon in the laboratory frame and  $E_p$  is the kinetic energy in the projectile rest frame. It must be noted here that the nucleon abrasion cross sections and their momentum distributions are evaluated in the rest frame of the projectile, while the differential cross sections are evaluated in the laboratory frame. Thus,

we need a proper mechanism for the conversion of the energy, momentum and the cross sections from one reference frame to another. A brief discussion on the frame transformations is presented below [82].

The transformation from the lab frame to the projectile frame can be obtained using the Lorentz transformation

$$\begin{pmatrix} E_p \\ p_{\parallel p} \end{pmatrix} = \begin{pmatrix} \gamma_{PL} & -\gamma_{PL}\beta_{PL} \\ -\gamma_{PL}\beta_{PL} & \gamma_{PL} \end{pmatrix} \begin{pmatrix} E_L \\ p_{\parallel L} \end{pmatrix} \quad (4.82)$$

and the inverse transformations from the projectile frame to the lab frame can be given by

$$\begin{pmatrix} E_L \\ p_{\parallel L} \end{pmatrix} = \begin{pmatrix} \gamma_{PL} & \gamma_{PL}\beta_{PL} \\ \gamma_{PL}\beta_{PL} & \gamma_{PL} \end{pmatrix} \begin{pmatrix} E_p \\ p_{\parallel p} \end{pmatrix} \quad (4.83)$$

where  $E_{L,p}$  represents the total energy of the nucleon with subscripts  $L$  and  $P$  representing the lab and the projectile rest frame respectively,  $\beta_{PL}$  is the relative speed of the projectile frame with respect to the lab frame, and  $\gamma_{PL}$  is the corresponding Lorentz factor. The parallel momentum term  $p_{\parallel}$ , in the appropriate reference frame, is given by

$$p_{\parallel p,L} = p_{p,L} \cos \theta \quad (4.84)$$

The Lorentz factor  $\gamma_{PL}$  can be expressed as

$$\gamma_{PL} = 1 + \frac{E_L}{m} \quad (4.85)$$

where  $E_L$  is the projectile kinetic energy in MeV/nucleon and  $m$  is the nucleon mass. Similarly, the relative speed can be expressed as

$$\beta_{PL} = \sqrt{1 - \frac{1}{\gamma_{PL}^2}} \quad (4.86)$$

Thus using the above equations, the Lorentz transformation for the energy from the lab frame to the projectile frame can be given by

$$E_P = \gamma_{PL} (E_L - \beta_{PL} p_L) \quad (4.87)$$

and the inverse transformation is given by

$$E_L = \gamma_{PL} (E_P + \beta_{PL} p_P) \quad (4.88)$$

In the similar manner, the conversion of the double differential cross sections from the lab frame to the projectile frame and vice versa can be obtained by

$$\frac{\partial^2 \sigma}{\partial E_L \partial \Omega_L} = \frac{\sin \theta_p}{\sin \theta_L} \frac{\partial^2 \sigma}{\partial E_p \partial \Omega_p} \quad (4.89)$$

where  $\theta_{p,L}$  represent the scattering angle in the projectile and the lab frame respectively and the transformation for angles from the lab frame to the projectile frame is given by

$$\tan \theta_L = \frac{\sin \theta_p}{\gamma_{pL} (\cos \theta_p + \varphi_p)} \quad (4.90)$$

with  $\varphi_p$  being defined as the ratio of the projectile velocity to the velocity of the outgoing particle. A detailed description of the frame transformations is given in reference [82].

## 5. Results

### 5.1. Comparison of Contributions of the Higher Order Correction Terms

Using the formalism described in the previous sections, comparisons of the total abrasion and the double differential cross sections for various projectile-target combinations at different energies and scattering angles have been calculated. The derivations of the higher order correction terms to the phase function were performed using high energy approximations, thus it is of interest to calculate the contributions of the corrections terms in the calculation of various cross sections, and also evaluate the stability of the approximations at different projectile energies.

We studied the contributions of the higher order correction terms in the calculation of the total abrasion cross section. It was observed that the first and the second order corrections terms had a significant contribution towards the total abrasion cross section. The amplitude of the correction terms was higher at the lower energies, with over a factor of one for the energies below 200 MeV/nucleon. The correction terms became smaller with the increasing energy. While the first two correction terms were stable at the lower energies, the third and the fourth correction term approximations fell apart for the energies below 100 MeV/nucleon, yielding extremely large negative results since at smaller energies the exponentials of correction terms become too large and unstable. The contributions from the third and the fourth correction terms were comparatively small at all energies above 100 MeV/nucleon and didn't have any significant impact on the total abrasion cross section.

Table (2) and (3) present the total abrasion cross section with contributions from the four correction terms at different incident energies for  $^{12}\text{C}$  projectile incident on  $^{27}\text{Al}$  Aluminum target at  $10^\circ$  scattering angle, and  $^{20}\text{Ne}$  projectile on  $^{16}\text{O}$  Oxygen target at  $20^\circ$  scattering angle.



Table 2: Total Abrasion Cross Section with Correction Terms for  $^{12}\text{C}$  on  $^{27}\text{Al}$  at 10 Degrees

Energy (MeV/Nucleon )	$\sigma \sum_{i=1} \chi_i$ (mb)	$\sigma \sum_{i=0}^1 \chi_i$ (mb)	$\sigma \sum_{i=0}^2 \chi_i$ (mb)	$\sigma \sum_{i=0}^3 \chi_i$ (mb)	$\sigma \sum_{i=0}^4 \chi_i$ (mb)
100	784.32	1368.40	1640.73	1690.05	1688.81
200	774.21	1074.81	1119.02	1122.45	1122.45
300	773.91	1022.38	1050.22	1051.92	1051.92
500	780.40	1035.56	1060.73	1062.08	1062.82
1000	783.19	1004.09	1019.68	1020.28	1020.28
3000	781.38	864.69	866.73	866.76	866.76
5000	781.60	833.82	834.58	834.59	834.59
10000	781.97	805.01	805.15	805.15	805.15

Table 3: Total Abrasion Cross Section with Correction Terms for  $^{20}\text{Ne}$  on  $^{16}\text{O}$  at 20 Degrees

Energy (MeV/Nucleon )	$\sigma \sum_{i=1} \chi_i$ (mb)	$\sigma \sum_{i=0}^1 \chi_i$ (mb)	$\sigma \sum_{i=0}^2 \chi_i$ (mb)	$\sigma \sum_{i=0}^3 \chi_i$ (mb)	$\sigma \sum_{i=0}^4 \chi_i$ (mb)
100	1476.63	2259.92	2577.92	2635.33	2633.68
200	1259.47	1604.47	1654.65	1658.55	1658.55
300	1251.13	1529.00	1559.52	1561.36	1561.36
500	1329.27	1604.52	1630.31	1631.64	1631.64
1000	1395.25	1623.86	1638.73	1639.27	1639.27
3000	1343.94	1421.68	1423.27	1423.29	1423.29
5000	1346.69	1390.02	1390.49	1390.50	1390.50
10000	1348.77	1364.36	1364.43	1364.43	1364.43

The comparison of the double differential cross sections for the different projectile-target combination at different energies and scattering angles concurs with the calculations of the total abrasion cross sections. The major contributions to the double differential cross sections were from the first two order correction terms, while the contributions of the third and the fourth order terms were comparatively negligible.

Figures (12) and (13) present the comparison of the double differential cross section for  $^{12}\text{C}$  on  $^{20}\text{Ne}$  for the abrasion and the ablation process respectively. The calculations are performed at 100 MeV/nucleon incident energy for  $10^\circ$  scattering angle. Similarly, figures (15) and (16) present the similar calculations for  $^{14}\text{N}$  on  $^{12}\text{C}$  at 400 MeV/nucleon incident energy at  $40^\circ$  scattering angle.

The calculations with two correction terms are represented by the red lines with cross marks and the four correction terms are represented by the blue lines with circles.

In figures (12) and (14), the solid lines represent the projectile contributions to the double differential cross sections from the abrasion process, while the dotted lines represent the target contributions.

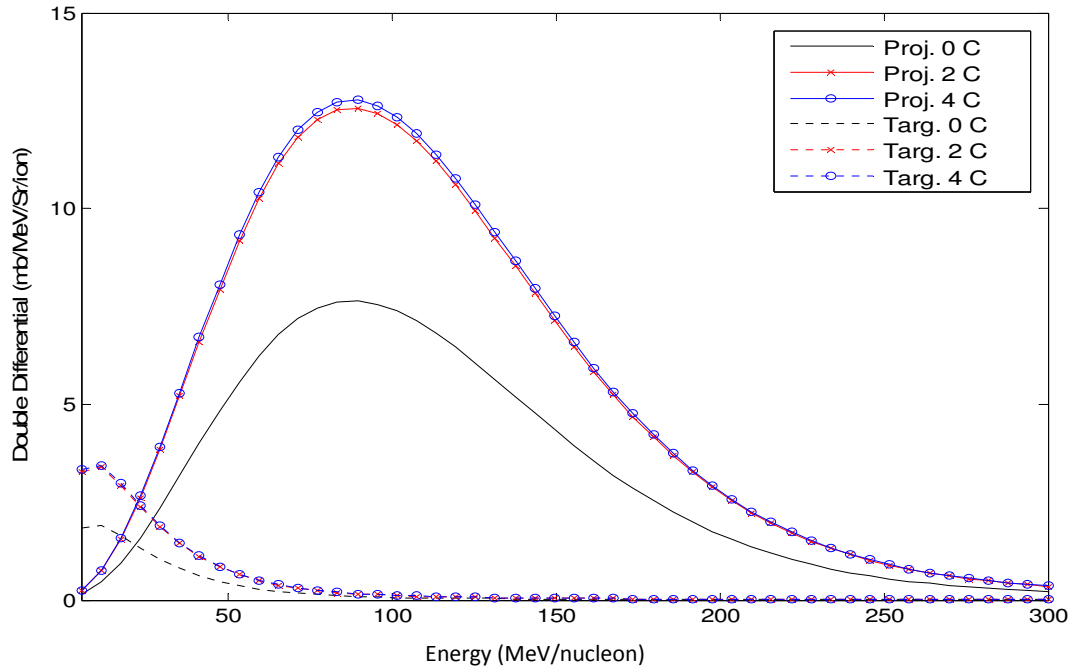


**Figure 12:** Comparison of differential cross section from **abrasion process** for 100 MeV/nucleon  $^{12}\text{C}$  on  $^{20}\text{Ne}$  at  $20^\circ$  scattering angle for 0, 2 and 4 correction terms.

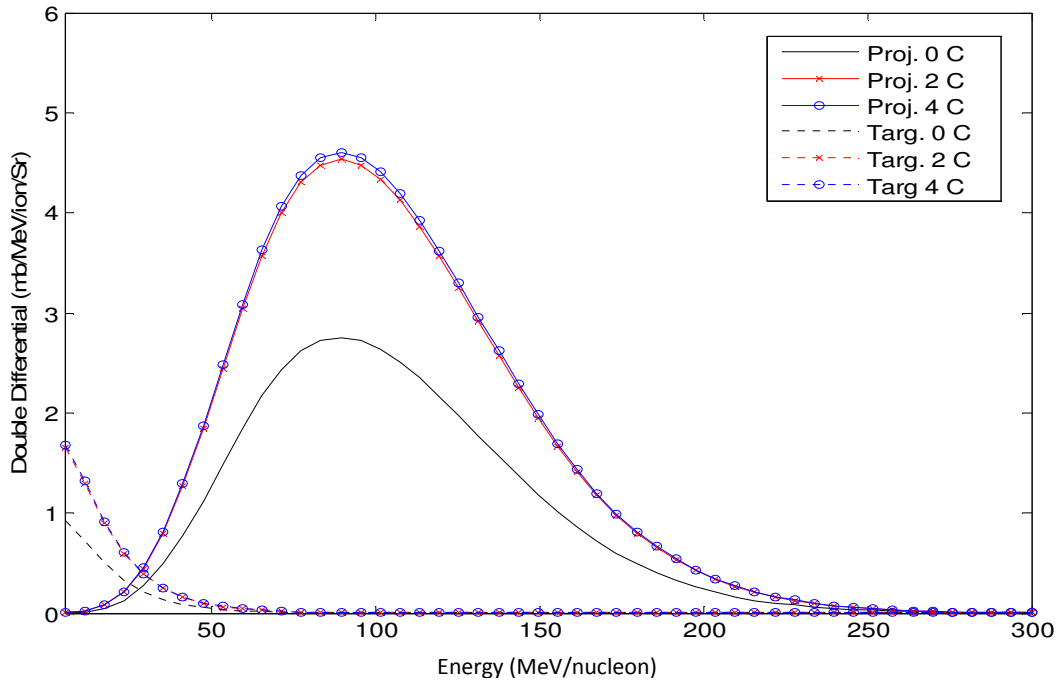


**Figure 13:** Comparison of differential cross section from **ablation process** for 100 MeV/nucleon  $^{12}\text{C}$  on  $^{20}\text{Ne}$  at  $20^\circ$  scattering angle for 0, 2 and 4 correction terms.

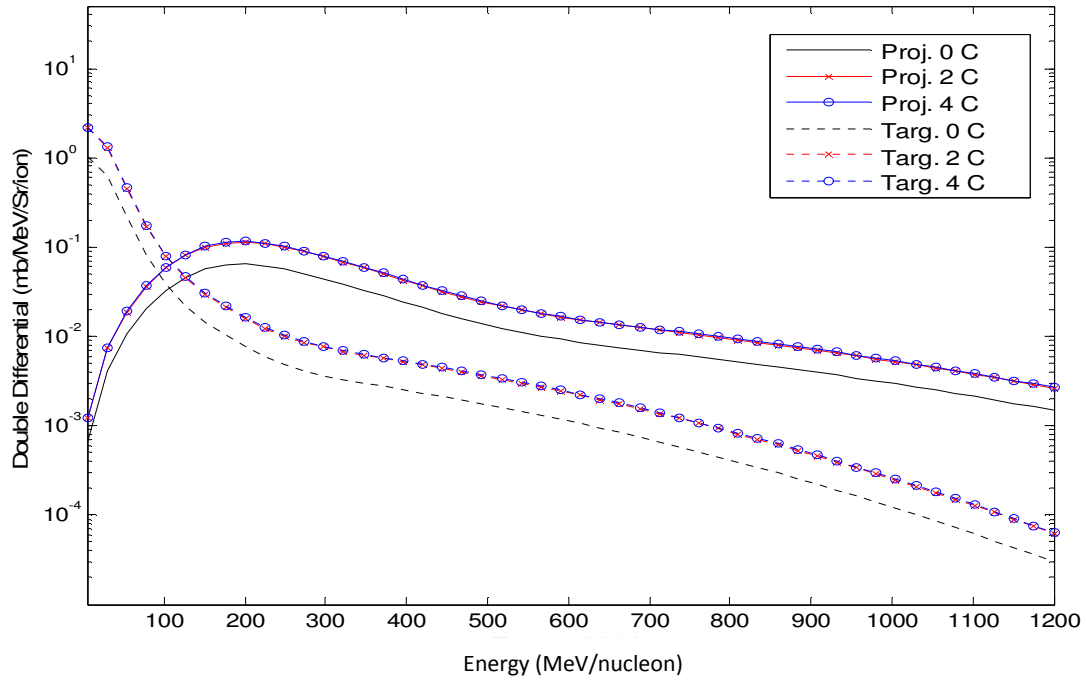


**Figure 14:** Comparison of differential cross section from **abrasion process** for 400 MeV/nucleon  $^{14}\text{N}$  on  $^{12}\text{C}$  at  $40^\circ$  scattering angle for 0, 2 and 4 correction terms.

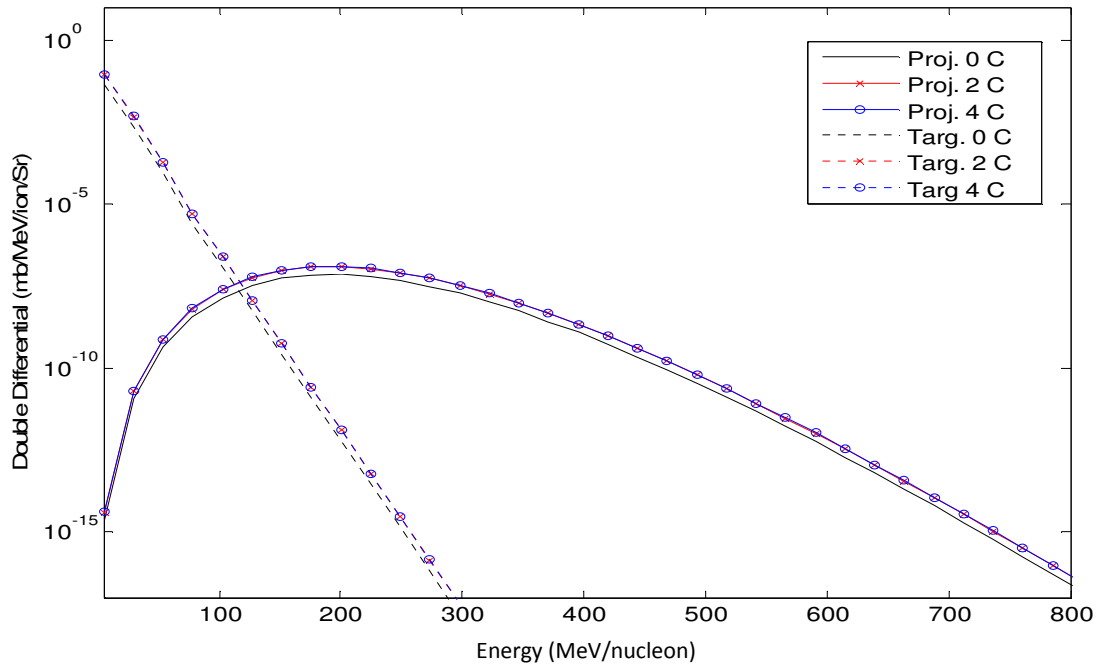


**Figure 15:** Comparison of differential cross section from **ablation process** for 400 MeV/nucleon  $^{14}\text{N}$  on  $^{12}\text{C}$  at  $40^\circ$  scattering angle for 0, 2 and 4 correction terms.

## 5.2. Comparison to the Experimental Data

A comparison of the calculations from present work to the experimental data from Nakamura and Heilbronn [3] has been done. The main purpose of the comparison is to examine the accuracy of the current calculations and also examine the effects of adding higher order correction terms. Since the contributions from the third and the fourth order correction terms were not significant, and the first two correction terms were more stable at the lower energies, only the first two correction terms are used in the calculations.

In figure (16) through (37), representative calculations of the double differential cross sections for the secondary neutron production are made at different scattering angles for the following reactions, with the experimental target exit beam energies listed in the parenthesis:

- 1) 290 MeV/nucleon  $^{12}\text{C}$  beam colliding on  $^{12}\text{C}$  target (272.3 MeV/nucleon)
- 2) 400 MeV/nucleon  $^{20}\text{Ne}$  beam colliding on  $^{64}\text{Cu}$  target (352.9 MeV/nucleon)
- 3) 400 MeV/nucleon  $^{14}\text{N}$  beam colliding on  $^{12}\text{C}$  target (382.8 MeV/nucleon)
- 4) 290 MeV/nucleon  $^{12}\text{C}$  beam colliding on  $^{64}\text{Cu}$  target (256.6 MeV/nucleon)

The comparisons show that the double differential cross sections increased with two correction terms added. There was an improvement when compared to experimental data at the lower scattering angles. At angles larger than 30 degrees, current work under predicts the double differential cross sections compared to the experimental data. Also, the relatively smaller cross sections below the beam energy are mainly caused due to lack the isobar formation and decay in the present work. In general, the calculations showed a fairly good agreement to the overall shape of double differential spectrum from the experimental data.

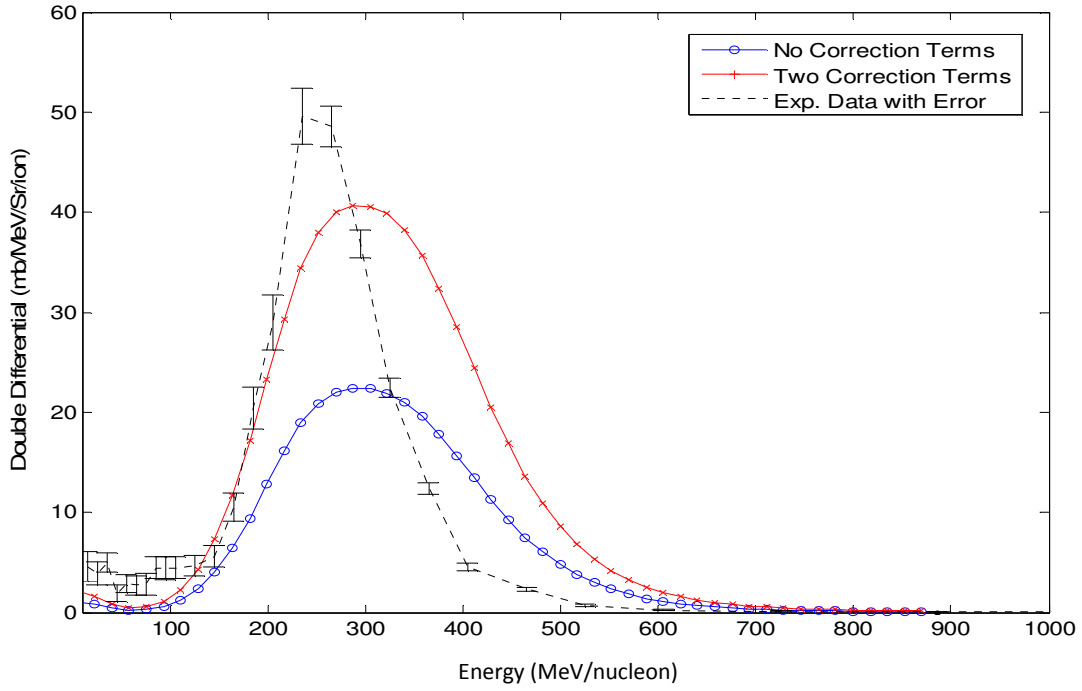


**Figure 16:** Double differential cross sections for 290 MeV/nucleon  $^{12}\text{C}$  on  $^{12}\text{C}$  at 5 degrees

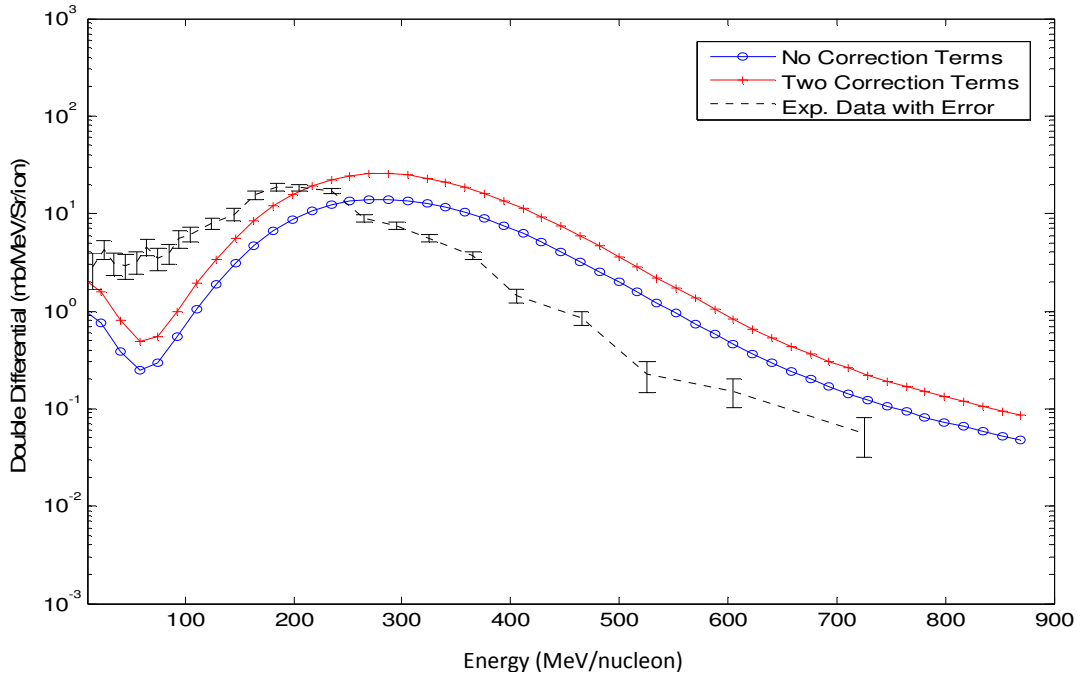


**Figure 17:** Double differential cross sections for 290 MeV/nucleon  $^{12}\text{C}$  on  $^{12}\text{C}$  at 10 degrees

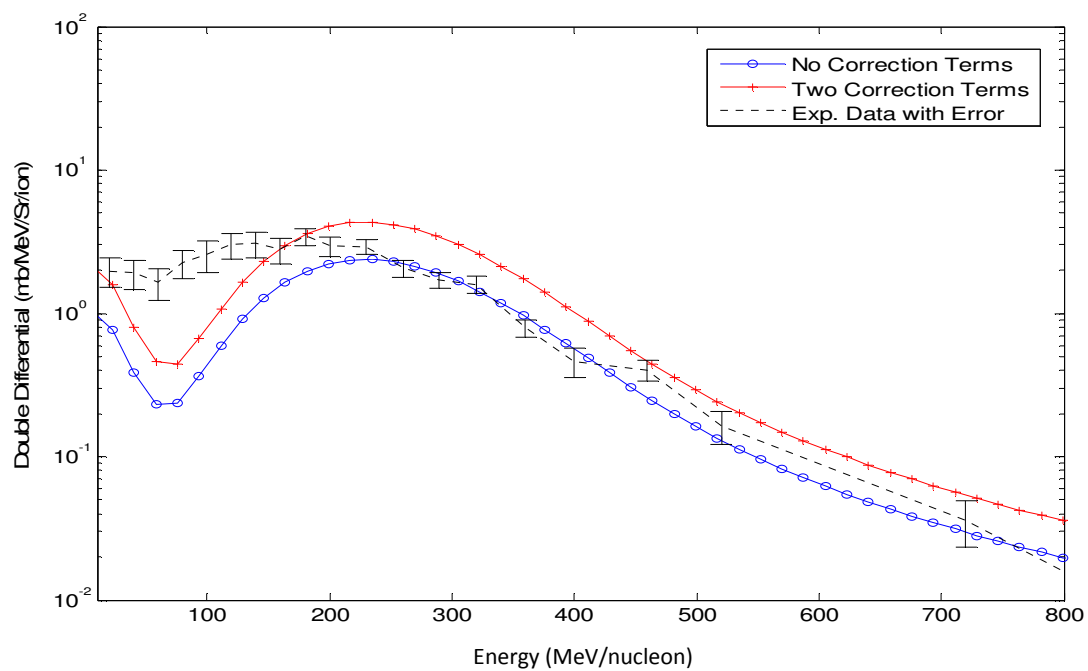


**Figure 18:** Double differential cross sections for 290 MeV/nucleon  $^{12}\text{C}$  on  $^{12}\text{C}$  at 20 degrees

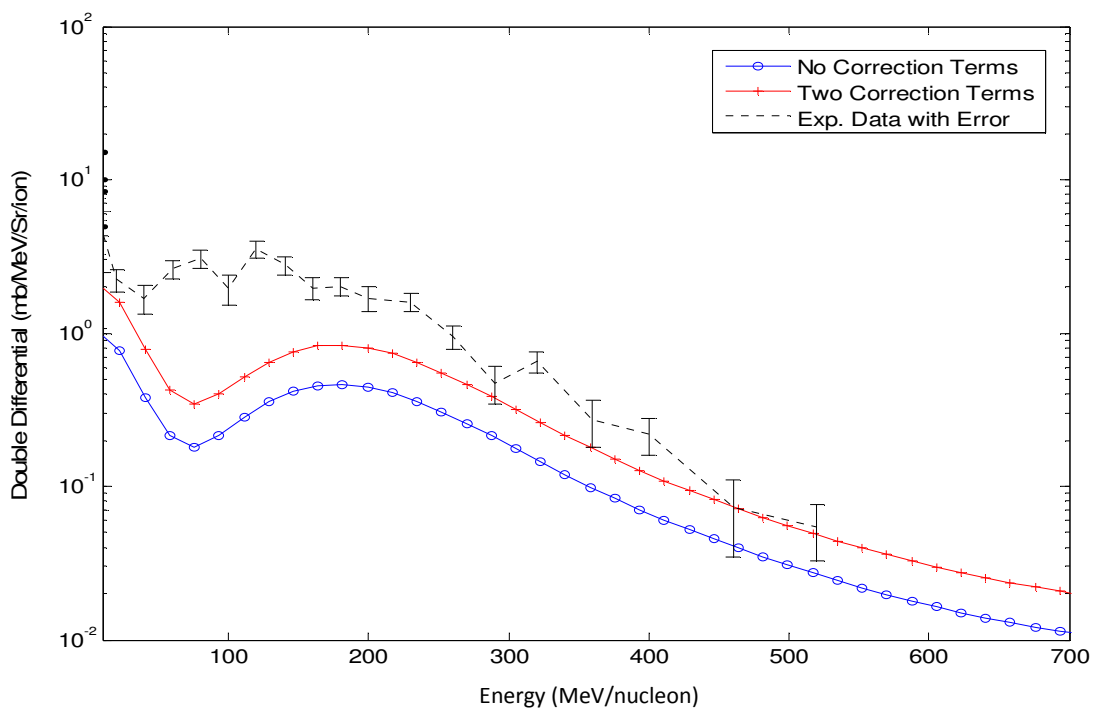


**Figure 19:** Double differential cross sections for 290 MeV/nucleon  $^{12}\text{C}$  on  $^{12}\text{C}$  at 30 degrees

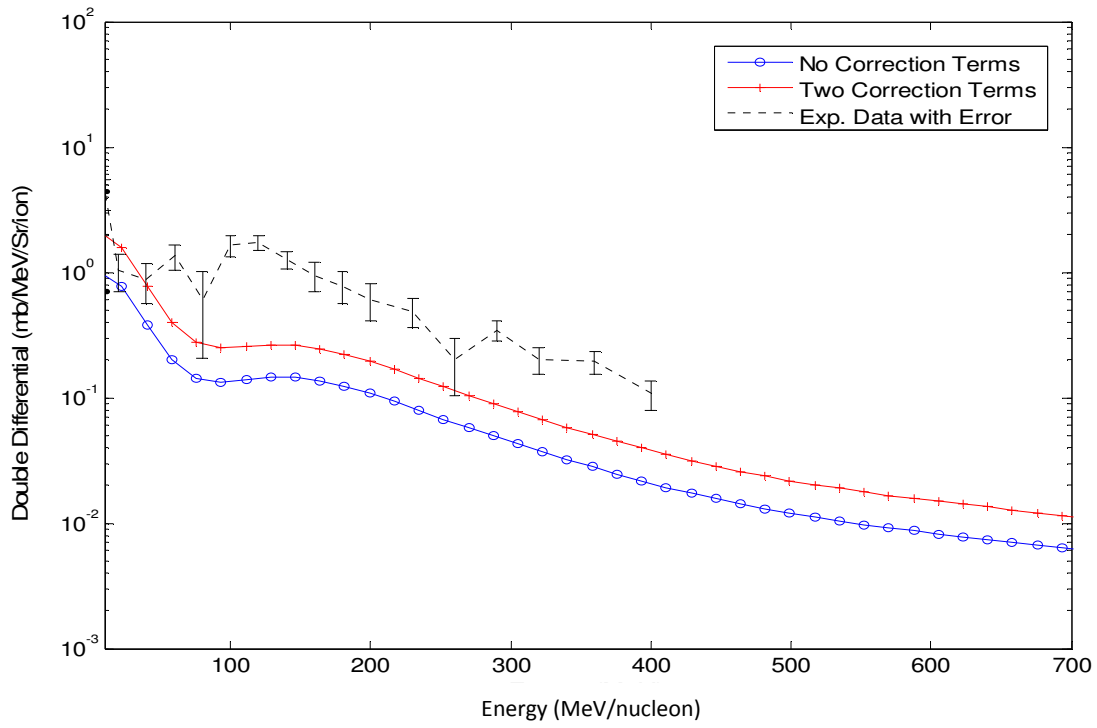


**Figure 20:** Double differential cross sections for 290 MeV/nucleon  $^{12}\text{C}$  on  $^{12}\text{C}$  at 40 degrees

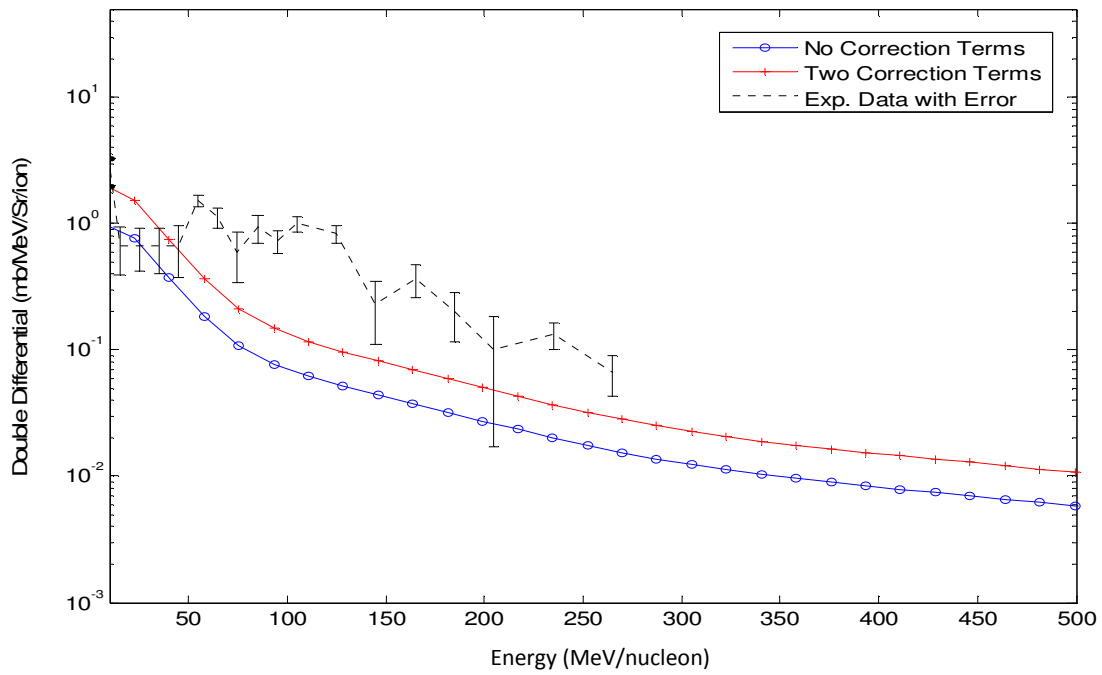


**Figure 21:** Double differential cross sections for 290 MeV/nucleon  $^{12}\text{C}$  on  $^{12}\text{C}$  at 60 degrees



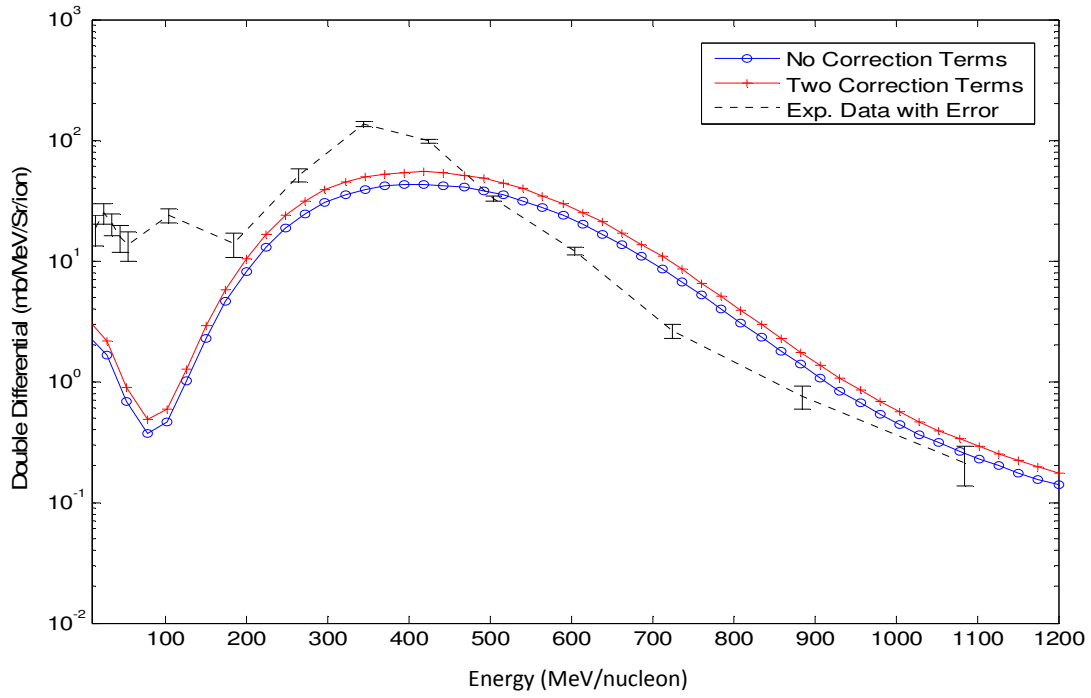


**Figure 22:** Double differential cross sections for 400 MeV/nucleon  $^{20}\text{Ne}$  on  $^{64}\text{Cu}$  at 5 degrees

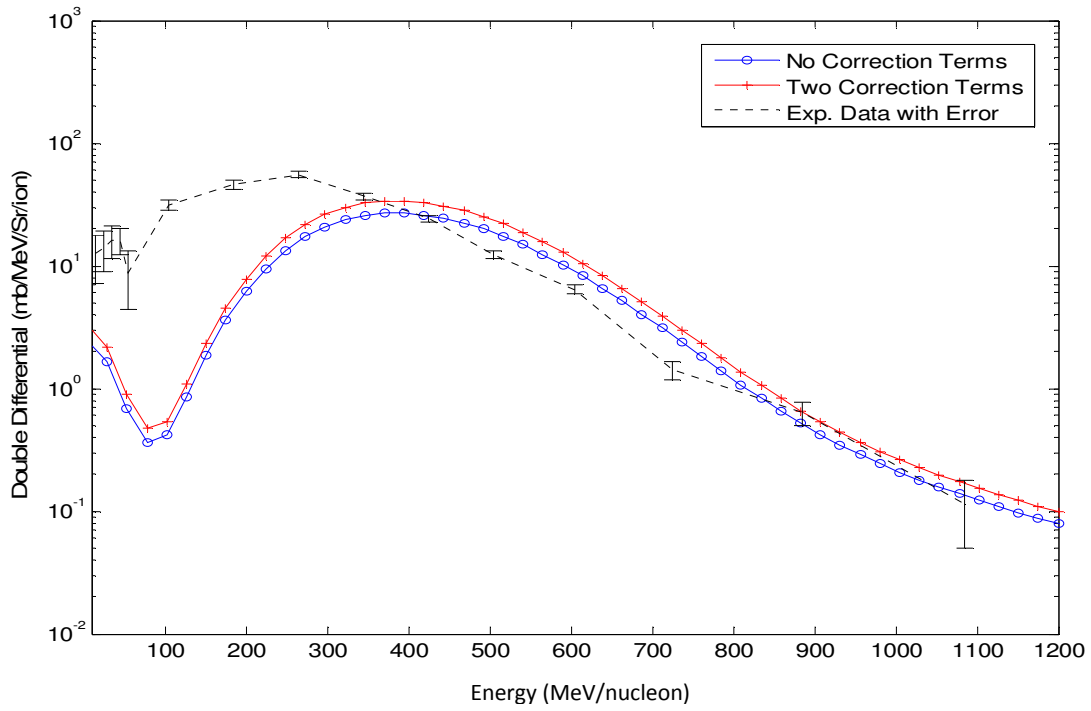


**Figure 23:** Double differential cross sections for 400 MeV/nucleon  $^{20}\text{Ne}$  on  $^{64}\text{Cu}$  at 10 degrees

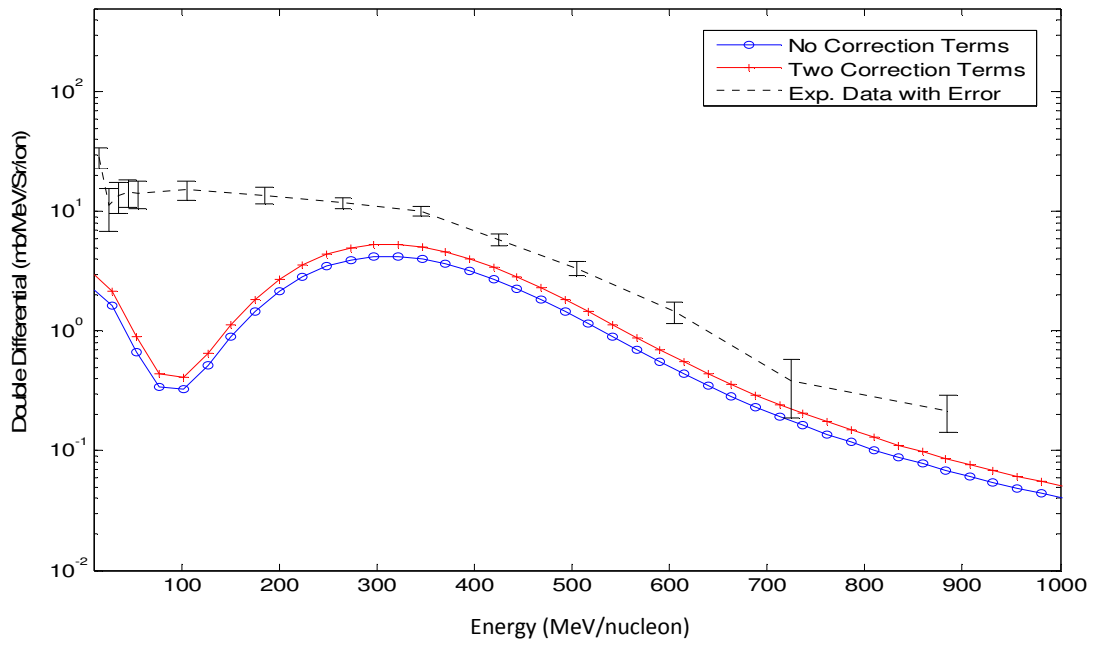


**Figure 24:** Double differential cross sections for 400 MeV/nucleon  $^{20}\text{Ne}$  on  $^{64}\text{Cu}$  at 20 degrees

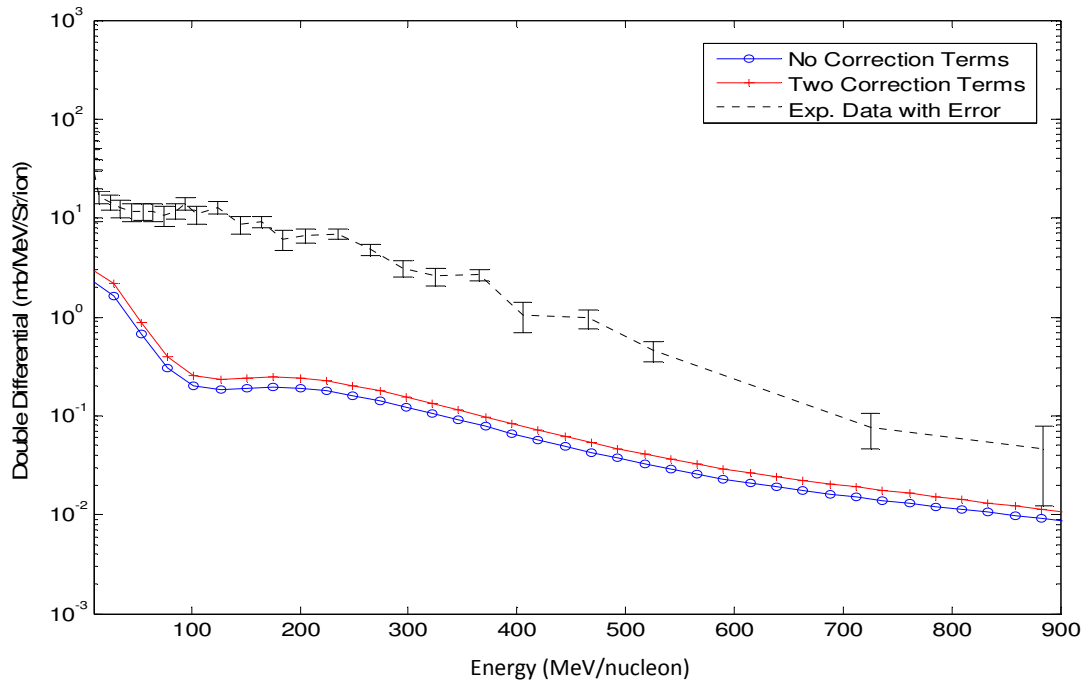


**Figure 25:** Double differential cross sections for 400 MeV/nucleon  $^{20}\text{Ne}$  on  $^{64}\text{Cu}$  at 40 degrees

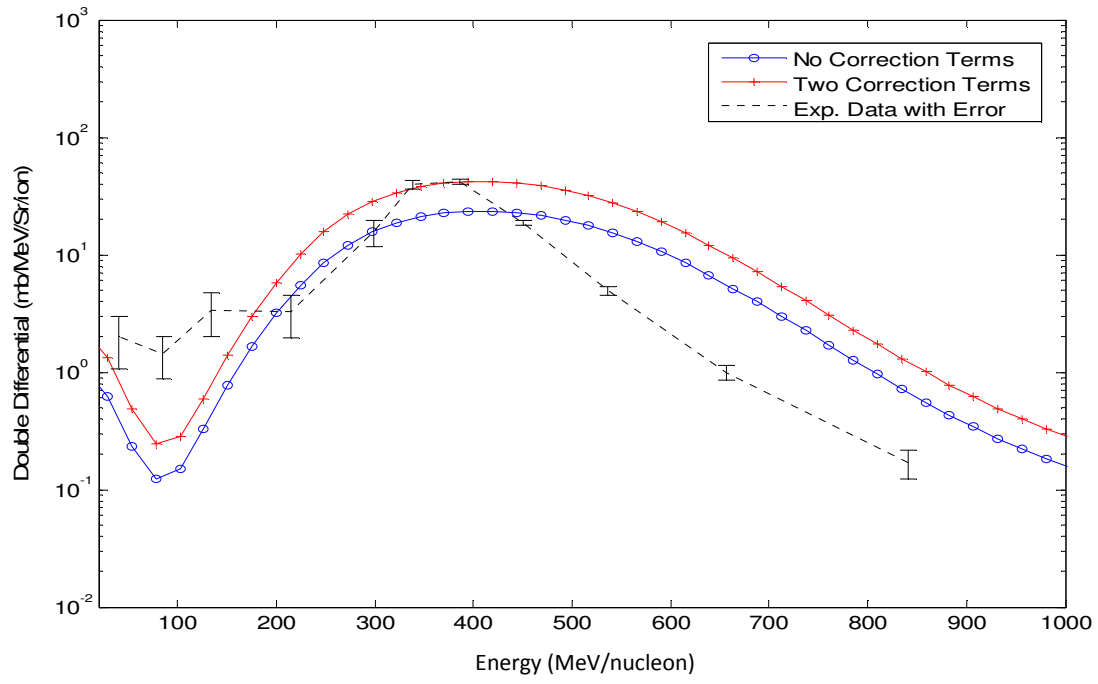


**Figure 26:** Double differential cross sections for 400 MeV/nucleon  $^{14}\text{N}$  on  $^{12}\text{C}$  at 5 degrees

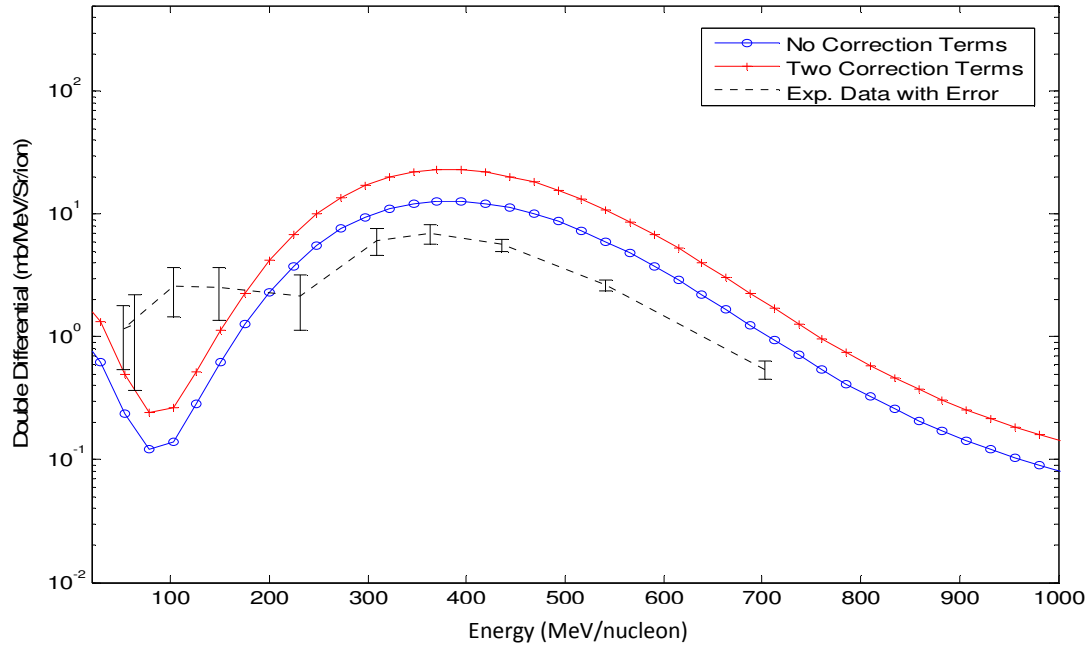


**Figure 27:** Double differential cross sections for 400 MeV/nucleon  $^{14}\text{N}$  on  $^{12}\text{C}$  at 10 degrees

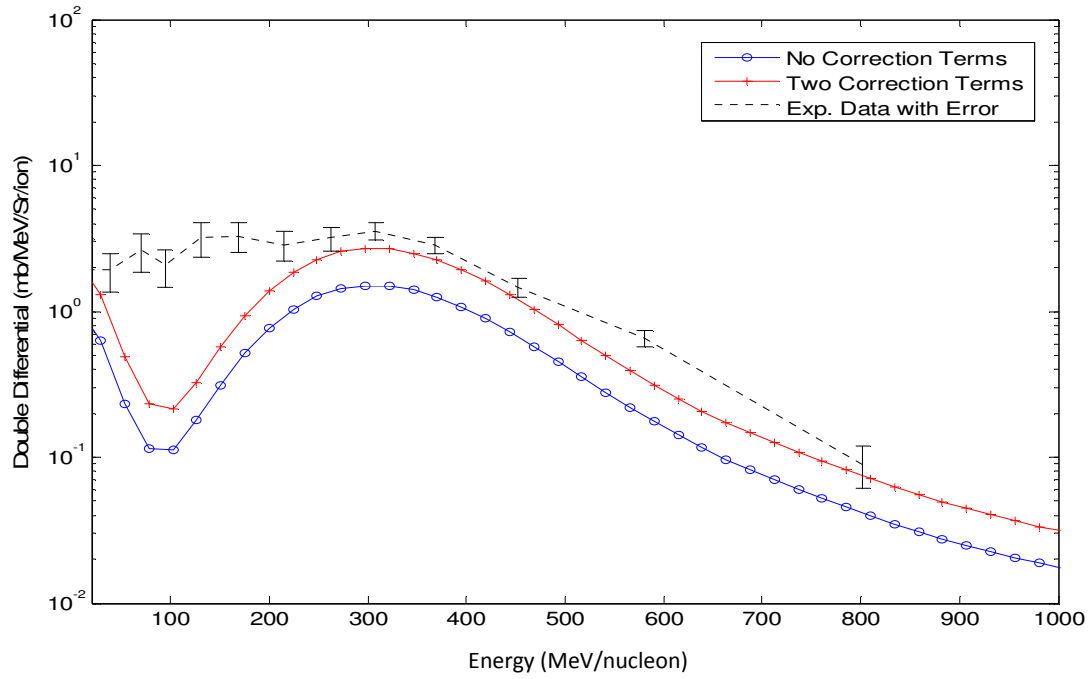


**Figure 28:** Double differential cross sections for 400 MeV/nucleon  $^{14}\text{N}$  on  $^{12}\text{C}$  at 20 degrees

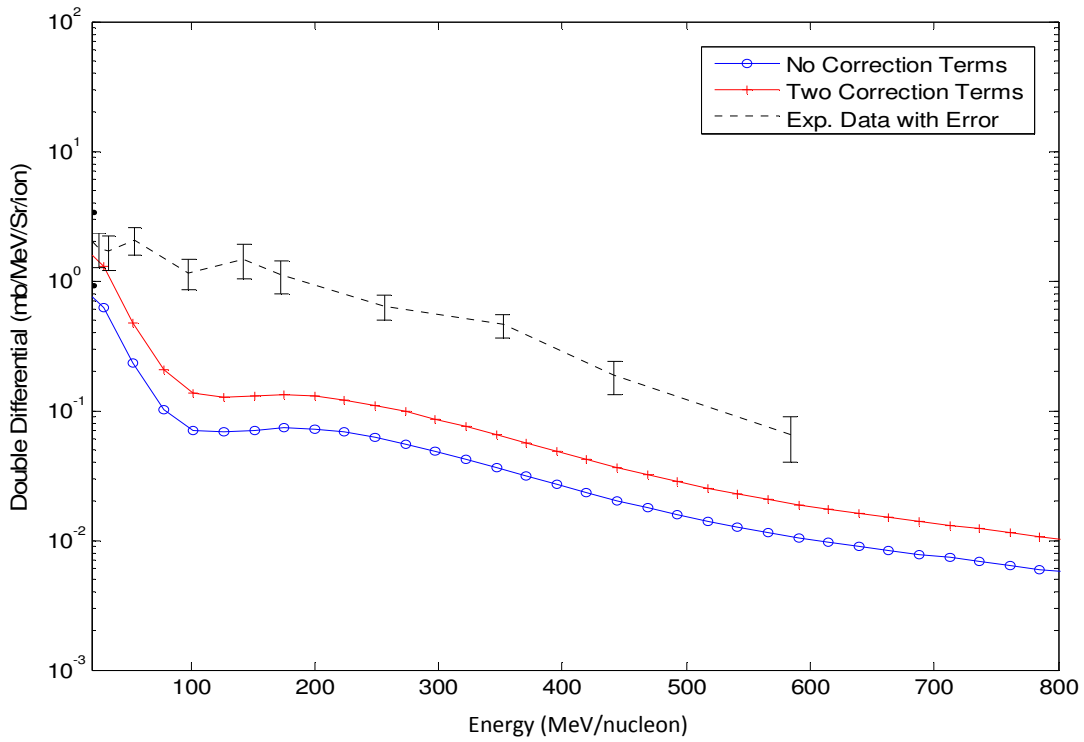


**Figure 29:** Double differential cross sections for 400 MeV/nucleon  $^{14}\text{N}$  on  $^{12}\text{C}$  at 40 degrees

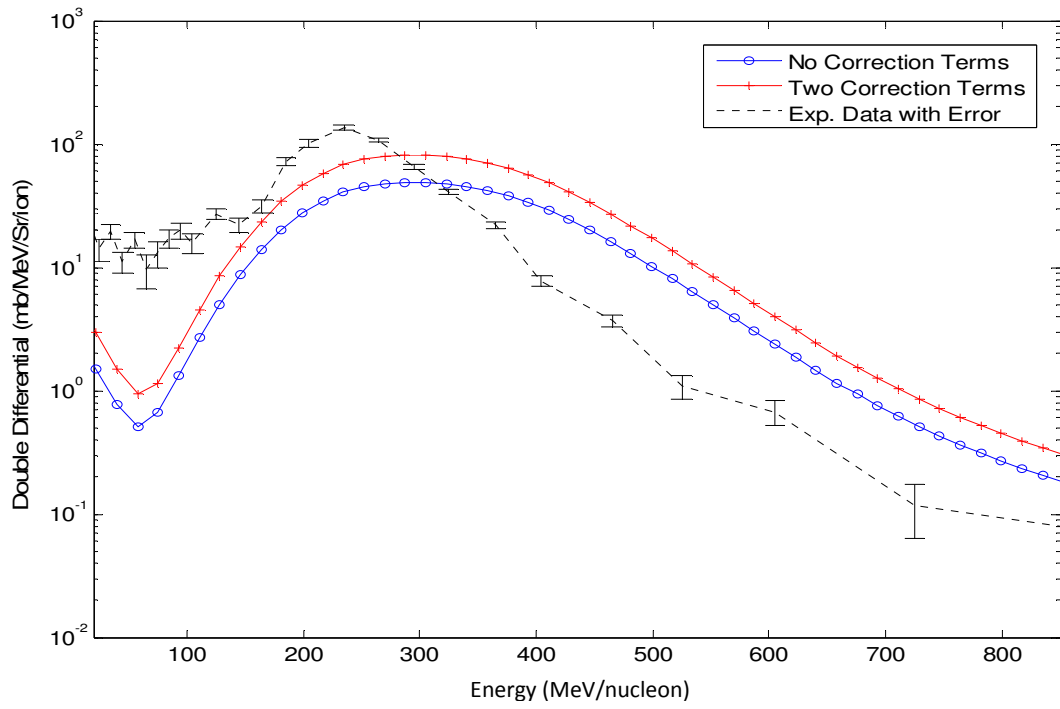


**Figure 30:** Double differential cross sections for 290 MeV/nucleon  $^{12}\text{C}$  on  $^{64}\text{Cu}$  at 5 degrees

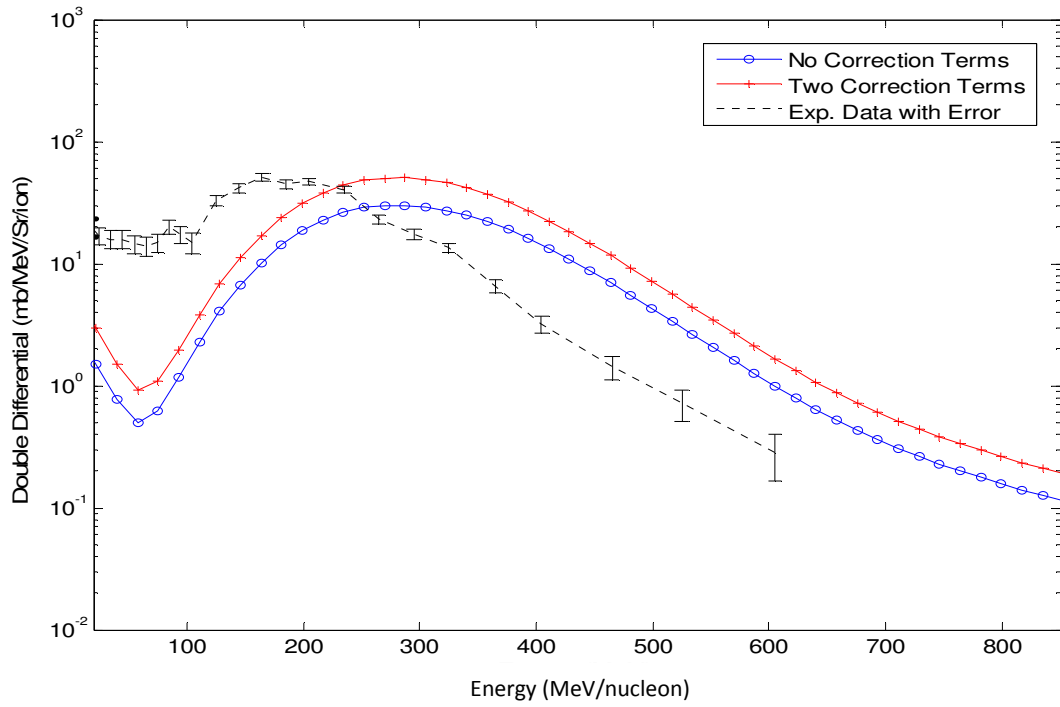


**Figure 31:** Double differential cross sections for 290 MeV/nucleon  $^{12}\text{C}$  on  $^{64}\text{Cu}$  at 10 degrees

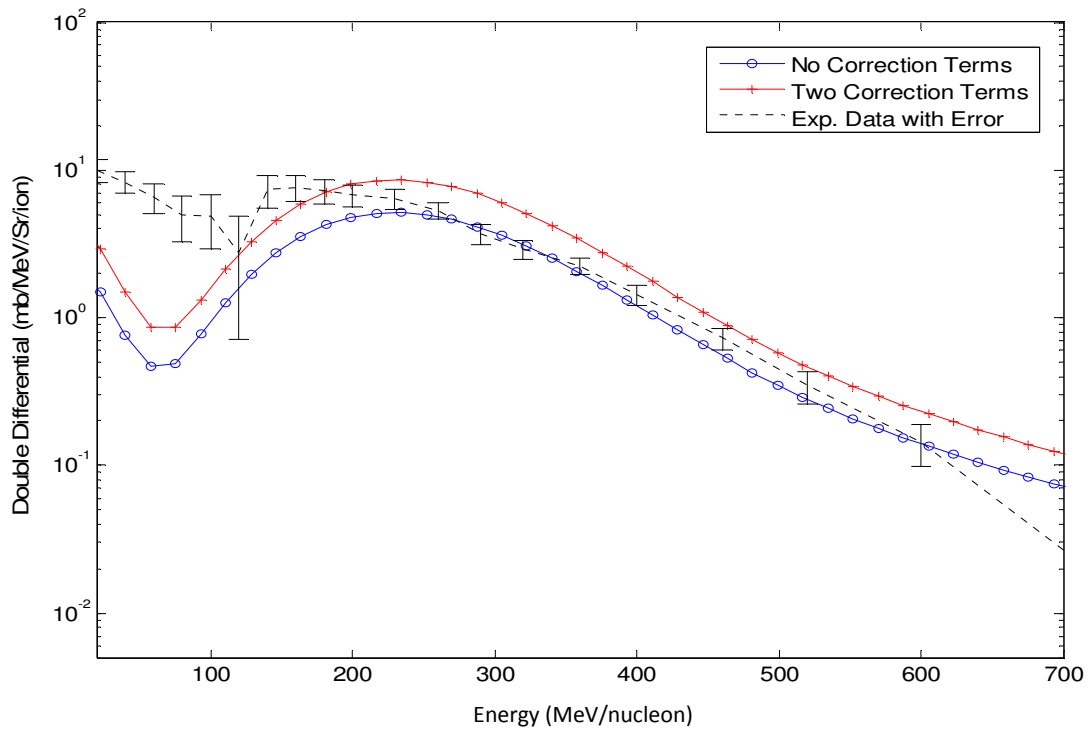


**Figure 32:** Double differential cross sections for 290 MeV/nucleon  $^{12}\text{C}$  on  $^{64}\text{Cu}$  at 20 degrees

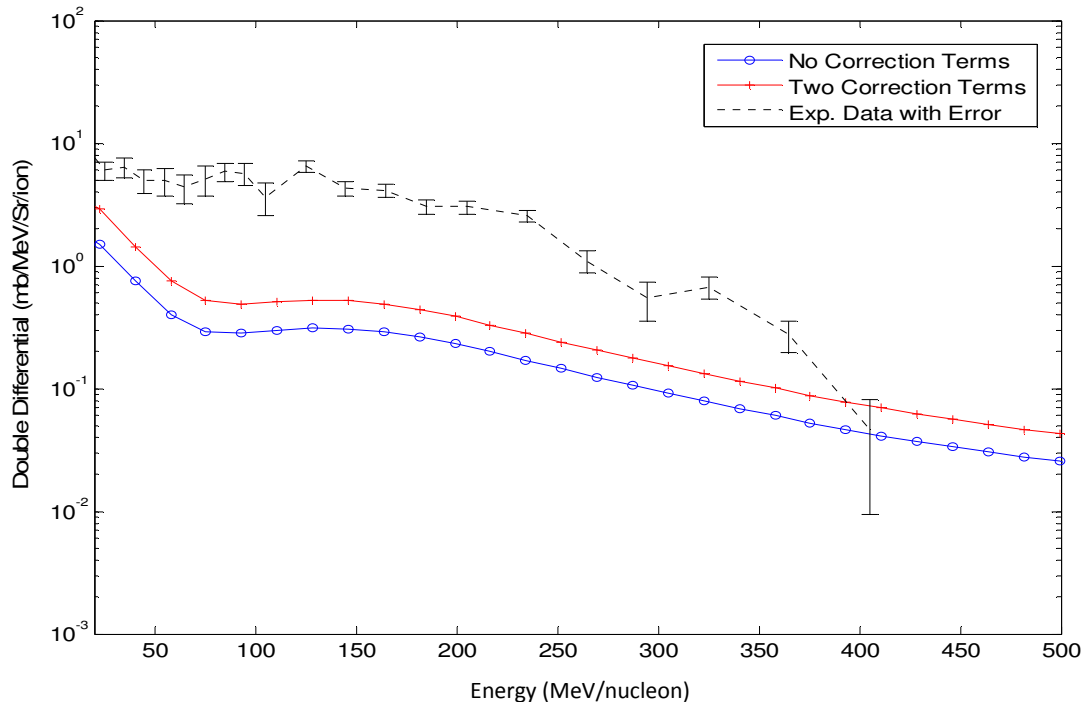


**Figure 33:** Double differential cross sections for 290 MeV/nucleon  $^{12}\text{C}$  on  $^{64}\text{Cu}$  at 40 degrees

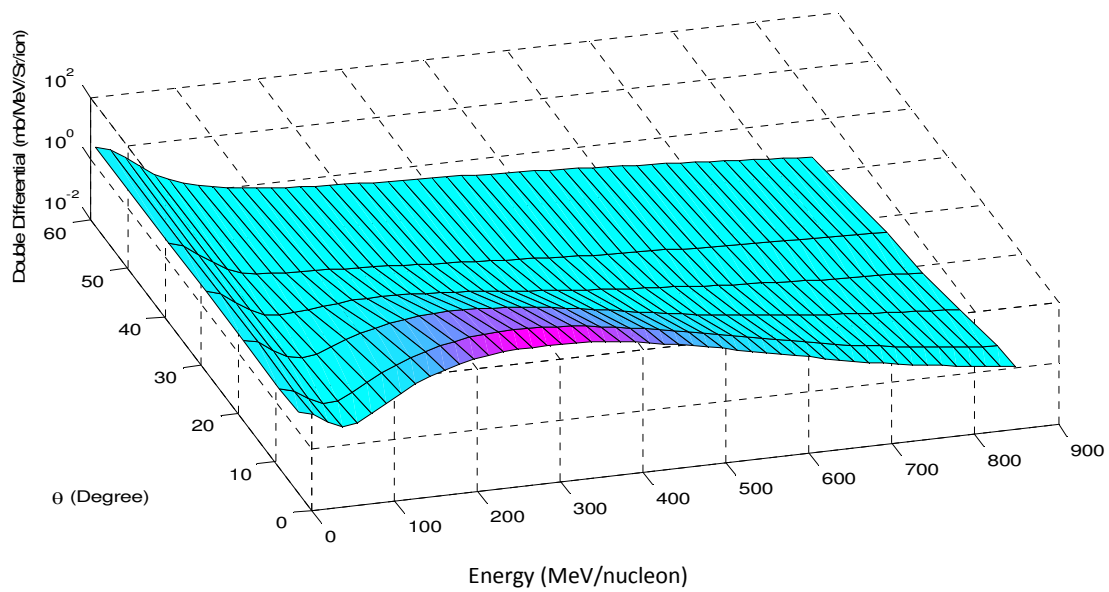


**Figure 34:** Surface plot of double differential cross section with two correction terms for 290 MeV/nucleon  $^{12}\text{C}$  on  $^{12}\text{C}$

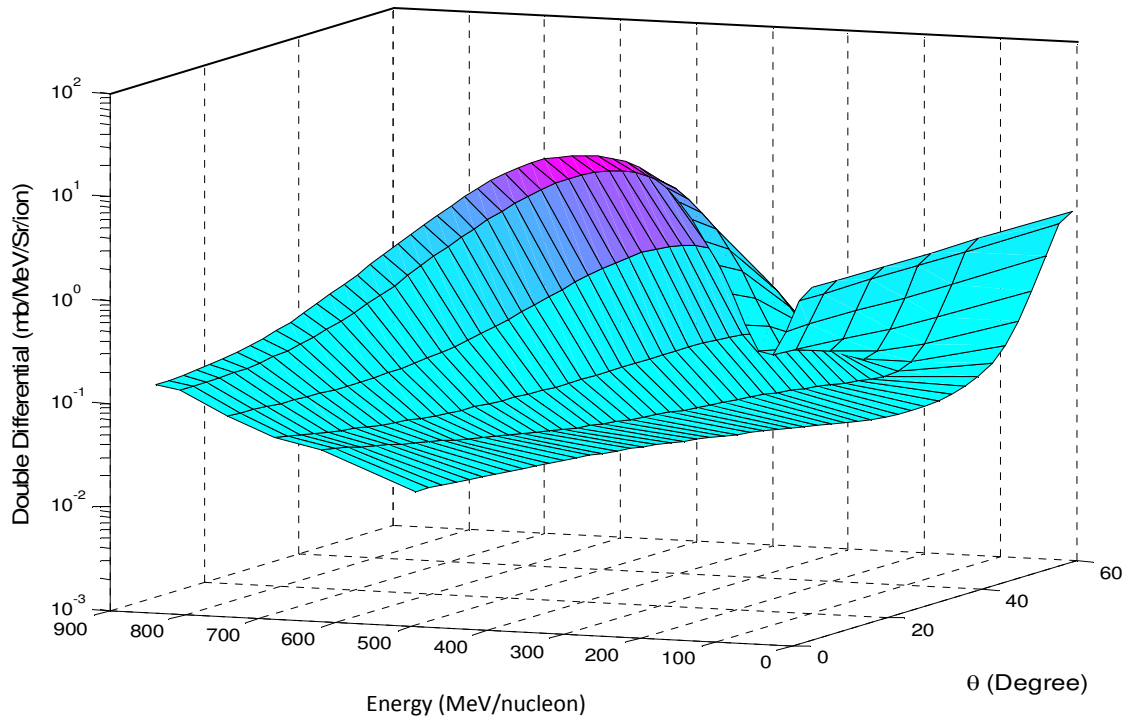


**Figure 35:** Same as Figure (34), except rotated

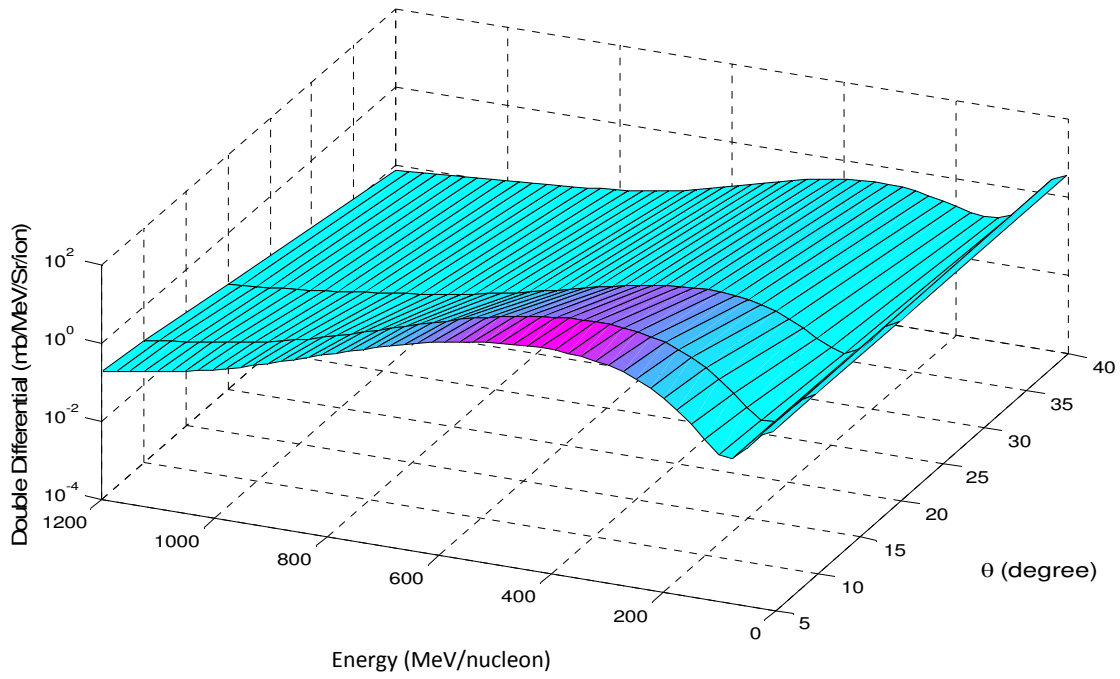


**Figure 36:** Surface plot of double differential cross section with two correction terms for 400 MeV/nucleon  $^{20}\text{Ne}$  on  $^{64}\text{Cu}$

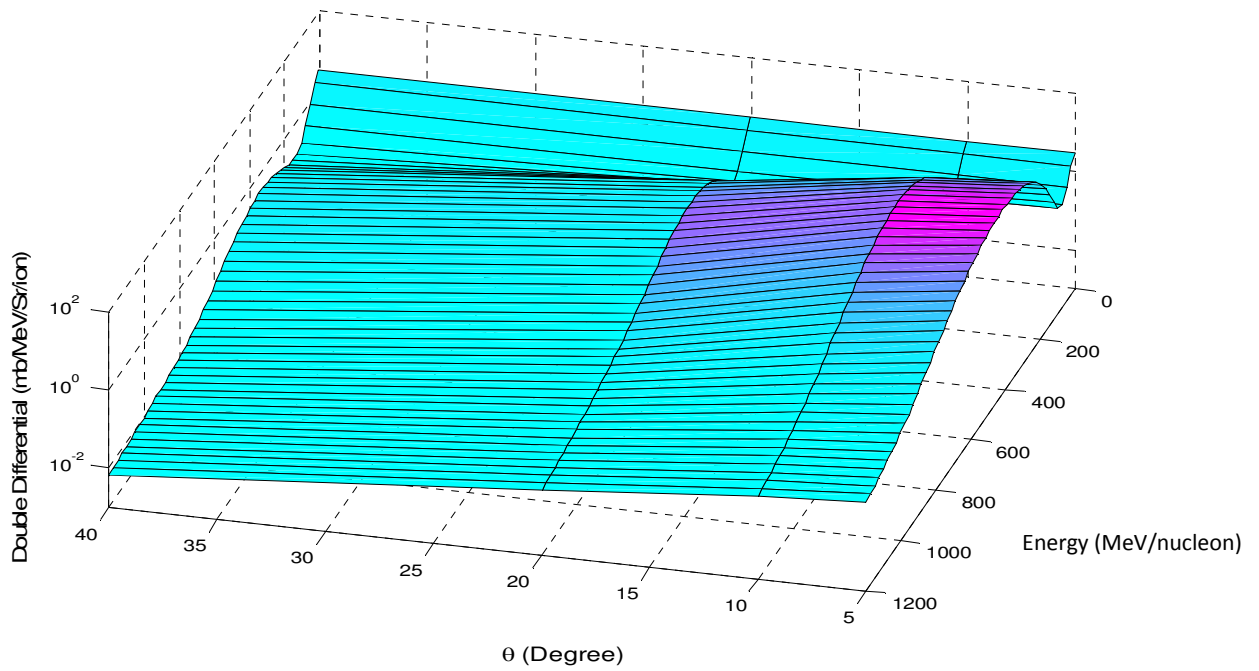


**Figure 37:** Same as Figure (36), except rotated



## 6. Conclusions and Future Work

The primary focus of this work was to relax the inherent small angle approximation in the formulation of the abrasion-ablation model. The existing abrasion formulation is based on the Eikonal approximations developed from the Glauber multiple scattering theory, considered in the high energy, small angle approximations. We used the Eikonal expansions and their higher order correction terms to the phase functions, developed by Wallace [19],[59] to re-derive the abrasion formulation, and thus derived four higher order correction terms to the phase factor. The optical potential in the development of the phase factor was derived using Gaussian approximations to the single particle nuclear densities. Previously, the single particle densities were described using a harmonic well distribution for lighter nuclei ( $A < 20$ ) and the Wood-Saxon distribution for heavier nuclei ( $A \geq 20$ ), which leads to too many terms in the calculation of the optical potential and becomes difficult to evaluate for the higher order correction terms. The use of the Gaussian approximations to the nuclear densities allowed for the optical potential to be expressed as a single term and thus was easier to evaluate. The validity of the Gaussian approximations was subsequently studied by comparing the total absorption cross sections calculated from the current model to the experimental data and the energy dependent parameterization from previous studies [77].

The improved formalism with four higher order correction terms was used to evaluate the total abrasion and the double differential cross sections. A comparison between the contributions from higher order terms in the calculation of the cross sections was done. It was observed that the major contribution to the total abrasion and the double differential cross sections was from the first two correction terms. The contribution from the third and the fourth correction terms was

fairly small. It was seen that the third and the fourth order corrections terms were unstable for the incident projectile energies below 100 MeV/nucleon, while the first two correction terms were stable at the lower energies. Since the contributions of the third and the fourth order correction terms were fairly small, and unstable at lower energies, only two higher order correction terms were used in the comparison of the neutron double differential cross sections to the experimental data. The comparisons for various projectile-target data at different incident projectile energies showed a fairly good agreement at smaller scattering angles. The current model under-predicted the cross sections at larger scattering angles, however an improvement in the comparison was seen with addition of the correction terms. The model also under predicted the cross section below the beam energy, which is due to lack of isobar formation in the current formalism. Further, the difference in the double differential cross section peaks compared to the experimental data are due to the difference between target exit energies of the beam from the experiment and the entrance beam energies used in the calculations. A better fit for cross section peaks when compared to experimental data can be expected by using an average of the entrance and exit energies in the calculations, which are slightly below the entrance energies.

The present work also indicated many areas of further investigation. These included:

- a) Implementation of the higher order correction terms developed in the present work to the current HZE transport codes and fragmentation models.
- b) Incorporation of the isobar formation and decay model to the current formalism. This will improve the double differential cross section predictions below the incident beam energy.
- c) Further investigation of the neutron momentum distribution models to improve the cross section prediction at larger scattering angles.

## **LIST OF REFERENCES**

- [1] J. W. Wilson, W. Schimmerling, L. W. Townsend, G. S. Khandelwal, F. Khan, J. E. Nearly, F. A. Cucinotta, and J. Norbury, "Transport methods and interactions for space radiation," NASA RP-1257, National Technical Information Service, 1991.
- [2] S. I. Sriprisan, "An improved knockout-ablation-coalescence model for predicting of secondary neutron and light ion production in cosmic ray interactions. Ph.D Dissertation, University of Tennessee," pp. 2-8, 2008.
- [3] T. Nakamura and L. H. Heilbronn, *Handbook on Secondary Particle Production and Transport by High-Energy Heavy Ions*. New Jersey (NJ): World Scientific, 2006.
- [4] F. A. Cucinotta, J. W. Wilson, and L. W. Townsend, "Abrasion-ablation model for neutron production in heavy ion collisions," *Nuclear Physics. A*, vol. 619, pp. 202-12, 1997.
- [5] F. A. Cucinotta, J. W. Wilson, and L. W. Townsend, "Abrasion-Ablation Model for Neutron Production in Heavy Ion Reactions," *NASA Technical Memorandum-4656*, 1995.
- [6] R. J. Glauber, "High energy collision theory," in *Lectures in theoretical physics*. vol. 1, W. E. Brittin and L. G. Dunham, Eds., ed New York (NY): Wiley-Interscience, Inc., 1959, pp. 315-414.
- [7] J. Bowman, W. Swiatecki, and C. Tsang, "Abrasion and ablation of heavy ions," *LBL-2908, University of California*, pp. 391-394, 1973.
- [8] J. Hufner, K. Schafer, and B. Schurmann, "Abrasion-ablation in reactions between relativistic heavy ions," *Physical Review A*, vol. 12, pp. 1888-1897, 1975.
- [9] M. Giacomelli, L. Sihver, J. Skvarc, N. Yasuda, and R. Illie, "Projectile like fragment emission angles in fragmentation reactions of light heavy ions in the energy region  $< 200$  MeV/nucleon: Modeling and simulations," *Physical Review C*, vol. 6, pp. 1-11, 1969.
- [10] J. Hufner, "Heavy fragments produced in proton-nucleus and nucleus-nucleus collisions at relativistic energies," *Physics Reports*, vol. 125, pp. 129-185, 1985.
- [11] L. F. Oliveria, R. Donangelo, and J. O. Rasmussen, "Abrasion-ablation calculations of large fragment yeilds from relativistic heavy ion reactions," *Physical Review C*, vol. 19, pp. 826-833, 1979.

- [12] J. W. Wilson, "Multiple scattering of heavy ions, Glauber theory, and optical model," *Physics Letters B*, vol. 52, pp. 149-152, 1974B.
- [13] L. W. Townsend, J. W. Wilson, F. A. Cucinotta, and J. Norbury, "Comparison of abrasion model differences in heavy ion fragmentation: Optical versus geometric models," *Physical Review C*, vol. 34, pp. 1491-1494, 1986.
- [14] L. W. Townsend, "Abrasion cross sections for 20-Ne projectiles at 2.1 GeV/nucleon," *Canadian Journal of Physics*, vol. A355, pp. 505-532, 1983.
- [15] V. Franco, "Small-angle high energy scattering by deuterons," *Physics Review Letters*, vol. 16, pp. 944-947, 1966.
- [16] F. A. Cucinotta, "Theory of alpha-nucleus collisions at high energies," Ph.D Dissertation, Physics Department, Old Dominion University, 1988.
- [17] V. F. Weisskopf and D. H. Ewing, "On the yield of nuclear reactions with heavy elements," *Physical Review*, vol. 57, pp. 472-485, 1940.
- [18] F. Carstoiu and R. J. Lombard, "Eikonal expansions for total cross sections of heavy ions," *Physical Review C*, vol. 48, 1993.
- [19] S. J. Wallace, "High energy expansion of scattering amplitudes," *Physical Review D*, vol. 8, pp. 180-193, 1973.
- [20] D. Waxman, C. Wilkin, J. F. Germond, and R. J. Lombard, "Eikonal corrections for spin-orbit potentials," *Physical Review C*, vol. 24, pp. 578-582, 1981.
- [21] S. J. Wallace, "Multiple-scattering eikonal expansion: systematic corrections to the Glauber theory," *Physical Review C*, vol. 8, pp. 2043-2055, 1971.
- [22] S. J. Wallace, "Comment on equivalence of the eikonal expansion and integral-equation methods for determining corrections to the Glauber approximation\*," *Physical Review D*, vol. 8, pp. 1934-1938, 1972.
- [23] R. Serber, "Nuclear Reactions at High Energies," *Physical Review C*, vol. 7, pp. 248-262, 1947.
- [24] M. L. Goldberger, "The interactions of high energy neutrons and heavy nuclei," *Physical Review*, vol. 74, pp. 1269-1277, 1948.
- [25] V. Franco, "High energy collisions between heavy nuclei," *Physics Letters B*, vol. 61, pp. 444-448, 1976.

- [26] G. F. Chew and M. L. Goldberger, "The scattering of elementary particles by complex nuclei-A generalization of impulse approximation," *Physical Review*, vol. 87, pp. 778-782, 1952.
- [27] G. F. Chew, "High energy elastic proton-deuteron scattering," *Physical Review*, vol. 84, pp. 1057-1058, 1951.
- [28] K. M. Watson, "Multiple scattering series and many body problems -applications to photomeson production in complex nuclei," *Physical Review*, vol. 89, pp. 557-587, 1953.
- [29] R. J. Glauber, "Cross sections in deuterium at high energies," *Physical Review*, vol. 100, pp. 242-248, 1955.
- [30] V. Franco and R. J. Glauber, "High energy deuteron cross sections," *Physical Review*, vol. 142, pp. 1195-1214, 1966.
- [31] W. Czyz and L. C. Maximon, "High energy, small angle elastic scattering of strongly interacting composite particles," *Annals of Physics*, vol. 52, pp. 59-121, 1969.
- [32] A. Dar and Z. Kirzon, "Simple explanation of elastic scattering of heavy ions," *Physics Letters B*, vol. 37, pp. 166-169, 1971.
- [33] D. R. Harrington, "Double scattering corrections to high energy diffraction scattering from deuterons," *Physics Review B*, vol. 135, pp. 358-364, 1964.
- [34] E. A. Remler, "High energy scattering by nuclei," *Physical Review*, vol. 176, 1968.
- [35] J. M. Eisenberg, "On the relationship between the Glauber Approximation and the Watson multiple scattering theory," *Annals of Physics*, vol. 71, pp. 542-555, 1972.
- [36] R. Blankenbecler and M. L. Goldberger, "Behavior of scattering amplitudes at high energies, bound states and resonances," *Physical Review*, vol. 126, pp. 766-785, 1962.
- [37] D. Harrington, "Multiple scattering, the Glauber approximation, and the off-shell eikonal approximation.," *Physics Review* vol. 184, pp. 1745-1749, 1969.
- [38] T. A. Osborn, "Glauber theory without the eikonal approximation," *Annals of physics*, vol. 58, pp. 417-453, 1970.
- [39] V. Franco and A. Tekou, "High energy heavy ion scattering and the optical phase shift function," *Physics Review C*, vol. 16, pp. 658-664, 1977.
- [40] G. F. Chew and G. C. Wick, "The impulse approximation," *Physical Review* vol. 85, pp. 636-642, 1952.

- [41] G. F. Chew, "The inelastic scattering of high energy neutrons bu deuterons according to impulse approximation," *Physical Review*, vol. 80, pp. 196-202, 1950.
- [42] N. M. Queen, "Corrections to impulse approximation for elastic nucleon-deuteron scattering," *Nuclear Physics* vol. 55, pp. 177-196, 1964.
- [43] O. Chamberlian, E. Segre, R. D. Tripp, C. Wiegand, and T. Ypsilantis, "Experiments with 315-MeV polarized protons: proton-proton and proton-nuetron scattering," *Physical Review*, vol. 105, pp. 288-301, 1957.
- [44] H. P. Stapp and T. J. Ypsilantis, "Phase shift analysis of 310-MeV proton-proton scattering experiments," *Physical Review*, vol. 105, pp. 302-310, 1957.
- [45] H. A. Bethe, "Scattering and polarization of protons by nuclei," *Annals of Physics*, vol. 3, pp. 190-240, 1958.
- [46] A. K. Kerman, H. McManus, and R. M. Thaler, "The scattering of fast nucleons from nuclei," *Annals of Physics*, vol. 8, 1959.
- [47] H. Feshbach and J. Hufner, "On scattering of nuclei at high energies," *Annals of Physics*, vol. 56, 1970.
- [48] J. W. Wilson, "Proton-deuteron double scattering," *Physical Review C*, vol. 10, pp. 369-376, 1974A.
- [49] J. W. Wilson and L. W. Townsend, "An optical model for composite nuclear scattering," *Canadian Journal of Physics*, vol. 59, pp. 1569-1576, 1981.
- [50] H. Postma and R. Wilson, "Elastic scattering of 146-MeV polarized protons by Deuterons," *Physical Review*, vol. 121, pp. 1229-1244, 1961.
- [51] S. J. Wallace, "Eikonal Expansion \* +," *Physics Review Letters*, vol. 27, 1971.
- [52] W. M. Cottingham and R. F. Peierls, "Impact parameter expansion of high-energy elastic-scattering-amplitudes," *Physics Review*, vol. 137, pp. B147-B154, 1964.
- [53] T. Adachi and T. Kotani, "An Impact Parameter Formalism. III ---Strong Absorption Model---," *Progress of Theoretical Physics* vol. 35, pp. 485-507, 1966.
- [54] A. Baker, "Second-order eikonal approximation for potential scattering," *Phys. Rev. D*, vol. 6, pp. 3462-3469, 1972.
- [55] L. Schiff, "High-Energy Scattering at Moderately Large Angles," *Physical Review*, vol. 176, pp. 1390-1394, 1968.

- [56] L. Schiff, "Approximation method for high-energy potential scattering," *Physical Review*, vol. 103, pp. 443-453, 1956.
- [57] D. K. Ross, "High-energy multiple scattering for large angles," *Phys. Rev.*, vol. 173, pp. 1695-1699, 1968.
- [58] S. Sarkar, "Higher-order terms in the eikonal expansion of the T-matrix for potential scattering," *Physical Review D*, vol. 21, pp. 3437-3459, 1980.
- [59] S. J. Wallace, "High-energy expansions of nuclear multiple scattering\*," *Physical Review C*, vol. 12, 1975.
- [60] M. Bleszynski and C. Sander, "Geometrical Aspects of high energy peripheral scattering," *Nuclear Physics A* vol. 326, pp. 525-535, 1979.
- [61] L. W. Townsend, "Lecture notes : Nuclear cross section modeling (NE-640)," University of Tennessee.
- [62] L. W. Townsend, C. R. Ramsey, R. K. Tripathi, F. A. Cucinotta, and J. W. Norbury, "Optical model methods of predicting nuclide production cross sections from heavy ion fragmentation," *Nuclear Instruments and Methods in Physics Research*, vol. 149, pp. 401-413, 1999.
- [63] F. A. Cucinotta and R. R. Dubey, "Final state interactions and inclusive nuclear collisions," NASA TP-3353, 1993.
- [64] K. Kikuchi and M. Kawai, *Nuclear matter and nuclear reactions*. Amsterdam (Germany): North Holland Publishing, 1968.
- [65] Y. Haneishi and T. Fujita, "Problem of backward proton production.,," *Physical Review C*, vol. 33, pp. 260-274, 1986.
- [66] G. S. Braley, L. W. Townsend, F. A. Cucinotta, and L. H. Heilbronn, "Modeling of secondary neutron production from space radiation interactions," *IEEE Transactions on Nuclear Science*, vol. 49, pp. 2800-2804, 2002.
- [67] D. Griffiths, "Introduction to elementary particles," 2nd ed Weinheim: Wiley-Vch Verlag GmbH & Co., 2009, pp. 160-165.
- [68] J. J. Sakurai, "Modern quantum mechanics," 1st ed California: The Benjamin/Cummings Publishing Company, Inc., 1985, pp. 392-397.



- [69] K. V. Shajesh, "Eikonal approximation", University of Oklahoma, Report submitted for partial fulfillment of general examination, 2004.
- [70] F. E. Ringia, T. Dobrowolski, H. R. Gustafson, L. W. Jones, M. J. Longo, E. F. Parker, and B. Cork, "Differential cross sections for small-angle neutron-proton and nucleus-nucleus elastic scattering at 4.8 GeV/c," *Physics Review Letters*, vol. 28, pp. 185-188, 1972.
- [71] C. W. De Jager, H. De Vries, and C. De Vries, "Nuclear charge and magnetization-density-distribution parameters from elastic electron scattering," *Atomic Data and Nuclear Data Tables*, vol. 14, pp. 479-508, 1974.
- [72] F. Borkowski, G. G. Simon, V. H. Walther, and R. D. Wendling, "On the determination of the proton RMS-radius from electron scattering data," *Z. Phys. A*, vol. 275, pp. 29-31, 1975.
- [73] L. W. Townsend, "Harmonic well matter densities and Pauli correlation effects in heavy ion collisions," NASA TP-2003, 1982.
- [74] J. W. Wilson and C. M. Costner, "Nucleon and heavy-ion total and reaction cross sections for selected nuclei," NASA TN D-8107, 1975.
- [75] K. M. Maung, P. A. Deutchman, and W. D. Royalty, "Integrals involving the three-parameter Fermi function," *Canadian Journal of Physics*, vol. 67, pp. 95-99, 1988.
- [76] H. B. Badisaria and L. W. Townsend, "Analytic optical potentials for nucleon-nucleus and nucleus-nucleus collisions involving light and medium nuclei," NASA Technical Memorandum-83224, 1982.
- [77] L. W. Townsend and J. W. Wilson, "Energy-dependent parameterization of heavy-ion absorption cross section," *Radiation Research*, vol. 106, pp. 283-287, 1986.
- [78] T. Koi and D. H. Wright. (2003). *Physics reference manual*  
Available:  
[http://geant4.cern.ch/G4UsersDocuments/UsersGuides/PhysicsReferenceManual/html/no\\_de8](http://geant4.cern.ch/G4UsersDocuments/UsersGuides/PhysicsReferenceManual/html/no_de8)
- [79] Wikipedia. Available: [http://en.wikipedia.org/wiki/Gaussian\\_quadrature](http://en.wikipedia.org/wiki/Gaussian_quadrature)
- [80] C. M. Werneth, M. Dhar, K. M. Maung, C. Sirola, and J. W. Norbury, "Numerical Gram-Schmidt orthonormalization," *European Journal of Physics*, vol. 31, pp. 693-700, 2010.

- [81] G. V. Winckel. *Legendre Gauss-quadrature weights and nodes*. Available: <http://www.mathworks.com/matlabcentral/fileexchange/4540-legendre-gauss-quadrature-weights-and-nodes>
- [82] J. W. Norbury and F. Dick, "Differential cross section kinematics for 3-dimensional transport codes," NASA TP-2008-215543, 2008.

## **APPENDIX**

## APPENDIX I

Table A.I. Generalized Bernoulli polynomials  $b_n(x) \equiv B_{(2n)}^{(2x)}(x)$

$b_0(x) = 1$
$b_1(x) = -x/6$
$b_2(x) = \frac{x(5x+1)}{60}$
$b_3(x) = -\frac{x(35x^2 + 21x + 4)}{504}$
$b_4(x) = \frac{x(175x^3 + 210x^2 + 101x + 18)}{2160}$
$b_5(x) = -\frac{x(385x^4 + 770x^3 + 671x^2 + 286x + 48)}{3168}$
$\frac{1}{(2n)!}b_n(x) = \frac{1}{n!}\left(-\frac{1}{12}x\right)^n - \frac{1}{5}\frac{1}{(n-2)!}\left(-\frac{1}{12}x\right)^{n-1} + \dots$

*(Table adapted from Wallace [19])*

## APPENDIX II

Table A.II. Nuclear Charge Distribution Parameters

Nucleus	Distribution	$\gamma$ or $t$ (fm)*	$a$ or $R$ (fm)*
<sup>2</sup> H	HW	0	1.71
<sup>4</sup> He	HW	0	1.33
<sup>7</sup> Li	HW	0.327	1.77
<sup>9</sup> B	HW	0.611	1.791
<sup>11</sup> Be	HW	0.811	1.69
<sup>12</sup> C	HW	1.247	1.649
<sup>14</sup> N	HW	1.291	1.729
<sup>16</sup> O	HW	1.544	1.833
<sup>20</sup> Ne	WS	2.517	2.74
<sup>27</sup> Al	WS	2.504	3.05
<sup>40</sup> Ar	WS	2.693	3.47
<sup>56</sup> Fe	WS	2.611	3.971
<sup>64</sup> Cu	WS	2.504	4.20
<sup>80</sup> Br	WS	2.306	4.604
<sup>108</sup> Ag	WS	2.354	5.139
<sup>138</sup> Ba	WS	2.621	5.517
<sup>208</sup> Pb	WS	2.416	6.624

\*  $\gamma$  and  $a$  are for HW distributions, and  $t$  and  $R$  are for WS distributions.

(Table adapted from Wilson et al.[1])

## APPENDIX III

### Phase Function Calculations

The phase function can be written in terms of optical potential in terms of sum of the series

$$\chi(b) = \sum_n -\frac{(\mu)^{n+1}}{k(n+1)!} \left[ \left( \frac{b}{k} \frac{\partial}{\partial b} - \frac{\partial}{\partial k} \right) \frac{1}{k} \right]^n \int_{-\infty}^{\infty} V^{n+1}(\vec{r}) dz \quad (\text{AIII.1})$$

where the optical potential is given as

$$V(\vec{r}) = -k M \exp(-Nx^2) \quad (\text{AIII.2})$$

The optical potential term already takes in account the nucleon mass , thus the series in equation (AIII.1) can be rewritten as

$$\chi(b) = \sum_n -\frac{1}{2k(n+1)!} \left[ \left( \frac{b}{k} \frac{\partial}{\partial b} - \frac{\partial}{\partial k} \right) \frac{1}{k} \right]^n \int_{-\infty}^{\infty} V^{n+1}(\vec{r}) dz \quad (\text{AIII.3})$$

We can now write the first term of the series as

$$\chi_0(b) = -\frac{1}{2k} \int_{-\infty}^{\infty} -kM \exp(-Nx^2) dz \quad (\text{AIII.4})$$

Separating  $x^2 = b^2 + z^2$ , allows us to write the equation above as

$$\chi_0(b) = \frac{1}{2} M \exp(-Nb^2) \int_{-\infty}^{\infty} \exp(-Nz^2) dz \quad (\text{AIII.5})$$

and further reduces to

$$\chi_0(b) = \frac{1}{2} \sqrt{\frac{\pi}{N}} M \exp(-Nb^2) \quad (\text{AIII.6})$$

In the similar manner, the first order correction term in the series can be written as

$$\chi_1(b) = -\frac{1}{4k} \left[ \left( \frac{b}{k} \frac{\partial}{\partial b} - \frac{\partial}{\partial k} \right) \frac{1}{k} \right] \int_{-\infty}^{\infty} V^2(\vec{r}) dz \quad (\text{AIII.7})$$

and further reduces to

$$\chi_1(b) = -\frac{1}{4k} \sqrt{\frac{\pi}{2N}} \left[ \left( \frac{b}{k} \frac{\partial}{\partial b} - \frac{\partial}{\partial k} \right) \frac{1}{k} \right] (k^2 M^2 \exp(-2Nb^2)) \quad (\text{AIII.8})$$

$$= -\frac{1}{4k} \sqrt{\frac{\pi}{2N}} (-4b^2 M^2 N - M^2) \exp(-2Nb^2) \quad (\text{AIII.9})$$

$$= \frac{1}{4k} \sqrt{\frac{\pi}{2N}} M^2 (4Nb^2 + 1) \exp(-2Nb^2) \quad (\text{AIII.10})$$

The second order correction term can be written in similar way as

$$\chi_2(b) = -\frac{1}{12k} \sqrt{\frac{\pi}{3N}} \left[ \left( \frac{b}{k} \frac{\partial}{\partial b} - \frac{\partial}{\partial k} \right) \frac{1}{k} \right]^2 \left( -k^3 M^3 \exp(-3Nb^2) \right) \quad (\text{AIII.11})$$

$$= -\frac{1}{12k} \sqrt{\frac{\pi}{3N}} \left[ \left( \frac{b}{k} \frac{\partial}{\partial b} - \frac{\partial}{\partial k} \right) \left( \frac{1}{k} \right) \right] \left( 6b^2 k M^3 N + 2k M^3 \right) \exp(-3Nb^2) \quad (\text{AIII.12})$$

$$= -\frac{1}{12k} \sqrt{\frac{\pi}{3N}} \left( -\frac{36}{k} b^4 M^3 N^2 \right) \exp(-3Nb^2) \quad (\text{AIII.13})$$

$$= -\frac{1}{12k^2} \sqrt{\frac{\pi}{3N}} M^3 \left( -36 b^4 N^2 \right) \exp(-3Nb^2) \quad (\text{AIII.14})$$

The third order correction term can be given as

$$\chi_3(b) = -\frac{1}{48k} \sqrt{\frac{\pi}{4N}} \left[ \left( \frac{b}{k} \frac{\partial}{\partial b} - \frac{\partial}{\partial k} \right) \frac{1}{k} \right]^3 \left( k^4 M^4 \exp(-4Nb^2) \right) \quad (\text{AIII.15})$$

$$= -\frac{1}{48k} \sqrt{\frac{\pi}{4N}} \left[ \left( \frac{b}{k} \frac{\partial}{\partial b} - \frac{\partial}{\partial k} \right) \left( \frac{1}{k} \right) \right]^2 \left( -8b^2 k^2 M^4 N - 3k^2 M^4 \right) \exp(-4Nb^2) \quad (\text{AIII.16})$$



$$= -\frac{1}{48k} \sqrt{\frac{\pi}{4N}} \left[ \left( \frac{b}{k} \frac{\partial}{\partial b} - \frac{\partial}{\partial k} \right) \left( \frac{1}{k} \right) \right] (16b^2 M^4 N + 64b^4 M^4 N^2 + 3M^4) \exp(-4Nb^2) \quad (\text{AIII.17})$$

$$= \frac{1}{48k^3} \sqrt{\frac{\pi}{4N}} M^4 (-24b^2 N - 192b^4 N^2 + 512b^6 N^3 - 3) \exp(-4Nb^2) \quad (\text{AIII.18})$$

The fourth order correction term in the series can be given by

$$\chi_4(b) = -\frac{1}{240k} \sqrt{\frac{\pi}{5N}} \left[ \left( \frac{b}{k} \frac{\partial}{\partial b} - \frac{\partial}{\partial k} \right) \frac{1}{k} \right]^4 (-k^5 M^5 \exp(-5Nb^2)) \quad (\text{AIII.19})$$

$$= -\frac{1}{240k} \sqrt{\frac{\pi}{5N}} \left[ \left( \frac{b}{k} \frac{\partial}{\partial b} - \frac{\partial}{\partial k} \right) \left( \frac{1}{k} \right) \right]^3 (10b^2 k^3 M^5 N + 4k^3 M^5) \exp(-5Nb^2) \quad (\text{AIII.20})$$

$$= -\frac{1}{240k} \sqrt{\frac{\pi}{5N}} \left[ \left( \frac{b}{k} \frac{\partial}{\partial b} - \frac{\partial}{\partial k} \right) \left( \frac{1}{k} \right) \right]^2 (-40b^2 k M^5 N - 100b^4 k M^5 N^2 - 8k M^5) \exp(-5Nb^2) \quad (\text{AIII.21})$$

$$= -\frac{1}{240k} \sqrt{\frac{\pi}{5N}} \left[ \left( \frac{b}{k} \frac{\partial}{\partial b} - \frac{\partial}{\partial k} \right) \left( \frac{1}{k} \right) \right] \left( \frac{1000}{k} M^5 N^3 b^6 \right) \exp(-5Nb^2) \quad (\text{AIII.22})$$

$$= -\frac{1}{240k^4} \sqrt{\frac{\pi}{5N}} M^5 (8000b^6 N^3 - 10000b^8 N^4) \exp(-5Nb^2) \quad (\text{AIII.23})$$

And the total phase is given by

$$\chi(b) = \chi_0(b) + \chi_1(b) + \chi_2(b) + \chi_3(b) + \chi_4(b) + \dots \quad (\text{AIII.24})$$

## Appendix IV

### Gaussian Quadrature

Gaussian quadrature numerical analysis method is an approximation of the definite integral of a function  $f$  , over interval  $[-1, 1]$  , given as

$$\int_{-1}^1 f(x) dx \approx \sum_{i=0}^{n-1} w_i f(x_i) \quad (\text{AIV.1})$$

where  $f$  is the desired function,  $x_i$  are the roots of Legendre Polynomials,  $n$  is the number of Gaussian points over which the function is summed over, and  $w_i$  are the weights determined from the derivatives of the Legendre polynomials as

$$w_i = \frac{2}{(1-x_i^2)[P'_l(x_i)]^2} \quad (\text{AIV.2})$$

where  $P'_l(x_i)$  are the derivatives of the Legendre Polynomials of  $x_i$ .

To transform integrals from  $[0, \infty]$  to  $[-1, 1]$  so we can use it to evaluate  $\int_0^{\infty} f(x') dx'$ , we use a

substitution function

$$x' = \tan \left[ \frac{\pi}{4} (x+1) \right] \quad (\text{AIV.3})$$

and

$$dx' = \frac{\pi}{4} \sec^2 \left[ \frac{\pi}{4}(x+1) \right] \quad (\text{AIV.4})$$

Thus using these substitutions, we can now write the function as

$$\int_0^\infty f(x') dx' = \int_{-1}^1 f \left( \tan \left[ \frac{\pi}{4}(x+1) \right] \right) \frac{\pi}{4} \sec^2 \left[ \frac{\pi}{4}(x+1) \right] dx \quad (\text{AIV.5})$$

$$\approx \sum_{i=0}^{n-1} f \left( \tan \left[ \frac{\pi}{4}(x_i+1) \right] \right) w_i \frac{\pi}{4} \sec^2 \left[ \frac{\pi}{4}(x_i+1) \right] \quad (\text{AIV.6})$$

With the variables been transformed, we can now compute the integral by carrying out the summation.

## Appendix V

### More Results:

Table 4: Total Abrasion Cross Section with Correction Terms for  $^{20}\text{Ne}$  on  $^{64}\text{Cu}$  at 5 Degrees

Energy (MeV/Nucleon)	$\sigma \sum_{i=1} \chi_i$ (mb)	$\sigma \sum_{i=0}^1 \chi_i$ (mb)	$\sigma \sum_{i=0}^2 \chi_i$ (mb)	$\sigma \sum_{i=0}^3 \chi_i$ (mb)	$\sigma \sum_{i=0}^4 \chi_i$ (mb)
100	2275.36	3550.03	4122.50	4230.03	4225.28
200	1979.06	2582.59	2677.46	2685.14	2685.14
300	1964.28	2454.06	2511.73	2515.35	2515.35
500	2069.31	2552.20	2600.72	2603.31	2603.31
1000	2157.17	2566.69	2595.73	2596.85	2596.85
3000	2088.78	2253.06	2257.27	2257.33	2257.33
5000	2092.44	2200.80	2202.55	2202.57	2202.57
10000	2095.13	2150.49	2150.92	2150.93	2150.93

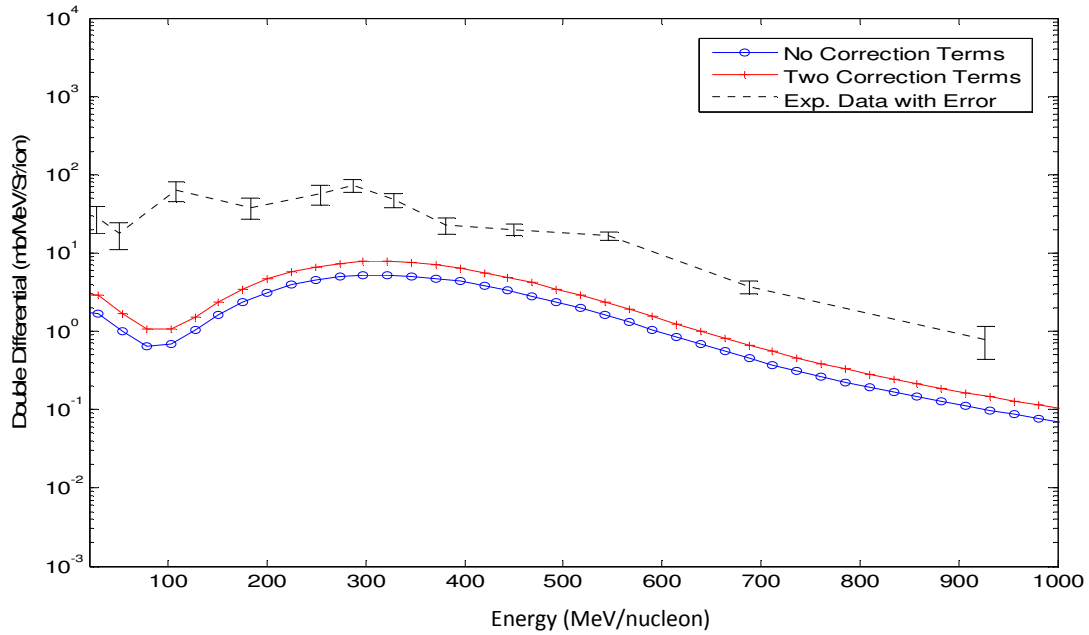
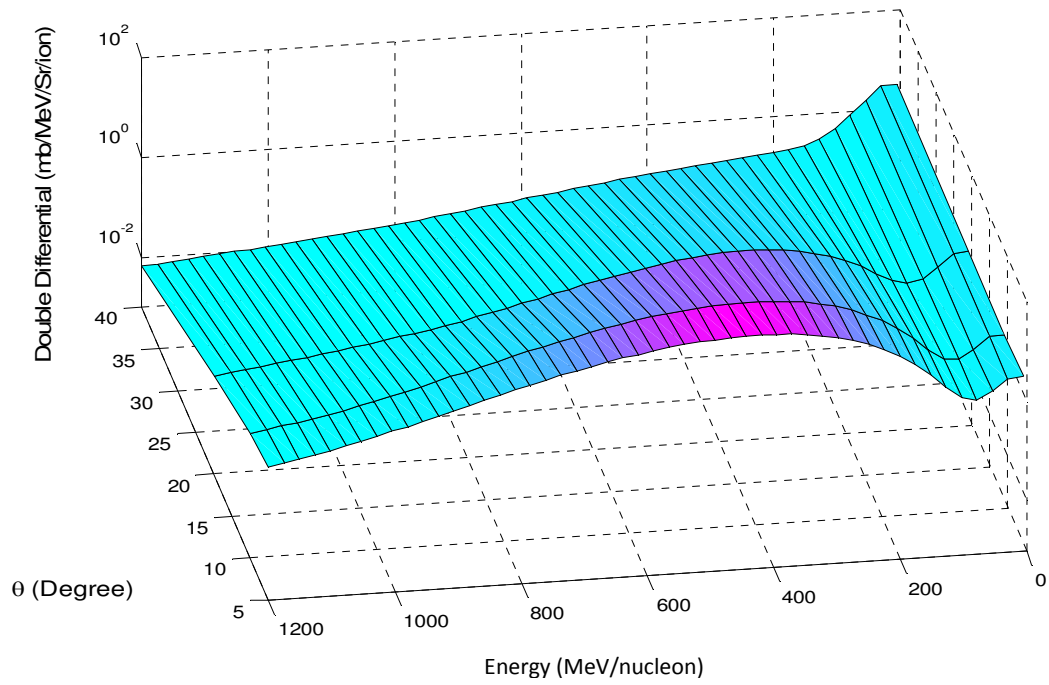
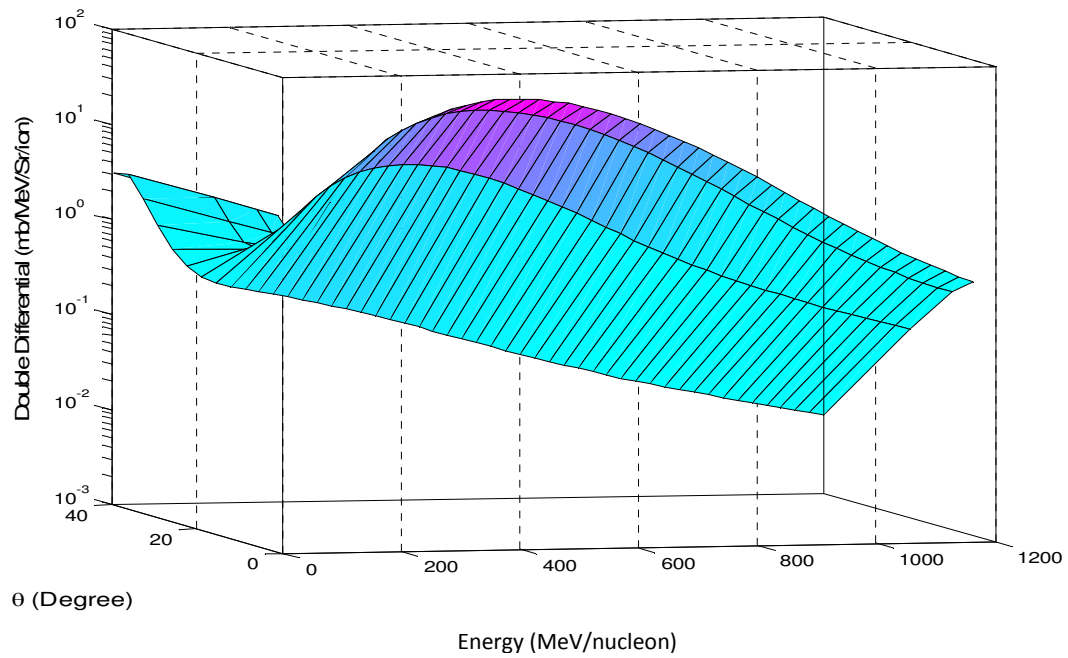


Figure 38: Double differential cross sections for 400 MeV/nucleon  $^{84}\text{Kr}$  on  $^{27}\text{Al}$  at 20 degrees



**Figure 39:** Surface plot of double differential cross section with two correction terms for 400 MeV/nucleon  $^{84}\text{Kr}$  on  $^{27}\text{Al}$



**Figure 40:** Same as figure (39), except rotated

## Appendix VI

### MATLAB code:

#### 1. Main Program:

```
%%%% The program calculates the Lorentz Invariant and the Double
%%%% differential cross sections from the abrasion process.
%%%% The cross sections from ablation are calculated using the abrasion
%%%% cross section generated by this program and the probability functions
%%%% from the UBERNSPEC code.

clc;
clear;

%% Input properties%%
%%%%%%%%%%%%%%%%%%%%%%%%%%%%%%%%%%%%%%%%

Tlab= input('\n Please Enter Projectile Lab. Energy      : ');
Ap= input('\n Please Enter Projectile Mass Number      : ');
At= input('\n Please Enter Target Mass Number         : ');
Zp= input('\n Please Enter Projectile Charge Number    : ');
Zt= input('\n Please Enter the Target Charge Number    : ');
theta= input('\n Please Enter the Scattering Angle (Degrees) : ');
hbar=197.36;

%% Change angle to Radians%%

AA=(theta*pi/180);

am=939.57; %%mass of nucleon
amp= Ap*(am-7); %% total projectile mass

%% Calculate the energy grid for outgoing Nucleon energy%%

Emin=5.00; %% MeV
Emax=3*Tlab; %% MeV

Ek(1)=Emin;
Ek(50)=Emax;
N=50;
NM1=N-1;
H=(Emax-Emin)/NM1;
W(1)=H/2;

for i=2:49
    Ek(i)=Ek(i-1)+H;
    W(i)=H;
end
```

```

%%%%%%%%Incoming Beam Calculations%%%%%%%%
PNN = sqrt(((Tlab+am)^2)-am^2);
T0lab=Tlab*Ap;
E0lab=(T0lab+amp);
P0lab=sqrt((E0lab^2)-amp^2);
Gamma = 1+ Tlab/am;
Beta= sqrt(1-(1/Gamma)^2);

%% Incoming nucleon %%

Ebeam=E0lab/Ap;
Pbeam=sqrt((Ebeam^2)-am^2);
Pn=Pbeam;
Tn=sqrt(am^2+Pn^2)-am;
Gamman= 1+Tn/am;
Betan= sqrt(1-(1/Gamman)^2);

%%% Calculation for nucleon momentum in projectile rest frame%%%

for n=1:50
    TL(n)=Ek(n);
    EF(n)=TL(n)+am;          %%% Lab Frame Nucleon energy
    Plab(n)=sqrt((EF(n))^2-am^2); %%% Lab Frame Momentum

    Pf(n)=Plab(n);
    PFL(n)=Gamman*(Pf(n)-(Betan*EF(n)));
    PFT(n)=Pf(n)*sin(AA);

    PFF(n)=sqrt(((PFL(n))^2)+((PFT(n))^2)); %%% Projectile rest frame
    EK1(n)=sqrt(((PFF(n))^2)+am^2);
    EZK(n)=sqrt((Plab(n))^2+am^2);
end

%% Calculate the Fermi Momentum and Momentum Distributions

KF=26*log(Ap)+129;
P1=KF*sqrt(2/5);
C1=1;
P2=KF*sqrt(6/5);
C2=0.03;
P3=500;
C3=0.0008;

% Normalization Constant

N0=1/((C1*(2*pi*P1^2)^1.5)+(C2*(2*pi*P2^2)^1.5)+((C3*(2*pi*P3^2)^1.5)));

```



```
%% Call the functions get the Abrasion cross section for the projectile
%% and the target
```

```
[SigA,SigA1,SigA2]=AbrasionCrs1(Tlab,Ap,At,Zp,Zt,AA) %projectile
[SigAt,SigAlt,SigA2t]=AbrasionCrs2(Tlab,At,Ap,Zt,Zp,AA) %Target
%% Calculation of Lorentz Invariant and Double Differential %%
```

```
for k=1:50
```

```
%Projectile, no correction terms
```

```
NuMom1(k)=(SigA)*N0*C1*exp(-(PFF(k))^2/(2*P1^2));
NuMom2(k)=(SigA)*N0*C2*exp(-(PFF(k))^2/(2*P2^2));
NuMom3(k)=(SigA)*N0*C3*exp(-(PFF(k))^2/(2*P3^2));
NuMom(k)=NuMom1(k)+NuMom2(k)+NuMom3(k);
```

```
%Projectile, two correction terms
```

```
NuMom1c2(k)=(SigA1)*N0*C1*exp(-(PFF(k))^2/(2*P1^2));
NuMom2c2(k)=(SigA1)*N0*C2*exp(-(PFF(k))^2/(2*P2^2));
NuMom3c2(k)=(SigA1)*N0*C3*exp(-(PFF(k))^2/(2*P3^2));
NuMomc2(k)=NuMom1c2(k)+NuMom2c2(k)+NuMom3c2(k);
```

```
%Projectile, four correction terms
```

```
NuMom1c4(k)=(SigA2)*N0*C1*exp(-(PFF(k))^2/(2*P1^2));
NuMom2c4(k)=(SigA2)*N0*C2*exp(-(PFF(k))^2/(2*P2^2));
NuMom3c4(k)=(SigA2)*N0*C3*exp(-(PFF(k))^2/(2*P3^2));
NuMomc4(k)=NuMom1c4(k)+NuMom2c4(k)+NuMom3c4(k);
```

```
% Target Contribution, no correction terms
```

```
NuMom1t(k)=(SigAt)*N0*C1*exp(-(Plab(k))^2/(2*P1^2));
NuMom2t(k)=(SigAt)*N0*C2*exp(-(Plab(k))^2/(2*P2^2));
NuMom3t(k)=(SigAt)*N0*C3*exp(-(Plab(k))^2/(2*P3^2));
NuMomt(k)=NuMom1t(k)+NuMom2t(k)+NuMom3t(k);
```

```
% Target, two correction terms
```

```
NuMom1tc2(k)=(SigAlt)*N0*C1*exp(-(Plab(k))^2/(2*P1^2));
NuMom2tc2(k)=(SigAlt)*N0*C2*exp(-(Plab(k))^2/(2*P2^2));
NuMom3tc2(k)=(SigAlt)*N0*C3*exp(-(Plab(k))^2/(2*P3^2));
NuMomtc2(k)=NuMom1tc2(k)+NuMom2tc2(k)+NuMom3tc2(k);
```

```
% Target, four correction terms
```

```
NuMom1tc4(k)=(SigA2t)*N0*C1*exp(-(Plab(k))^2/(2*P1^2));
NuMom2tc4(k)=(SigA2t)*N0*C2*exp(-(Plab(k))^2/(2*P2^2));
NuMom3tc4(k)=(SigA2t)*N0*C3*exp(-(Plab(k))^2/(2*P3^2));
NuMomtc4(k)=NuMom1tc4(k)+NuMom2tc4(k)+NuMom3tc4(k);
```

```

%% Lorentz Invariant for 0,2 & 4 correction terms

LnInv(k)= 10*(EK1(k)*NuMom(k)+EZK(k)*NuMomt(k));
LnInv1(k)= 10*(EK1(k)*NuMomc2(k)+EZK(k)*NuMomtc2(k));
%LnInv2(k)= 10*(EK1(k)*NuMomc4(k)+EZK(k)*NuMomtc4(k));

LnInv1t(k)=10*(EZK(k)*NuMomt(k));
LnInv1t(k)=10*(EZK(k)*NuMomtc2(k));
%LnInv2t(k)=10*(EZK(k)*NuMomtc4(k));

%Double Differential for 0,2 and 4 correction terms.

DbDiff(k)=Plab(k)*LnInv(k);
DbDiff1(k)=Plab(k)*LnInv1(k);
%DbDiff2(k)=Plab(k)*LnInv2(k);

DbDiff1t(k)=Plab(k)*LnInv1t(k);
DbDiff1t(k)=Plab(k)*LnInv1t(k);
%DbDiff2t(k)=Plab(k)*LnInv2t(k);

end

%%Display Results and plot

DbDiff'
DbDiff1'
plot(Ek, DbDiff, Ek, DbDiff1)

```

## 2. Function AbrasionCrs1

```

%% This function calculates the Abrasion cross section for the
projectile%%
%% Called by MainRun.m

function[SigAbr, SigAbr2, SigAbr4]=AbrasionCrs1(Tlab1,Ap1,At1,Zp1,Zt1,AA)

%% Calculate other constants%%

Np= Ap1-Zp1;           %% Number of Neutrons in the projectile
Nt= At1-Zt1;           %% Number of Neutrons in the Target
r0= 1.26;              %% Constant for radius calculation (fm)
Rp=r0*((Ap1)^(1/3));   %% Projectile radius (fm)
Rt= r0*((At1)^(1/3));   %% Target Radius (fm)
am=937.57;             %% Mass of Neutron MeV
amt= (am-7);           %% Atomic mass MeV
Mp=Ap1*amt;            %% Projectile total mass
Mt=At1*amt;            %% Target total mass
hbarc= 197.326;        %% MeV fm

```

```

%%% The values for density parameters taken from DeJager and DeVries.
%%% Call Density function %%%
%%% Calculate the Gauss density constants

[Cp,Dp]=density(Ap1);
[Ct,Dt]=density(At1);

%%% Call lgwt to do the Gauss Quadrature%%%
% Calculate the Gauss points for N=1000

Nint=1000;
a1= -1;
b1 = 1;

[x1,w1]=lgwt(Nint,a1,b1);

% Calculation of the energy and momentum in lab and projectile frame

Elab=Tlab1+am;
Gamma1= 1+Tlab1/am;
Beta1=sqrt(1-(1/Gamma1)^2);
Plab1=sqrt(Elab^2-am^2);
Pfl1=Gamma1*(Plab1*cos(AA)-Beta1*Elab);
Pft1=Plab1*sin(AA);
PK=sqrt(Pfl1^2+Pft1^2);
K=(PK)/(2*hbarc*sin(AA/2));

%%% The invariant in lab
S= ((Mp + Mt)^2)+ 2*Mt*Tlab1;

%% Calculate the Slope Parameter %%%

B= 0.0389*(10+ 0.5*log(((S)/1000000))));

%%% Calculate the nucleon-nucleon parameters

if Tlab1<=25
    Sigpp=exp(6.51*(exp(-Tlab1/135)^0.7))/10;
elseif Tlab1>25
    Sigpp =((1+(5/Tlab1))*(40+(109*(cos(0.199*((Tlab1)^0.5)))*exp(-0.451*((Tlab1-25)^(0.258))))))/10;
end
Sigpn=(38+12500*exp(-1.187*((Tlab1-0.1)^0.35)))/10;

Sig= ((Np+Nt)/(Ap1+At1))*(Sigpn)+Sigpp*((Zp1*Zt1+Np*Nt)/(Ap1*At1);

```

```

%% Calculate the constant values for the potential

W= Dp+(1/(2*B));
V= Dp-((Dp^2)/(W));
M1= Ap1*At1*Cp*Ct*Sig*((2*pi*B)^(-1.5))*((pi/W)^1.5)*((pi/(Dt+V))^1.5);
N1= V-((V)^2)/(Dt+V);

%%% Gaussian Weights %%%

for i=1:Nint
    triarg(i)=(pi/4)*(x1(i)+1);
    xb(i)=tan(triarg(i));
    wb(i)=((pi/4)*w1(i))/((cos(triarg(i)))*(cos(triarg(i))));
end

for k=1:Ap1

    for n=1:Nint
        argb(n)= xb(n);
        X1(n)= ((M1)/2)*((pi/N1)^0.5)*exp(-N1*(argb(n))^2);
        X2(n)=(1/(4*K))*((M1^2))*((pi/((2*N1)))^0.5)*((4*N1*(argb(n))^2)+1)*exp(-
2*N1*(argb(n))^2);
        X3(n)= -1*((M1^3)/(12*K^2))*((pi/(3*N1))^0.5)*((argb(n))^2)*(-
1*(36*(N1)^2*(argb(n))^2))*exp((-3*N1*(argb(n))^2));
        X4(n)=(1*(M1^4)/(48*K^3))*((pi/(4*N1))^0.5)*((-24*N1*(argb(n))^2)-
(192*(N1^2)*(argb(n)^4))+(512*(N1^3)*(argb(n)^6))-(3))*exp((-
4*N1*(argb(n))^2));
        X5(n)=-(1*(M1^5)/(240*K^4))*((pi/(5*N1))^0.5)*((8000*(N1^3)*(argb(n)^6))-
(10000*(N1^4)*(argb(n)^8)))*exp((-5*N1*(argb(n))^2));

        Pb1(n)=exp(-2*X1(n)/Ap1);
        Pb2(n)=exp(-2*X2(n)/Ap1);
        Pb3(n)=exp(-2*X3(n)/Ap1);
        Pb4(n)=exp(-2*X4(n)/Ap1);
        Pb5(n)=exp(-2*X5(n)/Ap1);

        Zsum1(n)= 2*pi*((argb(n)*wb(n))*((1-Pb1(n))^k)*((Pb1(n))^(Ap1-k))));
        ZCsum2(n)=2*pi*((argb(n)*wb(n))*((1-Pb2(n))^k)*((Pb2(n))^(Ap1-k))));
        ZCsum3(n)=2*pi*((argb(n)*wb(n))*((1-Pb3(n))^k)*((Pb3(n))^(Ap1-k))));
        ZCsum4(n)=2*pi*((argb(n)*wb(n))*((1-Pb4(n))^k)*((Pb4(n))^(Ap1-k))));
        ZCsum5(n)=2*pi*((argb(n)*wb(n))*((1-Pb5(n))^k)*((Pb5(n))^(Ap1-k))));

        ZCsumTwo(n)=Zsum1(n)+ZCsum2(n)+ZCsum3(n);
        ZCsumFour(n)=Zsum1(n)+ZCsum2(n)+ZCsum3(n)+ZCsum4(n)+ZCsum5(n);
    end

    Z1(k)= nchoosek(Ap1,k)*sum(Zsum1);
    Z2C(k)=nchoosek(Ap1,k)*sum(ZCsumTwo);
    Z4C(k)=nchoosek(Ap1,k)*sum(ZCsumFour);
end

```

```

Ksum1=sum(Z1);
Ksum2=sum(Z2C);
Ksum4=sum(Z4C);

SigAbr=Ksum1    % Abrasion with no correction terms
SigAbr2=Ksum2;  % Abrasion with two correction terms
SigAbr4=Ksum4;  % Abrasion with four correction terms

```

### 3. Function AbrasionCrs2

```

%%%This function calculates the Abrasion cross section for the Target
%%% Called by MainRun.m

function[SigAbr, SigAbr2, SigAbr4]=AbrasionCrs2(Tlab1,Ap1,At1,Zp1,Zt1,AA)

%%%%% Calculate other constants%%%%%%%%

Np= Ap1-Zp1;          % Number of Neutrons in the projectile
Nt= At1-Zt1;          % Number of Neutrons in the Target
r0= 1.26;             % Constant for radius calculation (fm)
Rp=r0*((Ap1)^(1/3));  % Projectile radius (fm)
Rt= r0*((At1)^(1/3)); % Target Radius (fm)
am=937.57;            % Mass of Neutron MeV
amt= (am-7);          % Atomic mass MeV
Mp=Ap1*amt;           % Projectile total mass
Mt=At1*amt;           % Target total mass
hbarc= 197.326;       % MeV fm

%%% The values for density parameters taken from Dejager and Devries.
%%% Call Density function %%%%
%%% Calculate the Gauss density constants

[Cp,Dp]=density(Ap1);
[Ct,Dt]=density(At1);

%%% Call lgwt to do the Gauss Quadrature%%%
% Calculate the Gauss points for N=1000

Nint=1000;
a1= -1;
b1 = 1;
[x1,w1]=lgwt(Nint,a1,b1);

% Calculation of energy and momentum in lab and projectile frame

Elab=Tlab1+am;

```

```

Gamma1= 1+Tlab1/am;
Beta1=sqrt(1-(1/Gamma1)^2);
Plab1=sqrt(Elab^2-am^2);
Pfl1=Gamma1*(Plab1*cos(AA)-Beta1*Elab);
Pft1=Plab1*sin(AA);
PK=sqrt(Pfl1^2+Pft1^2);
K=(PK)/(2*hbarc*sin(AA/2));

%%% The invariant in lab
S= ((Mp + Mt)^2)+ 2*Mt*Tlab1;

%% Calculate the Slope Parameter %%%

B= 0.0389*(10+ 0.5*log(((S)/1000000))));

%%% Calculate the N-N parameters

if Tlab1<=25
    Sigpp=exp(6.51*(exp(-Tlab1/135)^0.7))/10;
elseif Tlab1>25
    Sigpp =((1+(5/Tlab1))*(40+(109*(cos(0.199*((Tlab1)^0.5)))*exp(-0.451*((Tlab1-25)^(0.258))))))/10;
end
Sigpn=(38+12500*exp(-1.187*((Tlab1-0.1)^0.35)))/10;

Sig=((Np+Nt)/(Ap1+At1))*(Sigpn)+Sigpp*((Zp1*Zt1+Np*Nt)/(Ap1*At1);

%%% Constants for the calculation

%%% Calculate the Values of Potential

W= Dp+(1/(2*B));
V= Dp-((Dp^2)/(W));
M1= Ap1*At1*Cp*Ct*Sig*((2*pi*B)^(-1.55))*((pi/W)^1.5)*(((pi/(Dt+V))^1.5));
N1= V-((V)^2)/(Dt+V);

%%% Gaussian weights are being put in now

for i=1:Nint
    triarg(i)=(pi/4)*(x1(i)+1);
    xb(i)=tan(triarg(i));
    wb(i)=(pi/4)*w1(i)/(cos(triarg(i)))/(cos(triarg(i)));
end

for k=1:3;

    for n=1:Nint
        argb(n)= xb(n);
        X1(n)= ((M1)/2)*((pi/N1)^0.5)*exp(-N1*(argb(n))^2);
    end
end

```

```

X2(n)=(1/(4*K))*(M1^2)*(pi/((2*N1)))^0.5)*((4*N1*(argb(n))^2)+1)*exp(-
2*N1*(argb(n)^2));
X3(n)= -1*((M1^3)/(12*K^2))*(pi/(3*N1))^0.5)*((argb(n))^2)*(-
1*(36*(N1)^2*(argb(n)^2))*exp((-3*N1*(argb(n))^2));
X4(n)=(1*(M1^4)/(48*K^3))*(pi/(4*N1))^0.5)*((argb(n))^2)*((-24*N1)-
(192*(N1^2)*(argb(n)^2))+(512*(N1^3)*(argb(n)^4))-(3/(argb(n)^2)))*exp((-
4*N1*(argb(n))^2));
X5(n)=-
(1*(M1^5)/(240*K^4))*(pi/(5*N1))^0.5)*((argb(n))^2)*((8000*(N1^3)*(argb(n)^4
))-(10000*(N1^4)*(argb(n)^6)))*exp((-5*N1*(argb(n))^2));

Pb1(n)=exp(-2*X1(n)/Ap1);
Pb2(n)=exp(-2*X2(n)/Ap1);
Pb3(n)=exp(-2*X3(n)/Ap1);
Pb4(n)=exp(-2*X4(n)/Ap1);
Pb5(n)=exp(-2*X5(n)/Ap1);

Zsum1(n)= 2*pi*((argb(n)*wb(n)*((1-Pb1(n))^k)*((Pb1(n))^(Ap1-k)))));
ZCsum2(n)=2*pi*((argb(n)*wb(n)*((1-Pb2(n))^k)*((Pb2(n))^(Ap1-k)))));
ZCsum3(n)=2*pi*((argb(n)*wb(n)*((1-Pb3(n))^k)*((Pb3(n))^(Ap1-k)))));
ZCsum4(n)=2*pi*((argb(n)*wb(n)*((1-Pb4(n))^k)*((Pb4(n))^(Ap1-k)))));
ZCsum5(n)=2*pi*((argb(n)*wb(n)*((1-Pb5(n))^k)*((Pb5(n))^(Ap1-k)))));
ZCsumTwo(n)=Zsum1(n)+ZCsum2(n)+ZCsum3(n);
ZCsumFour(n)=Zsum1(n)+ZCsum2(n)+ZCsum3(n)+ZCsum4(n)+ZCsum5(n);

end

Z1(k)=nchoosek(Ap1,k)*sum(Zsum1);
Z2C(k)=nchoosek(Ap1,k)*sum(ZCsumTwo);
Z4C(k)=nchoosek(Ap1,k)*sum(ZCsumFour);

end
Ksum1=sum(Z1);
Ksum2=sum(Z2C);
Ksum4=sum(Z4C);

SigAbr=Ksum1;
SigAbr2=Ksum2;
SigAbr4=Ksum4;

```

#### 4. Function Density

```

%% This subroutine calculates the nuclear single particle densities
%% Called bt AbrasionCrs1.m and AbrasionCrs2.m

function[C1,D1]=density(A)
rp= 0.87;
pi=3.1416;

```

```

%% Gauss approximation to Harmonic Well Distributions

if (A < 20)
%% Values up to A=16 from DeJager and Devries A from 16-20 extrapolated

a = [1.2 1.77 1.51 1.33 1.7 1.75 1.77 1.78 1.79 1.8 1.69 1.649 1.7 1.729 1.8
1.833, 1.835, 1.86 1.88 1.89];
g = [0.0 0.0 0.0 0.0 0.1 0.2 0.327 0.45 0.611 0.81 1.0 1.247 1.28 1.291 1.4
1.544 1.61 1.63 1.64 1.65];

s= (((a(A))^2)/4)-((rp^2)/6))^0.5
D=1/(4*(s^2));
A1=((a(A)^3)/(8*s^3))*(1+(3*g(A)/2)-((3*g(A)*(a(A)^2))/(8*s^2)));
B= ((a(A)^3)/(8*s^3))*((g(A)*(a(A)^2))/(16*(s^4)));
rho0= 1/((((pi/D)^(3/2)))+(3*B/2)*(((pi^3)/(D^5))^0.5)));

C1= 0.66*(rho0*(a(A))^3/(8*s^3))*(1.5+(3*(g(A))/2)-
(3*g(A)*(a(A))^2/(8*s^2)))+(g(A)*(a(A))^2*(1)/(16*s^4))
D1 = 1/(4*(1 +0.52*g(A))*s^2);

%% Gauss approximation to Wood Saxon Distribution

elseif (A>=20)

a= (-6e-5*(A)^2)+(0.0342*A)+2.0976;
g=0.000005*(A^2)-0.0017*A+2.5955;
beta=exp(4.4*rp/(g*sqrt(3)));
ta=(8.8*rp/sqrt(3))*((log((3*beta-1)/(3-beta)))^-1);
rho02=(1/((((4*pi*((a^3)/3)+ ((pi^2)*(ta^2)*a/3))))));

C1=(a/g)^0.3*rho02;
D1= -0.0109*a+0.1234;

end

```

## 5. Function lgwt

```

% This script is computes definite integrals using Legendre-Gauss
% Quadrature. Computes the Legendre-Gauss nodes and weights on an interval
% [a,b] with truncation order N
% (Adapted from Greg von Winckel - 02/25/2004)

function [x,w]=lgwt(N,a,b)

N=N-1;
M1=N+1; M2=N+2;

kx=linspace(-1,1,M1)';

```



```

% Initial guess
y=cos((2*(0:N)' +1)*pi/(2*N+2))+(0.27/M1)*sin(pi*kx*N/M2);

% Legendre-Gauss Vandermonde Matrix
K=zeros(M1,M2);

% Derivative of LGVM
Kp=zeros(M1,M2);

% Compute the zeros of the N+1 Legendre Polynomial
% using the recursion relation and the Newton-Raphson method

y0=2;

% Iterate until new points are uniformly within epsilon of old points
while max(abs(y-y0))>eps

    K(:,1)=1;
    Kp(:,1)=0;

    K(:,2)=y;
    Kp(:,2)=1;

    for k=2:M1
        K(:,k+1)=( (2*k-1)*y.*K(:,k)-(k-1)*K(:,k-1) )/k;
    end

    Kp=(M2)*( K(:,M1)-y.*K(:,M2) )./(1-y.^2);

    y0=y;
    y=y0-K(:,M2)./Kp;

end

% Linear map from[-1,1] to [a,b]
x=(a*(1-y)+b*(1+y))/2;

% Compute the weights
w=(b-a)./( (1-y.^2) .*Kp.^2)*(M2/M1)^2;

```

## **VITA**

Santosh Bhatt was born in Baitadi, Nepal. He graduated his High school from Siddhanath Science Campus in Mahendranagar, Nepal. In August 2002, he moved to United States and graduated with B.S. in Engineering Physics from Southwestern Oklahoma State University in Weatherford, Oklahoma. He received his M.S. in Nuclear Engineering from University of Cincinnati in Cincinnati, Ohio, where his research area was study of fast reactor fuel burn up using computer code REBUS-PC. He joined University of Tennessee in January, 2008. His dissertation work was sponsored by the National Aeronautics and Space Administration (NASA).